Supplemental material

Dietary caloric input and tumor growth accelerate senescence and modulate liver and adipose tissue crosstalk

José Xavier do Nascimento Júnior1, Júlia da Conceição Gomes1, Ricardo Imbroisi Filho, Helber de Maia Valença, Jéssica Ristow Branco, Amanda Bandeira Araújo, Amanda de Oliveira Esteves Moreira, Letícia Diniz Crepaldi, Larissa Pereira Paixão, Alan C. Ochioni, Thainá M. Demaria, João Gabriel Bernardo Leandro, Livia Marques Casanova, Mauro Sola-Penna, Patricia Zancan

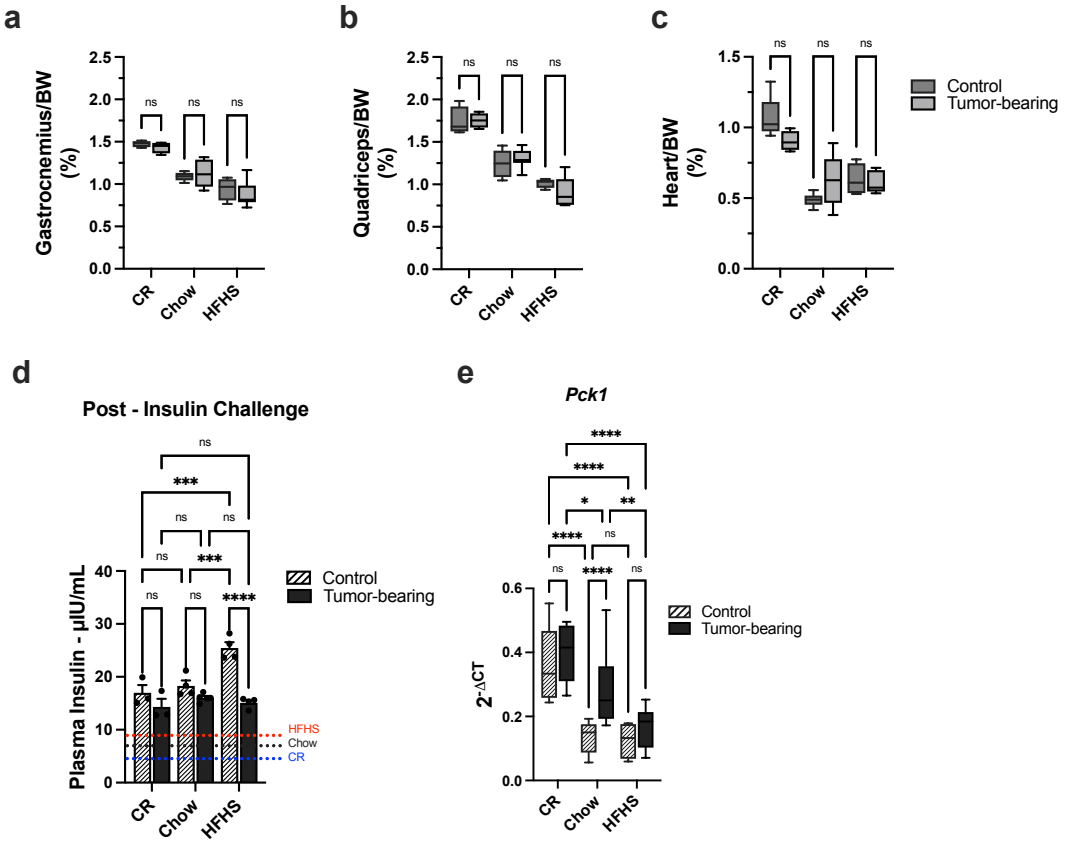

Fig. S1. HFHS diet enhances body weight gain, glucose intolerance, and tumor growth which, in turn, induces weight loss in the HFHS group and glucose intolerance in the Chow group. (a) Gastroc. (b) Quadriceps. (c) Heart-relative weight. (d) Plasma insulin levels after insulin challenge during the euthanasia. Dotted lines indicate fasting insulinemia in tumor-free mice. (e) qPCR analysis of phosphoenolpyruvate carboxykinase 1 (*Pck1*) level in liver samples. Each test was performed with at least nine animals (n = 9–20), and plotted values are mean ± S.E.M. * $P < 0.05$; ** $P < 0.01$; *** $P < 0.001$; **** $P < 0.0001$. For all Panels, a two-way ANOVA was performed, followed by Tukey's post-test.

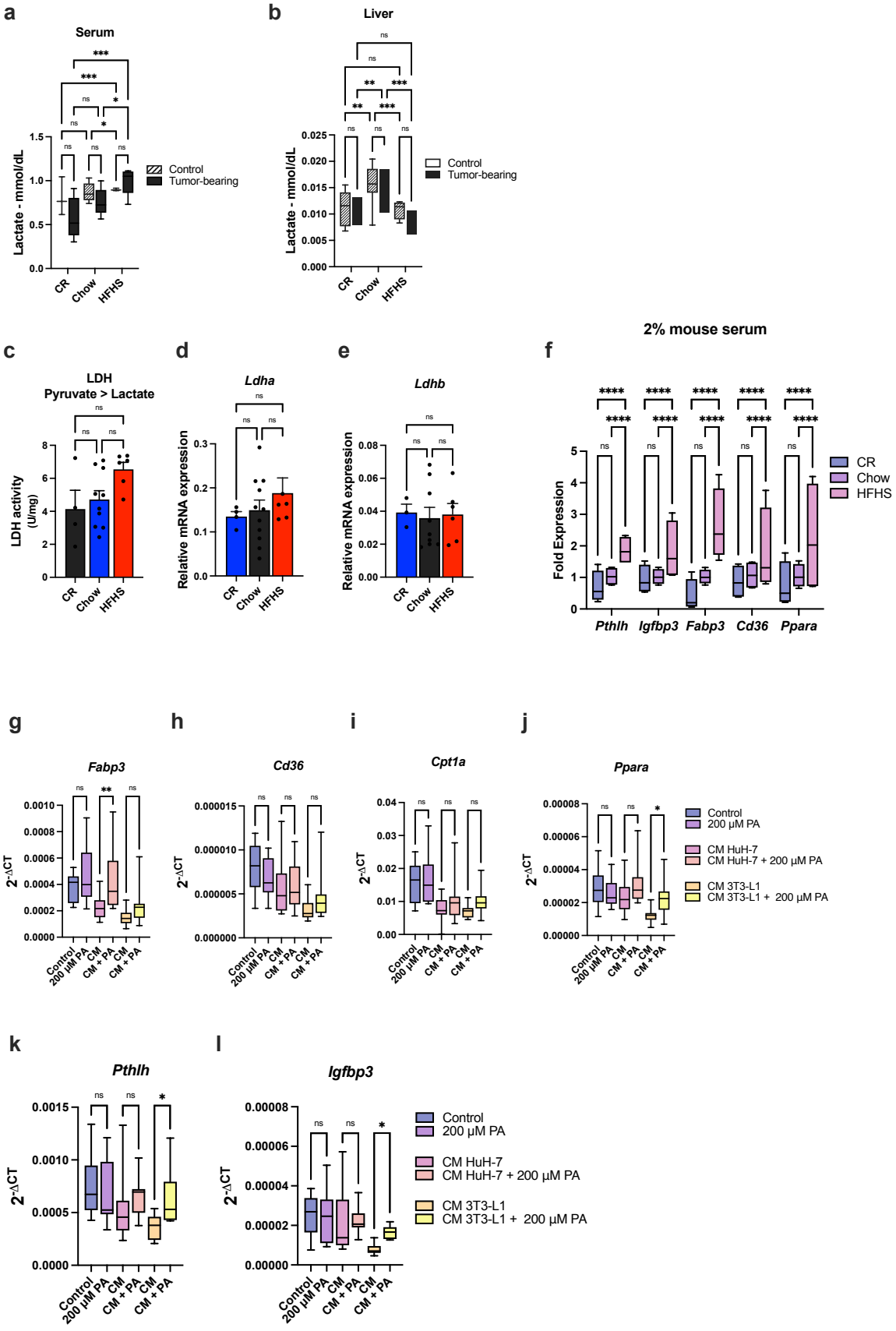
a
Serum
Lactate - mmol/dL
Control
Tumor-bearing
CR
Chow
HFHS
b
Liver
Lactate - mmol/dL
c
LDH
Pyruvate > Lactate
LDH activity (U/mg)
d
Ldha
Relative mRNA expression
e
Ldhb
Relative mRNA expression
f
2% mouse serum
Fold Expression
Pthlh
Igfbp3
Fabp3
Cd36
Ppara
CR
Chow
HFHS
g
Fabp3
h
Cd36
i
Cpt1a
j
Ppara
2-ΔCT
Control
200 µM PA
CM HuH-7
CM HuH-7 + 200 µM PA
CM 3T3-L1
CM 3T3-L1 + 200 µM PA
k
Pthlh
l
Igfbp3

Fig. S2. HFHS improves lipid and glucose metabolism in tumors and increases the expression of disruptors of energy balance. (a) Serum lactate levels. (b) Liver lactate levels measured as described in the Materials and Methods section in all groups. (c) Tumor LDH (Pyruvate to Lactate) activity. (d-e) Tumor *Ldha* (d) and *Ldhb* (e) mRNA expression. (f) qPCR analysis of *Pthlh*, *Igfbp3*, *Fabp3*, *Cd36* and *Ppara* mRNA expression in B16F10 cells treated during 48h with 2% mouse serum from CR, Chow and HFHS mice. (g-l) qPCR analysis of *Fabp3* (g), *Cd36* (h), *Cpt1a* (i), *PPara* (j), *Pthlh* (k) and *Igfbp3* (l) expression in B16F10 cell treated with 200 µM Palmitic acid (PA) or high glucose conditioned media (CM) from HuH7 or 3T3L1 cells incubated (or not) with 200 µM PA during 24h. All liver samples were analyzed. Plotted values are mean ± S.E.M. For all panels, two-way ANOVA was performed, followed by Tukey's post-test. * $P < 0.05$; ** $P < 0.01$; *** $P < 0.001$; **** $P < 0.0001$.

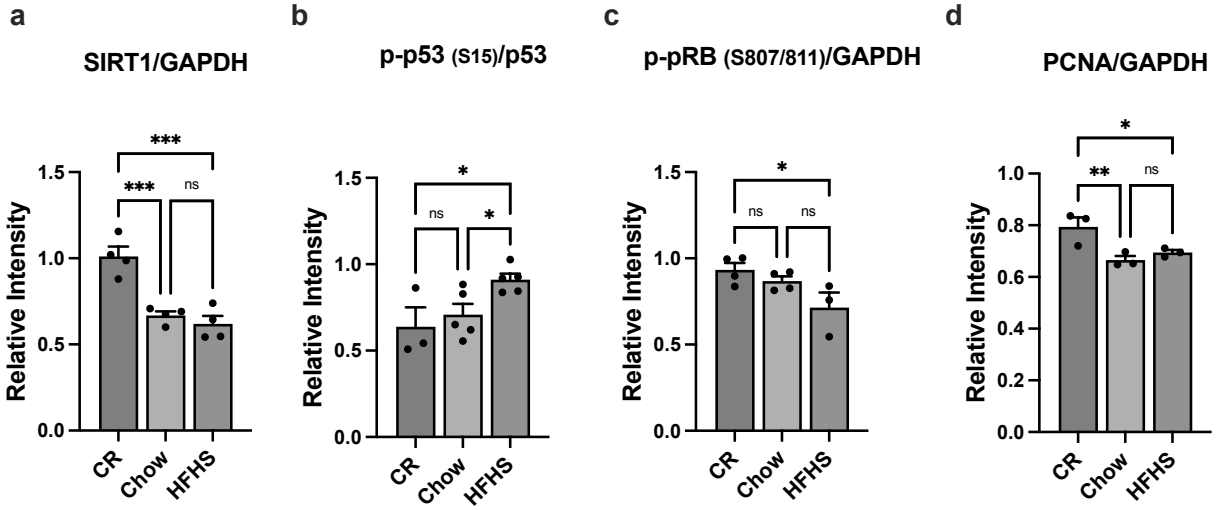

Fig. S3. HFHS diet and tumor growth induce liver senescence, steatosis and fibrosis. (a-d) Western blotting densitometries of (a) SIRT1/GAPDH, (b) p-p53 (S15)/p53, (c) p-pRB (S808/811)/GAPDH, and (d) PCNA/GAPDH. Plotted values are mean ± S.E.M. For all panels, One-way or two-way ANOVA was performed, followed by Tukey's post-test. * $P < 0.05$; ** $P < 0.01$; *** $P < 0.001$; **** $P < 0.0001$.

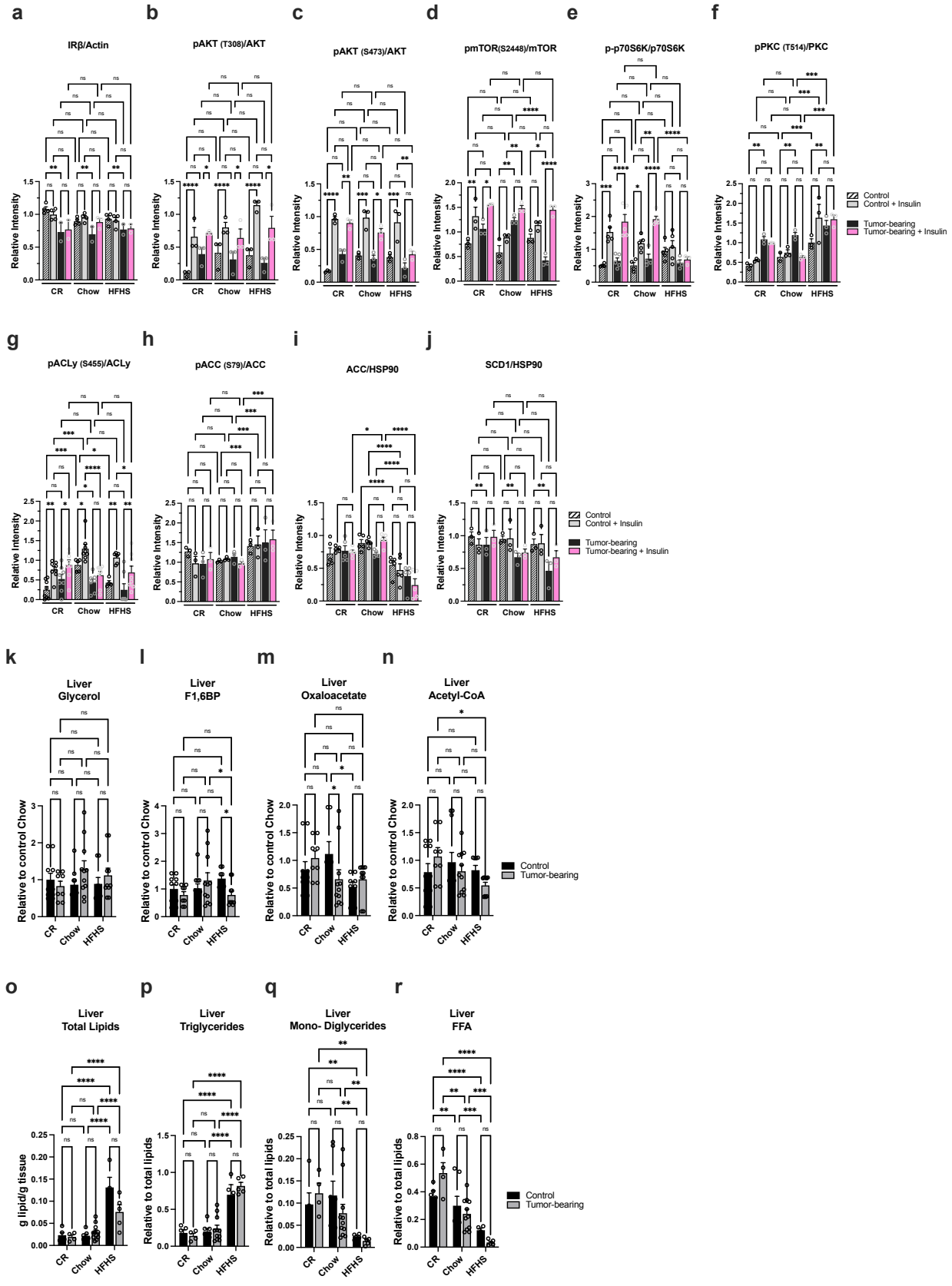
a
IRβ/Actin
b
pAKT (T308)/AKT
c
pAKT (S473)/AKT
d
pmTOR(S2448)/mTOR
e
p-p70S6K/p70S6K
f
pPKC (T514)/PKC
Relative Intensity
CR
Chow
HFHS
Control
Control + Insulin
Tumor-bearing
Tumor-bearing + Insulin
g
pACLy (S455)/ACLy
h
pACC (S79)/ACC
i
ACC/HSP90
j
SCD1/HSP90
k
Liver Glycerol
l
Liver F1,6BP
m
Liver Oxaloacetate
n
Liver Acetyl-CoA
Relative to control Chow
Control
Tumor-bearing
o
Liver Total Lipids
p
Liver Triglycerides
q
Liver Mono- Diglycerides
r
Liver FFA
g lipid/g tissue
Relative to total lipids

Fig. S4. Tumor and diet-induced hepatic insulin resistance, impaired lipid metabolism and liver-WAT crosstalk. (a–e) Western blotting densitometries of hepatic insulin signaling pathway analysis: (a) IRβ/Actin, (b) pAKT (T308)/AKT, (c) pAKT (S473)/AKT, (d) p-mTOR (S2448)/mTOR, and (e) p-p70S6K (T421/S424)/p70S6K. (f) Western blotting densitometries of hepatic pPKC (T514)/PKC. (g–j) Western blotting densitometries of (h) pACLy (S455)/ACLy, (i) pACC (S79)/ACC, (j) ACC/HSP90, and (k) SCD1/HSP90. Band intensities were quantified using ImageJ software (NIH, USA). (k-n) Liver metabolites flux analysis: (k) glycerol, (l) fructose 1,6-bisphosphate (F1,6BP), (m) oxaloacetate, and (n) acetyl-CoA quantification. (o-r) Liver lipids metabolites analysis: (o) total lipids, (p) triglycerides, (q) monoglycerides/diglycerides, and (r) free fat acids (FFA) quantification. The results are depicted as the mean ± SEM. * $P < 0.05$; ** $P < 0.01$; *** $P < 0.001$; **** $P < 0.0001$. For all panels, a two-way ANOVA was performed, followed by Tukey's post-test.

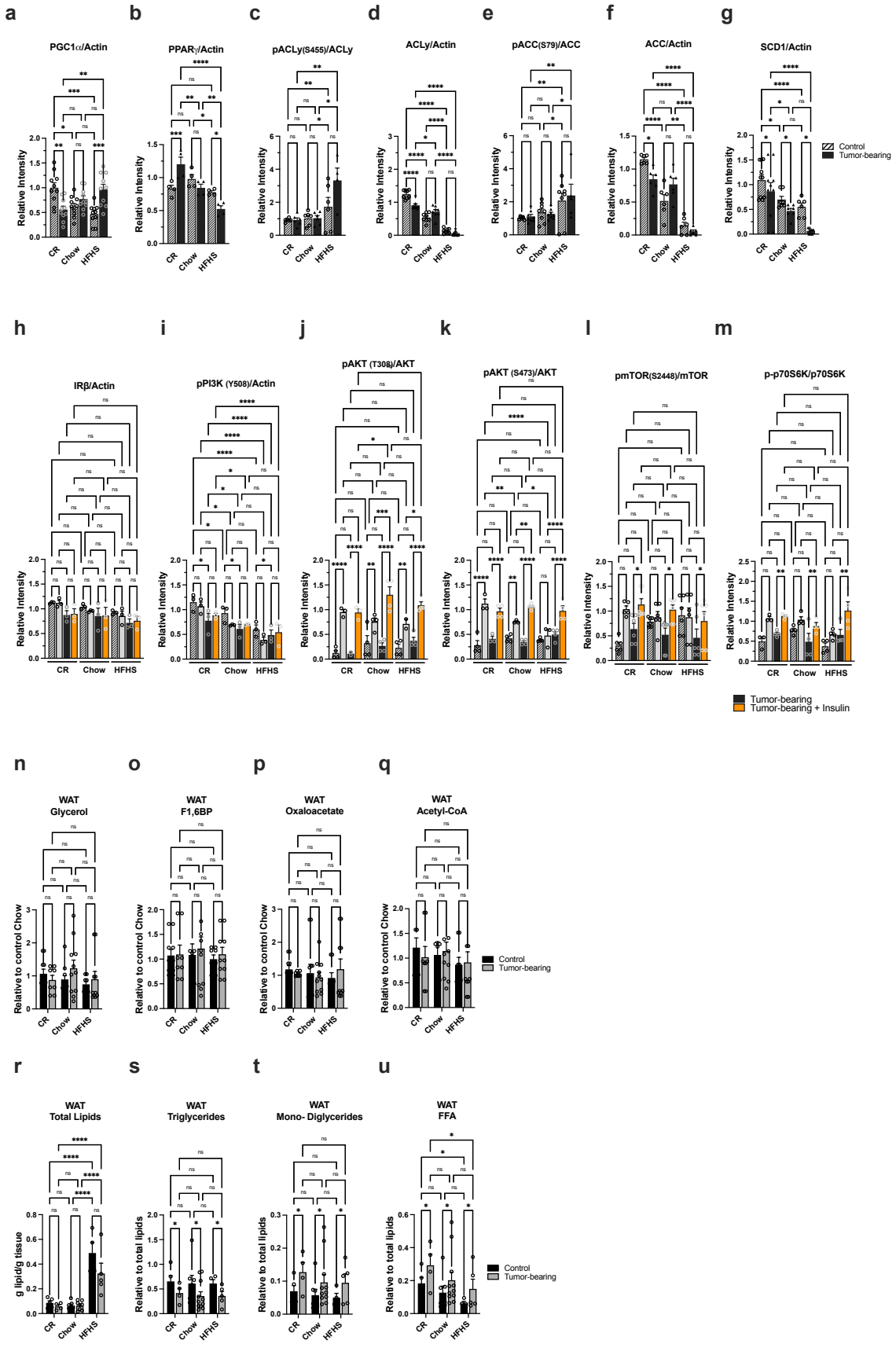
a
PGC1α/Actin
b
PPARγ/Actin
c
pACLy(S455)/ACLy
d
ACLy/Actin
e
pACC(S79)/ACC
f
ACC/Actin
g
SCD1/Actin
Relative Intensity
CR
Chow
HFHS
Control
Tumor-bearing
h
IRβ/Actin
i
pPI3K (Y508)/Actin
j
pAKT (T308)/AKT
k
pAKT (S473)/AKT
l
pmTOR(S2448)/mTOR
m
p-p70S6K/p70S6K
Tumor-bearing
Tumor-bearing + Insulin
n
WAT Glycerol
o
WAT F1,6BP
p
WAT Oxaloacetate
q
WAT Acetyl-CoA
Relative to control Chow
r
WAT Total Lipids
s
WAT Triglycerides
t
WAT Mono- Diglycerides
u
WAT FFA
g lipid/g tissue
Relative to total lipids

Fig. S5. Tumor growth induces browning and reverts insulin resistance in WAT from HFHS-fed mice. (a–g) Western blotting densitometries of lipid and metabolic regulation in gWAT: (a) PGC1α/Actin, (b) PPARγ/Actin, (c) pACLy (S455)/ACLy, (d) ACLy/Actin, (e) pACC (S79)/ACC, (f) ACC/Actin, and (g) SCD1/Actin. (h–m) Western blotting densitometries of gWAT insulin signaling pathway analysis: (h) IRβ/Actin, (i) pPI3K (Y508)/Actin, (j) pAKT (T308)/AKT, (k) pAKT (S473)/AKT, (l) pmTOR (S2448)/mTOR, and (m) p-p70S6K (T421/S424)/p70S6K. Band intensities were quantified using ImageJ software (NIH, USA). (n-q) WAT metabolites flux analysis: (n) glycerol, (o) fructose 1,6-bisphosphate (F1,6BP), (p) oxaloacetate, and (q) acetyl-CoA quantification. (r-u) WAT lipids metabolites analysis: (r) total lipids, (s) triglycerides, (t) monoglycerides/diglycerides, and (u) free fat acids (FFA) quantification. The results are presented as the mean ± SEM and represent three independent experiments (n = 3). * $P < 0.05$; ** $P < 0.01$; *** $P < 0.001$; **** $P < 0.0001$. For all panels, a two-way ANOVA was performed, followed by Tukey's post-test.

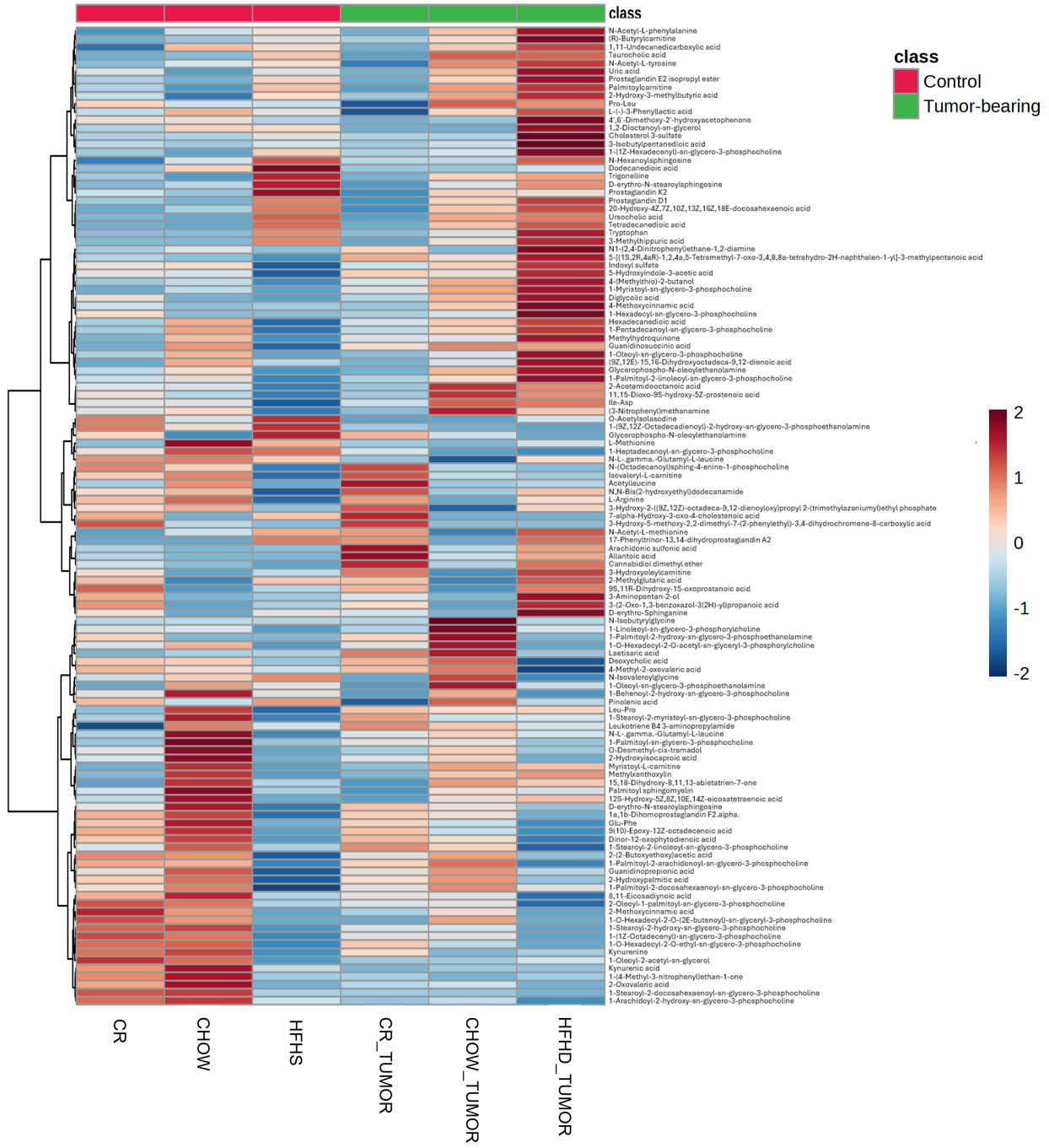

Fig. S6. Heat map analysis of identified differential serum metabolites from NMR based metabolomics. Each row represents the ion intensity of a metabolite. Each column shows the metabolic patterns of mice control groups: CR, Chow and HFHS, or tumor-bearing groups: CR_Tumor, Chow_Tumor and HFHS_Tumor. The red color of the tile indicates high abundance and blue indicates low abundance of metabolites.

Table S1. Primary antibodies used for Western Blotting

Antigen	Host	Dilution	Manufacturer	Catalogue number
β-*Actin*	Rabbit	1:1000	Cell Signaling	#4967
ACC	Rabbit	1:1000	Cell Signaling	#3662
p-ACC (S79)	Rabbit	1:1000	Cell Signaling	#3661
ACLy	Rabbit	1:10000	Abcam	ab40793
p-ACLy (S455)	Rabbit	1:5000	Abcam	ab46796
AKT	Rabbit	1:1000	Cell Signaling	#9272
p-AKT (S473)	Rabbit	1:1000	Cell Signaling	#9271
p-AKT (T308)	Rabbit	1:1000	Cell Signaling	#9275
eEF2	Rabbit	1:1000	Cell Signaling	#2332
GAPDH	Rabbit	1:5000	Sigma-Aldrich	G9545
HSP90	Rabbit	1:1000	SCBT	sc-7947
IKKα	Rabbit	1:1000	Cell Signaling	#2682
p-IKKα/β (S176/180)	Rabbit	1:1000	Cell Signaling	#2697
IR-β	Rabbit	1:1000	SCBT	sc-711
mTOR	Rabbit	1:1000	Cell Signaling	#2972
p-mTOR (S2448)	Rabbit	1:1000	Cell Signaling	#2971
Nos2 (iNOS)	Rabbit	1:1000	Cloud-Clone Corp	PAA837Mu01
p53	Mouse	1:1000	SCBT	sc-99
p-p53 (S15)	Rabbit	1:1000	Cell Signaling	#9284
p70S6K	Rabbit	1:1000	Cell Signaling	#9202
p-p70S6K (T421/S424)	Rabbit	1:1000	Cell Signaling	#9204
PCNA	Mouse	1:2000	Cell Signaling	#2586
p-PI3K (Y508)	Goat	1:1000	SCBT	sc-12929
PKC	Mouse	1:1000	SCBT	Sc-8393
p-PKC (T514)	Rabbit	1:1000	Cell Signaling	#9379
PGC1a	Goat	1:1000	SCBT	sc-5816

PPARγ	Rabbit	1:1000	Cell Signaling	#2443
p-Rb (S807/811)	Rabbit	1:1000	Cell Signaling	#9308
SCD1	Rabbit	1:1000	Cell Signaling	#2794
SIRT1	Rabbit	1:1000	SCBT	sc-15404
TLR4	Rabbit	1:500	Cloud-Clone Corp	PAA753Mu01
TNFα	Mouse	1:1000	Abcam	ab1793

Table S2 **Primers used for quantitative RT-PCR**

Gene	Protein	Primer sequence		Amplicon length (bp)
		Forward	Reverse	
Acadl	Acyl-Coenzyme A dehydrogenase	GTAGCTTATGAATGTGTGCAACTC	GTCTTGCGATCAGCTCTTTCATTA	139
Actb	β-Actin	TGAACCCTAAGGCCAACC	CACAATGCCTGTGGTACG	128
Adipoq	Adiponectin	GACTAATGAGACCTGGCCACT	AGTAGCATCCTGAGCCCTTTT	89
Apob	Apolipoprotein B	TACTTCCACCCACAGTCCCCT	CCTTAGAAGCCTTGGGCACAT	166
Cd36	CD36	AGAATTCTCAGCTGCTCCGC	CACATTTCAGAAGGCAGCAAC	137
Cdkn1a	P21 (cyclin dependent kinase inhibitor 1A)	CAGCAGAATAAAAGGTGCCACAGG	CGGAACAGGTCGGACATCAC	61
Cdkn2a	P16 (cyclin dependent kinase inhibitor 2A)	GCGCTCTGGCTTTCGTGAAC	GTTGCCCATCATCATCACCTGG	96
Cpt1a	Carnitine O-palmitoyltransferase 1	TGGACCCAAATTGCAGTGGT	CTCCCACCAGTCACTCACATAA	73
Emr1 (F4/80)	Adhesion G protein-coupled receptor E1	CCGTCAGGTACGGGATGAAT	AGAAGTCTGGGAATGGGAGC	73
Fabp3	Fatty acid bindind protein 3	CGGAAGGTCAAGTCACTGGT	TTCCCGTCAACTAGCTCCCT	104
Fasn	Fatty acid synthase	CCATGGCAGCTGTTGGTTTG	GTGTCCTCAGAGTTGTGGCA	88
Fgf21	Fibroblast growth factor 21	AGCTCTCTATGGATCGCCTC	CACAGGTCCCCAGGATGTTG	163
Hprt1	Hypoxanthine phosphoribosyltransferase 1	CCCTGGTTAAGCAGTACAGCCCC	AGTCTGGCCTGTATCCAACACTTCG	90
Igfbp3	Insulin-like growth factor binding protein 3	CTCAAAGCACAGACACCCAGA	GCGGCAGGGACCGTATT	68
Il6	Interleukin-6	TCGTGGAAATGAGAAAAGAGTTGT	ACTCCAGAAGACCAGAGGAAA	174
Krt18	Keratin 18	GTGGATGCCCCCAAATCTCA	CCTCAATCTGCTGAGACCAGT	121
Ldha	lactate dehydrogenase A	TGGGGTTGGTGCTGTTGGA	GGAAGAGGCTGCCATGCTGA	137
Ldhb	lactate dehydrogenase B	TCAGCGTGGCTGACCTCATCG	AGGATGCACGGGAGACTGAGGA	124
Mmp9	Matrix metalloproteinase-9	GCGTCATTCGCGTGGATAAG	AGGCTTTGTCTTGGTACTGGA	78
Pck1	Phosphoenolpyruvate carboxykinase 1	GCAGAACACAAGGGCAAGAT	TTGTAGCCGAAGAAGGGTCG	65
Pnpla2	ATGL	CCAGACTCAATGAGGCCCTG	CGCACTGGTAGCATGTTGG	82
Ppara	PPAR-alpha	GCAACAACCCGCCTTTTGTC	TTGGCCACAAGCGTCTTCTC	70
Ppargc1a	PGC-1alpha	CTTGGAACTGCAGGCCTAA	CAAGAGGGCTTCAGCTTTGG	95
Ppia	Peptidylprolyl isomerase A	CAGACGCCACTGTCGCTTT	TGTCTTTGGAACTTTGTCTGCAA	133
Prdm16	PR domain containing 16	CGAGATGAACCAGGCATCCA	GTCTTGGATCTCAGGCCGTT	52
Pthlh	Parathyroid hormone-like peptide	TTTTTGCCTGTGCGGTTTGAG	CTGGCTCTGGGGACTTGTGTAG	69

Scd1	Stearoyl-Coenzyme A desaturase 1	CACCTGCCTCTTCGGGATTTT	GGCCCATTCGTACACGTCA	166
Tert	Telomerase reverse transcriptase	TGCAGTCTGTGTTTCGGAGA	CGTAAAAGCAACCCATCCCG	71
Tgfb1	Transforming growth fator beta 1	TACCAACTATTGCTTCAGCTCCAC	CCAACCCAGGTCCTTCCTAAA	82
Tnfa	Tumor necrosis fator-alpha	TGAGAAGTTCCCAAATGGCCT	CCACTTGGTGGTTTGTGAGTG	74
Ucp1	Uncoupling protein 1	ACTGCCACACCTCCAGTCATT	CTTTGCCTCACTCAGGATTGG	123
Vim	Vimentin	TCCTCTGGTTGACACCCACT	TGATCACCTGTCCATCTCTGGT	74
Xbp1s	X-box binding protein 1	GAGTCCGCAGCAGGTG	GTGTCAGAGTCCATGGGA	65

S7. Metabolomic analysis of animal serum pools

Sample preparation

In a 2 mL centrifuge tube (Eppendorf), 50 µL of serum and 100 µL of ice-cold methanol with internal standard (p-fluoro-DL-phenylalanine and furosemide, final concentration of 2.5 µg/mL) were added. The mixture was homogenized by vortexing for 10 s, followed by an ultrasound bath with ice for 10 min and homogenized again for 10 s. Subsequently, the samples were incubated at -20 °C for 15 min for protein precipitation, followed by centrifugation at 10,000 xg for 15 min. In a new tube, the supernatant (120 µL) was collected and dried in a Turbovap equipment in a water bath at 45 °C and N2 gas pressure regulated at 7 psi for approximately 30 min. The dried extract was reconstituted in 60 µL of injection solvent (methanol:water, 1:1) with internal standard (Caffeine, final concentration of 1 µg/mL) and vortexed for 10 s. For solubilization, the reconstituted samples were placed in an ultrasonic bath for 5 min and centrifuged again at 10,000 x g for 5 min. Finally, an aliquot (50 µL) was collected in a 2 mL vial with a 150 µL insert. Prior to analysis, 5 µL of each sample was collected and mixed in a vial to create a quality control (QC) solution, which was analyzed at the beginning and at periodic intervals throughout the injection list.

Description of the high-resolution mass spectrometry system

Liquid chromatograph

Thermo Dionex Ultimate 3000 coupled to the high-resolution and mass-accuracy mass spectrometer Thermo QExactive Plus with electrospray ionization source operating in positive and negative analysis modes. General ionization source conditions: Sheath gas and auxiliary gas: 45 and 15 arbitrary units, respectively; spray voltage: + or - 3600 V; S-lens voltage: 50 V; capillary temperature: 300 °C; source temperature: 400 °C. Chromatographic conditions: Separation was achieved using a Thermo Scientific® Hypersil Gold C18 column (50 x 2.1 mm x 1.9 µm particle diameter) maintained at 40 °C at a flow rate of 0.350 mL/min of mobile phase and injection of 5 µL of sample. The mobile phases (FM) were: (FM A) ultrapure water with 0.1% formic acid and 5 mM ammonium formate, and (FM B) methanol with 0.1% formic acid. The chromatographic separation was performed using the gradient elution mode: 0-1.0 min 15% B; 1.0-10.0 min 100% B; 10.0-15.0 min 100% B; 15.0-15.1 min 15% B; 15.1-20.0 min 15% B.

Mass spectrometry experiments

Data acquisitions were performed in full scan mode in the m/z range 100-1000 using a resolution of 35,000 FWHM (Full Width at Half Maximum), AGC 1e6 and IT 100ms, combined with the data dependent acquisition (DDA, from English Data Dependent Analysis; ddMS2 TOP 3) experiment using a resolution of 17,500 FWHW, AGC 1e5, IT 50 ms; NCE 15-35% and isolation window of 1.2 Da.

Data processing

The processing of the raw .RAW files obtained from the analyses by Liquid Chromatography coupled to High Resolution Mass Spectrometry (LC-EMAR) was performed in the MS-DIAL software (RIKEN, version 4.9) for the extraction of the detected signals, spectral deconvolution and peak alignments. The parameters used in the processing were: tolerance for MS1 of 0.005 Da and MS2 of 0.05 Da; minimum peak height of 1.0E6; mass width of 0.05 Da; sigma value of the deconvolution window of 0.5; and tolerance for alignment of 0.3 min and 0.005 Da. A sample blank (extraction solvent) was used to subtract interfering signals. For the putative annotation of the main metabolites, the experimental MS/MS spectra were compared with data from a laboratory spectral library that combined the Mass Bank of North America public library and the commercial NIST MSMS 2020, considering a similarity level between the spectra greater than 80%. An error of less than 8 ppm was also considered for similarity between the experimental and theoretical m/z values. The detected ions were exported to Excel (Microsoft Office 2016) to obtain a data matrix table. Inconsistent data were filtered based on i) the coefficient of variation (CV) of the signal areas detected in the quality controls (pooled QC, a mixture of samples and analyzed at periodic intervals throughout the injection list), where variables with CV > 30% were removed; and ii) by evaluating the chromatographic peaks (Gaussian profile) obtained in all samples.

S8. Uncropped blot/gels

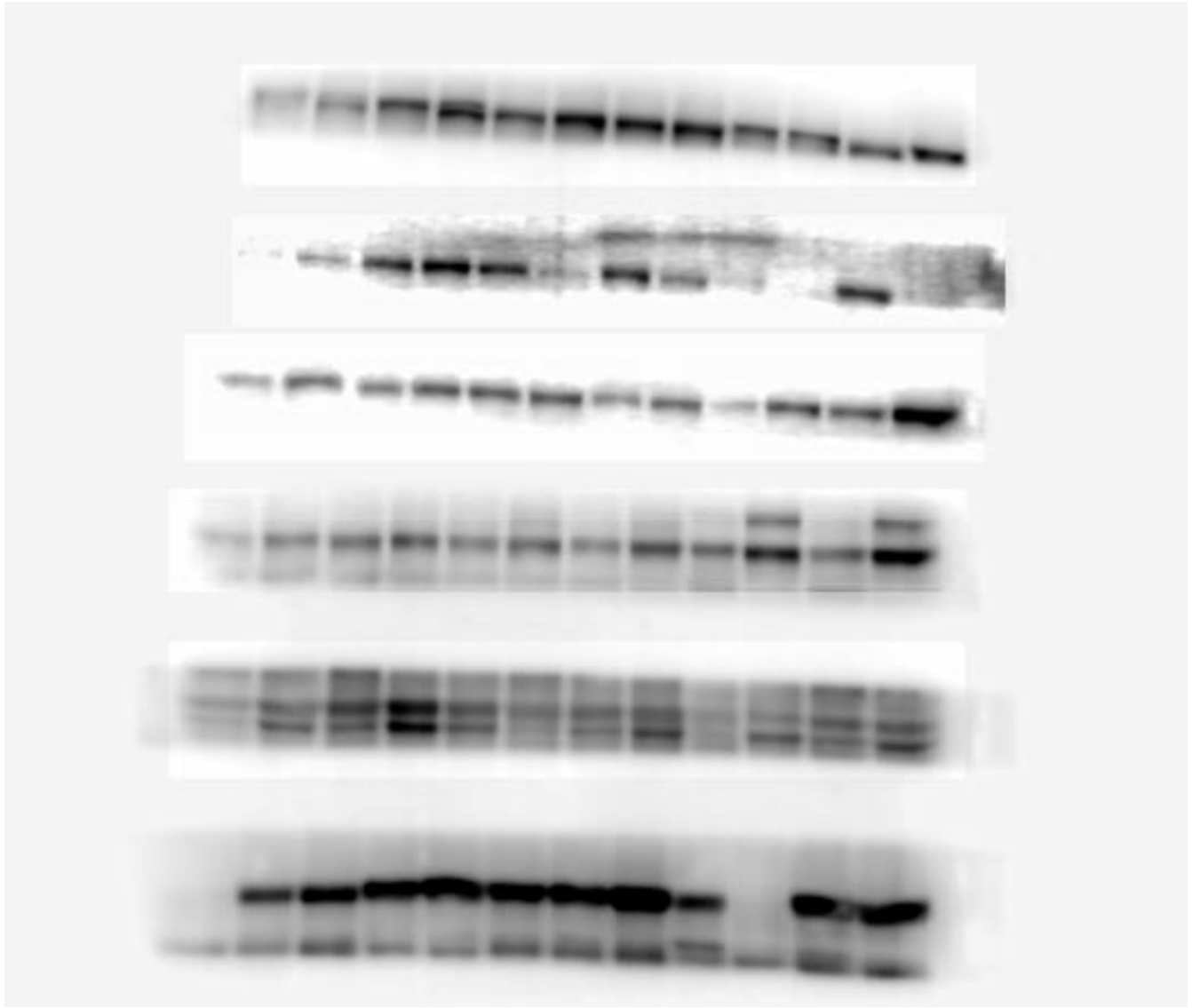
mTOR
p-ACLy
PGC1a
p-p70S6K
p-ERK
p-S6

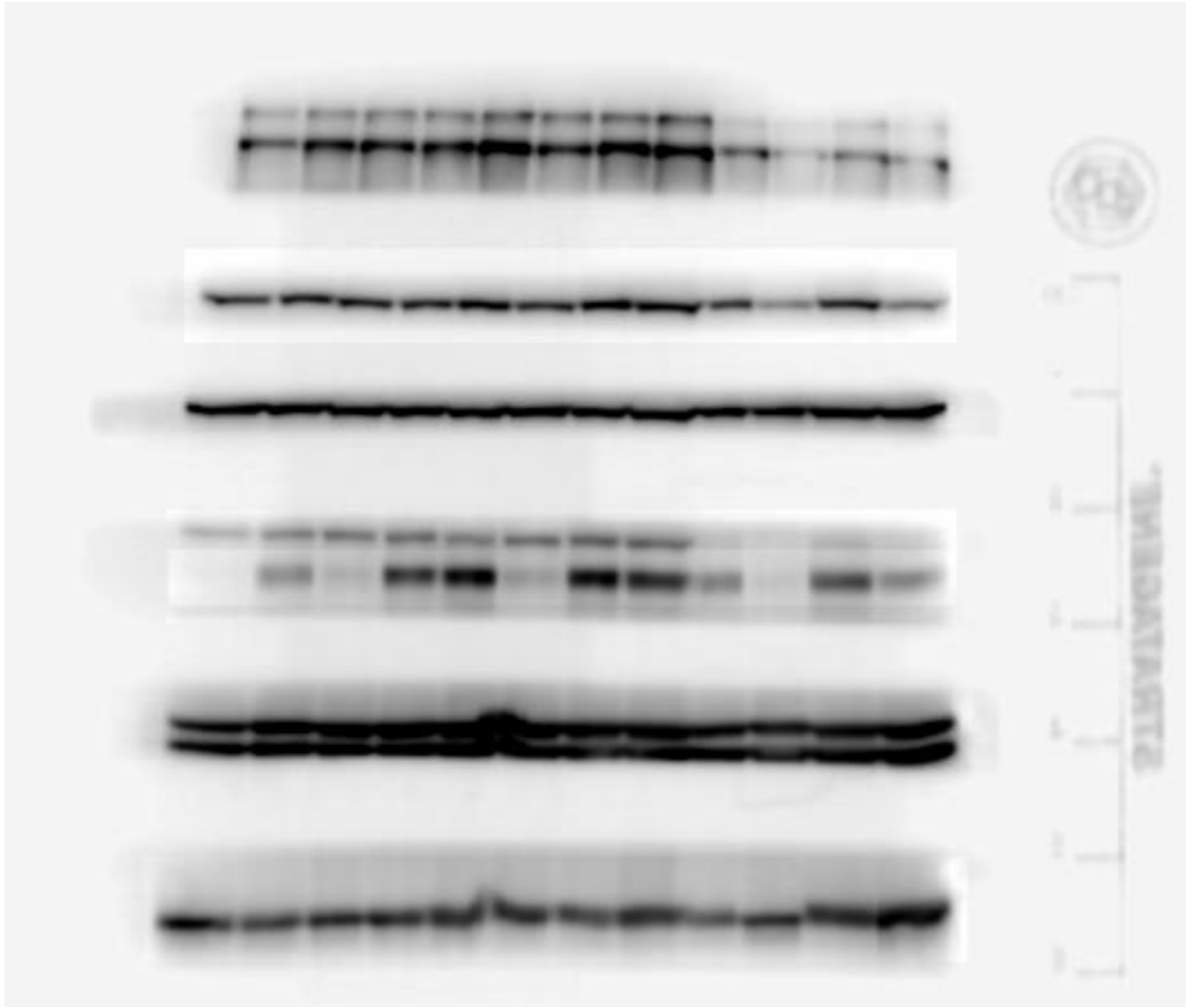
p-ACC
ACLy
eEF2
p-p70S6K
ERK
S6

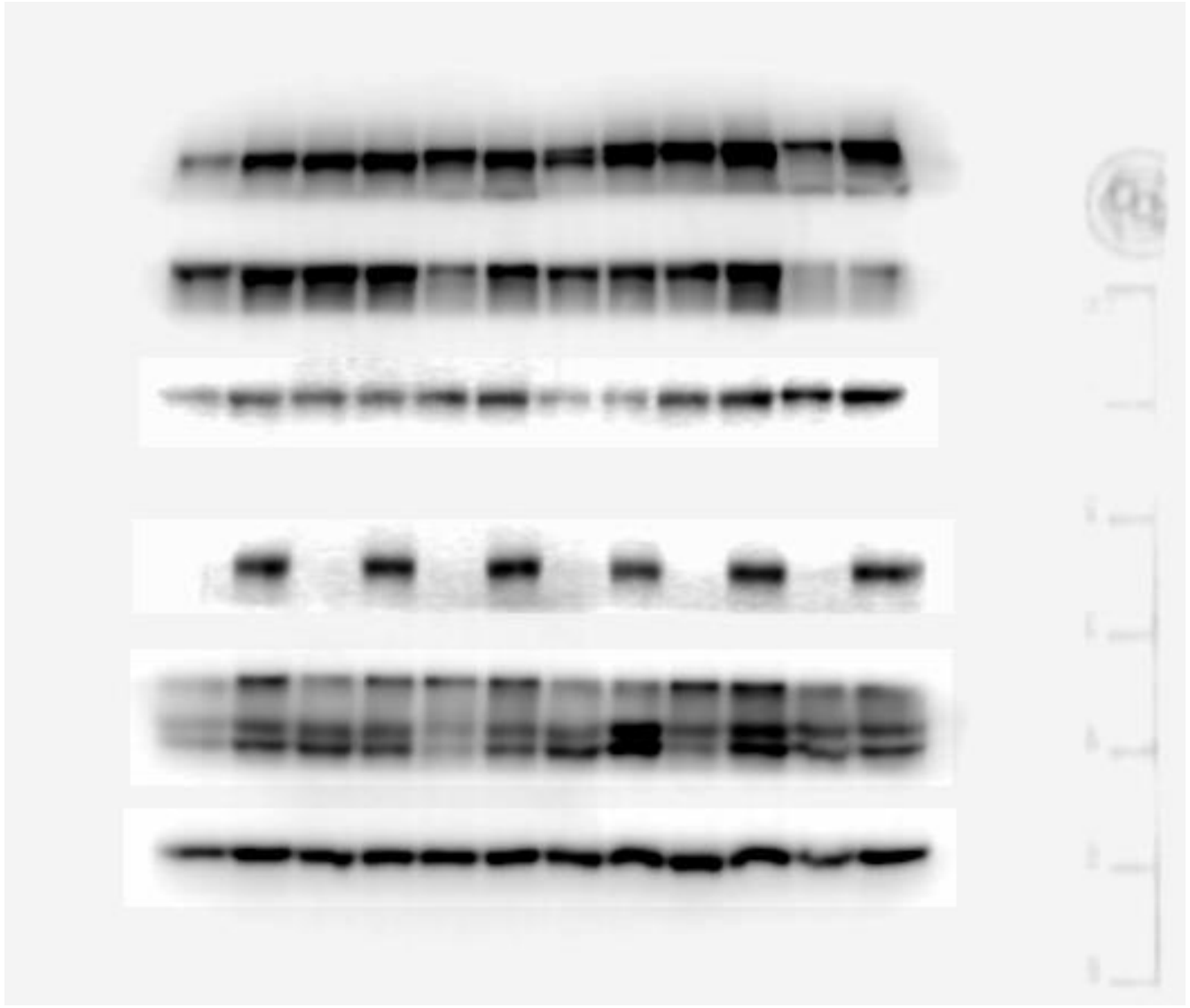
p-mTOR
ACLy
eEF2
p-AKTthr – FIG4A
p-ERK
GAPDH

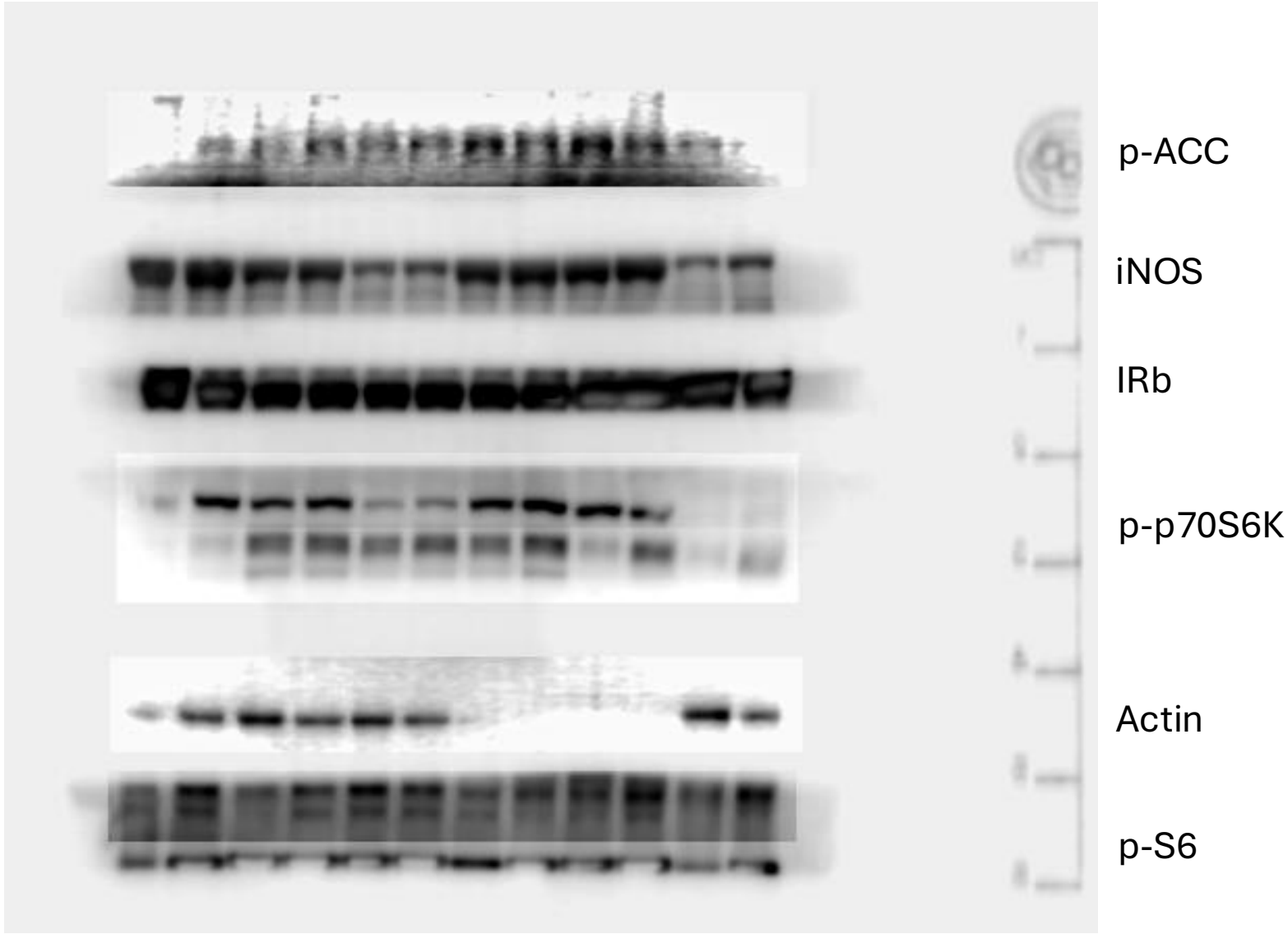
p-ACC
iNOS
IRb
p-p70S6K
Actin
p-S6

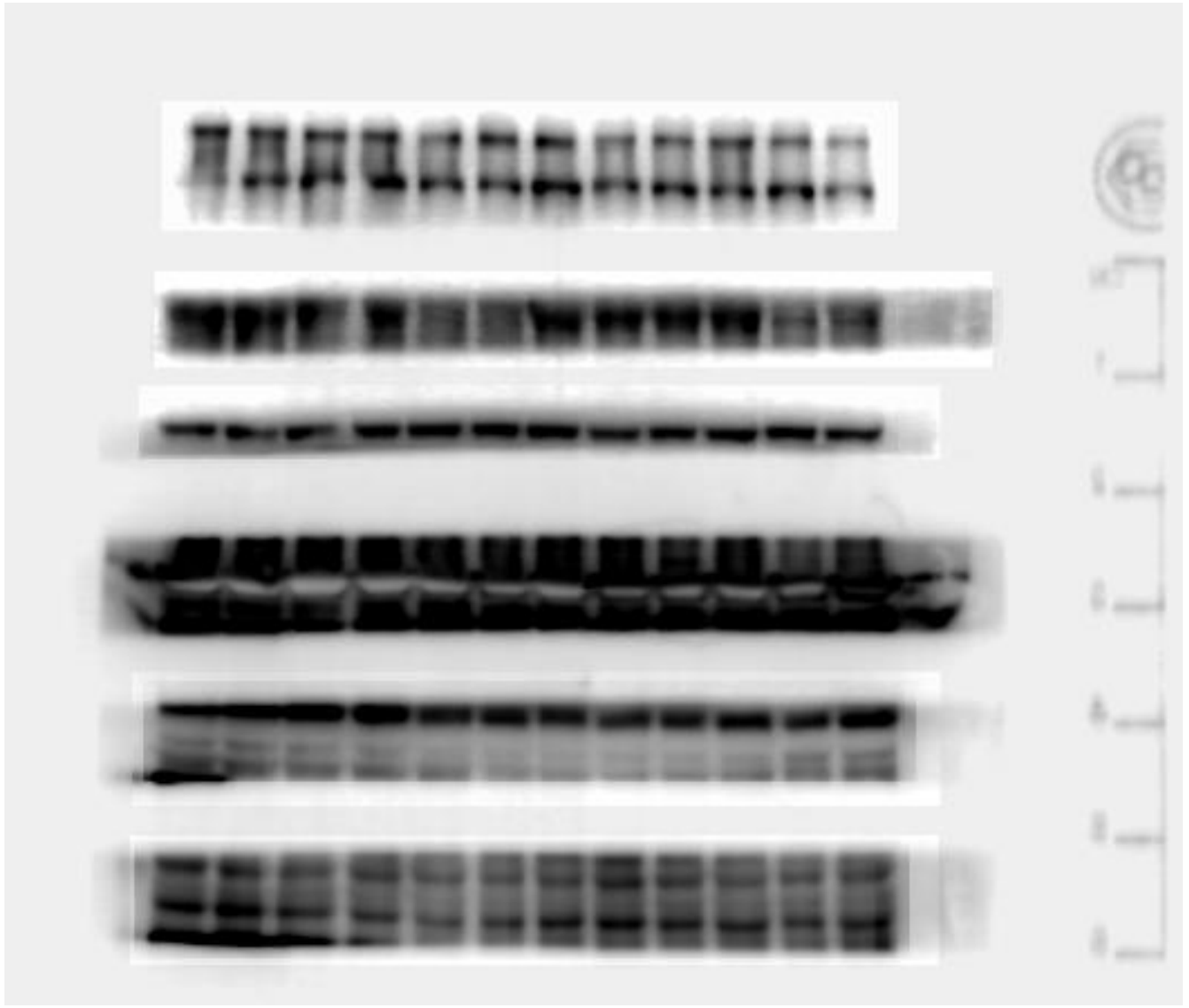
ACC
PGC1a
eEF2
SDHa
Arg1
SDHb

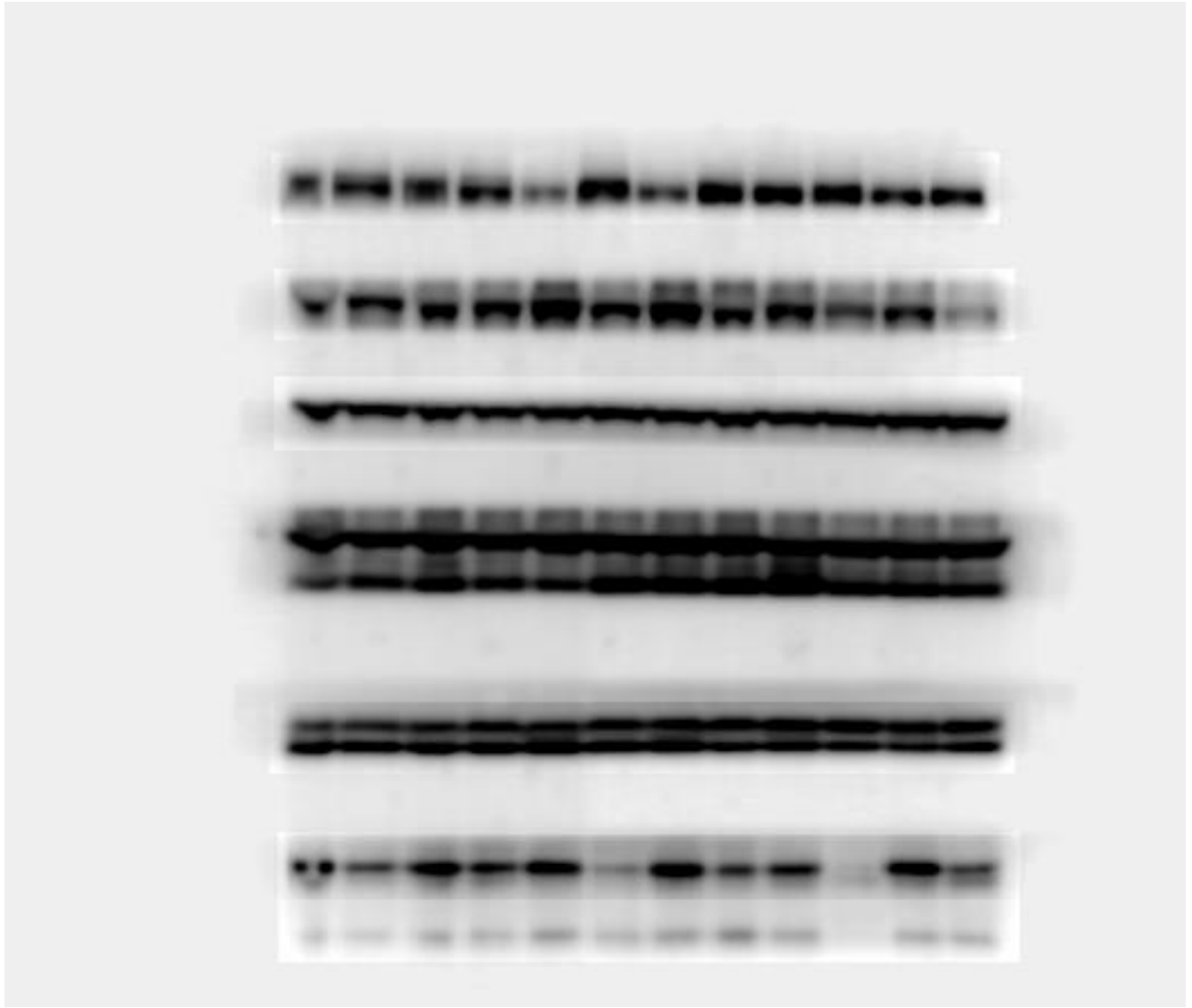
mTOR
ACLy
eEF2
SDHa
ERK
SCD1

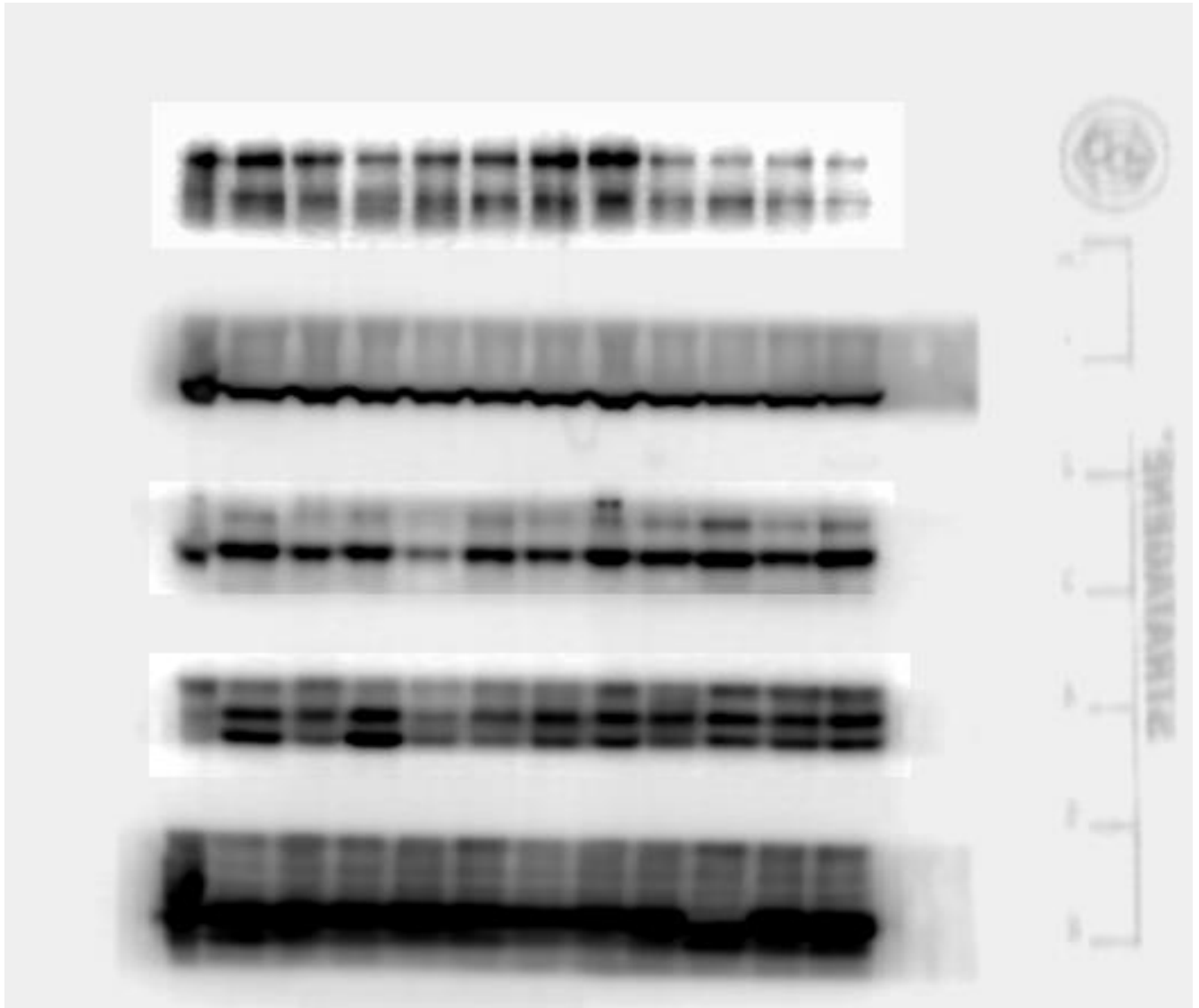
ACC
PGC1a
p70S6K
p-ERK
S6

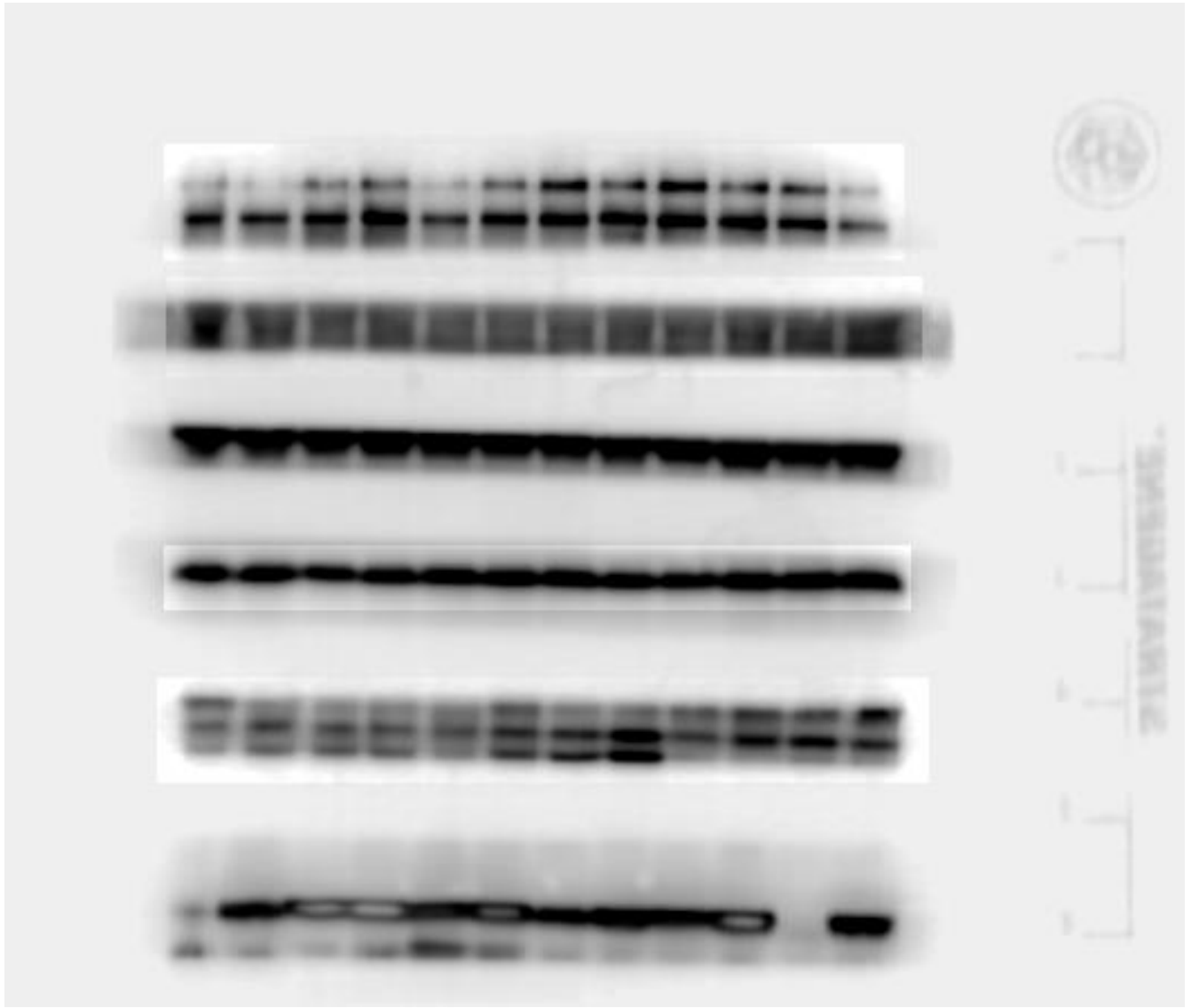
p-ACC
PGC1a
IRb
AKT
p-ERK
p-S6

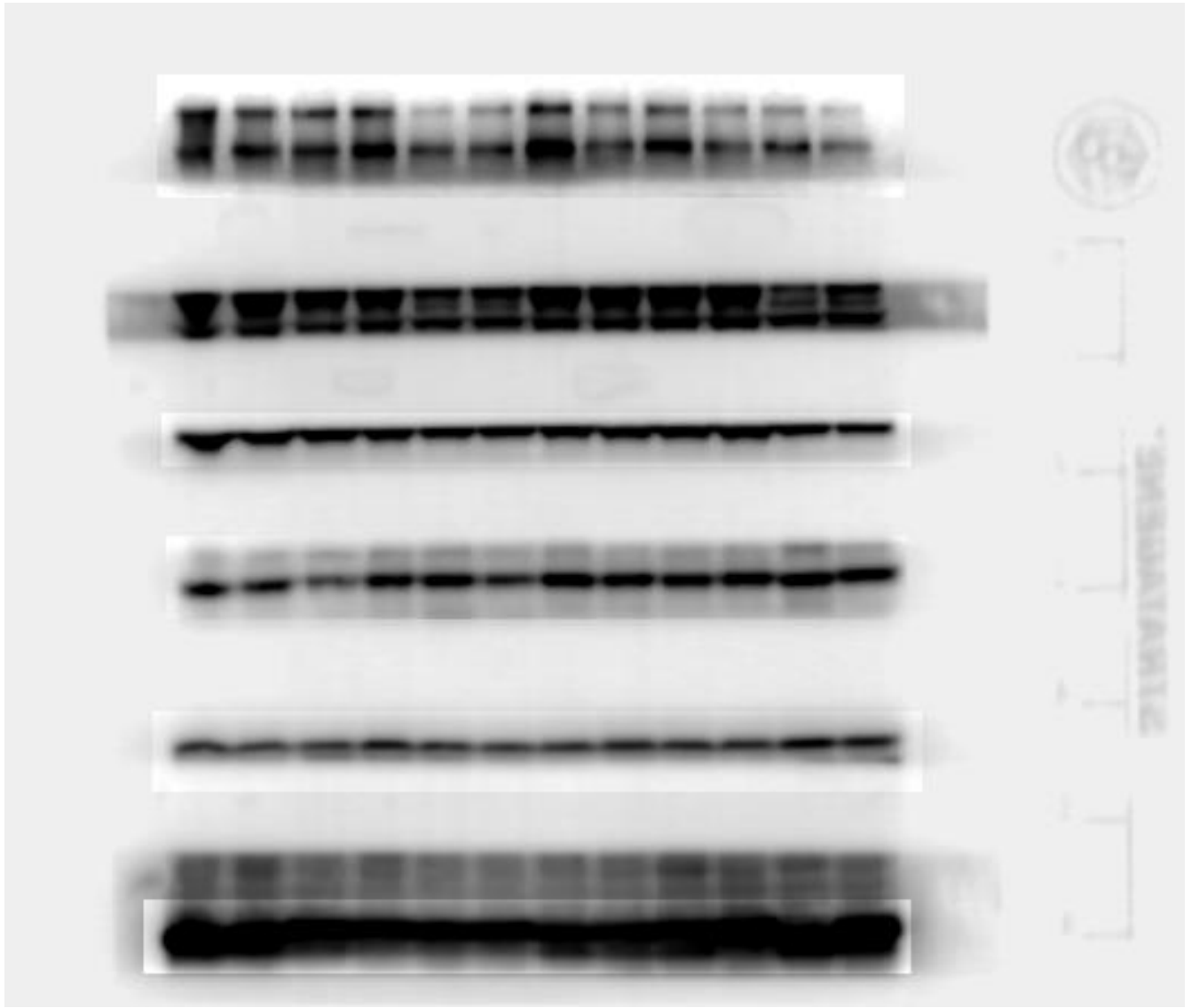
ACC
TLR4
eEF2
p70S6K
ERK
S6

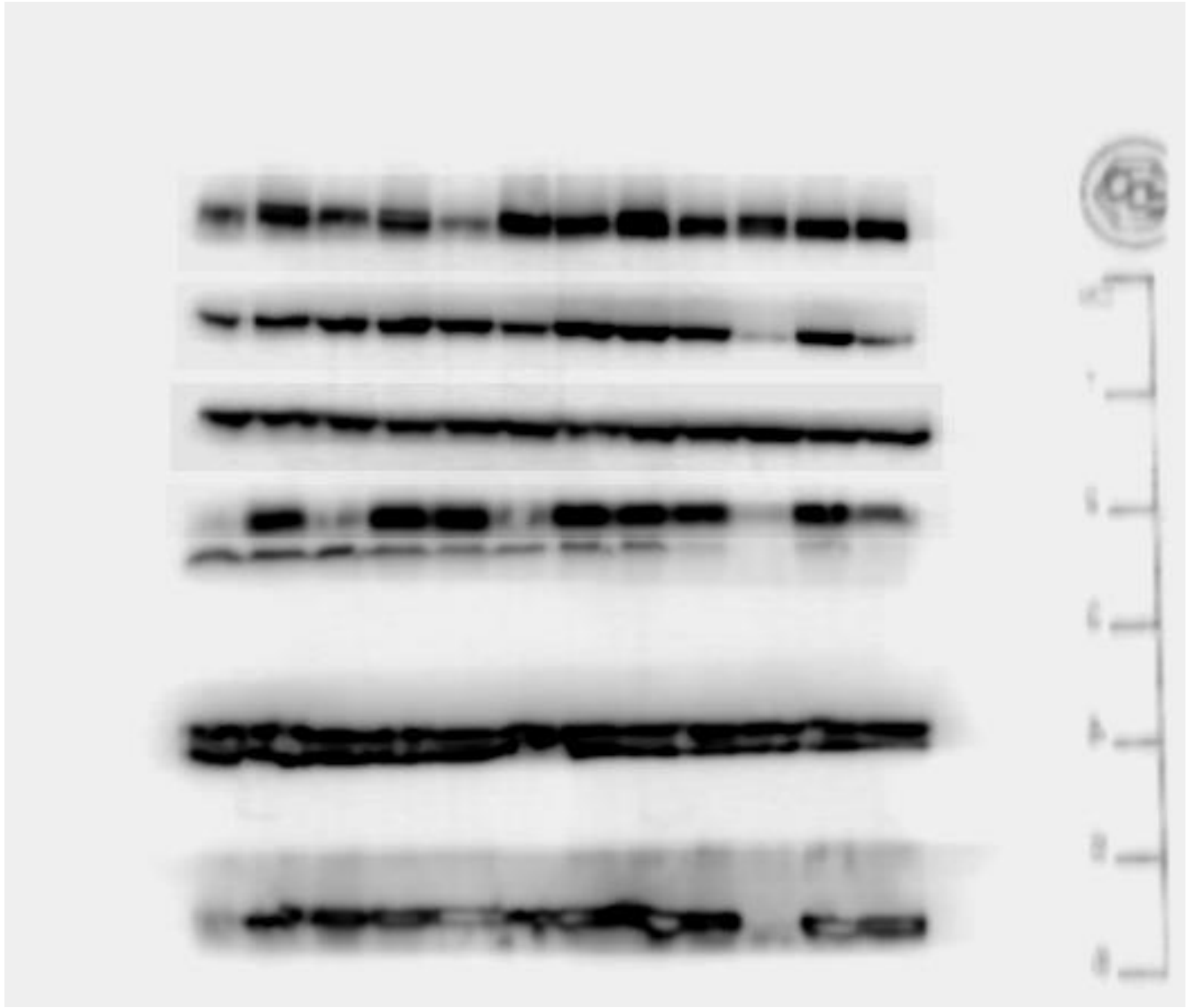
p-mTOR
p-ACLy
eEF2
p-p70S6K
p-ERK
p-S6

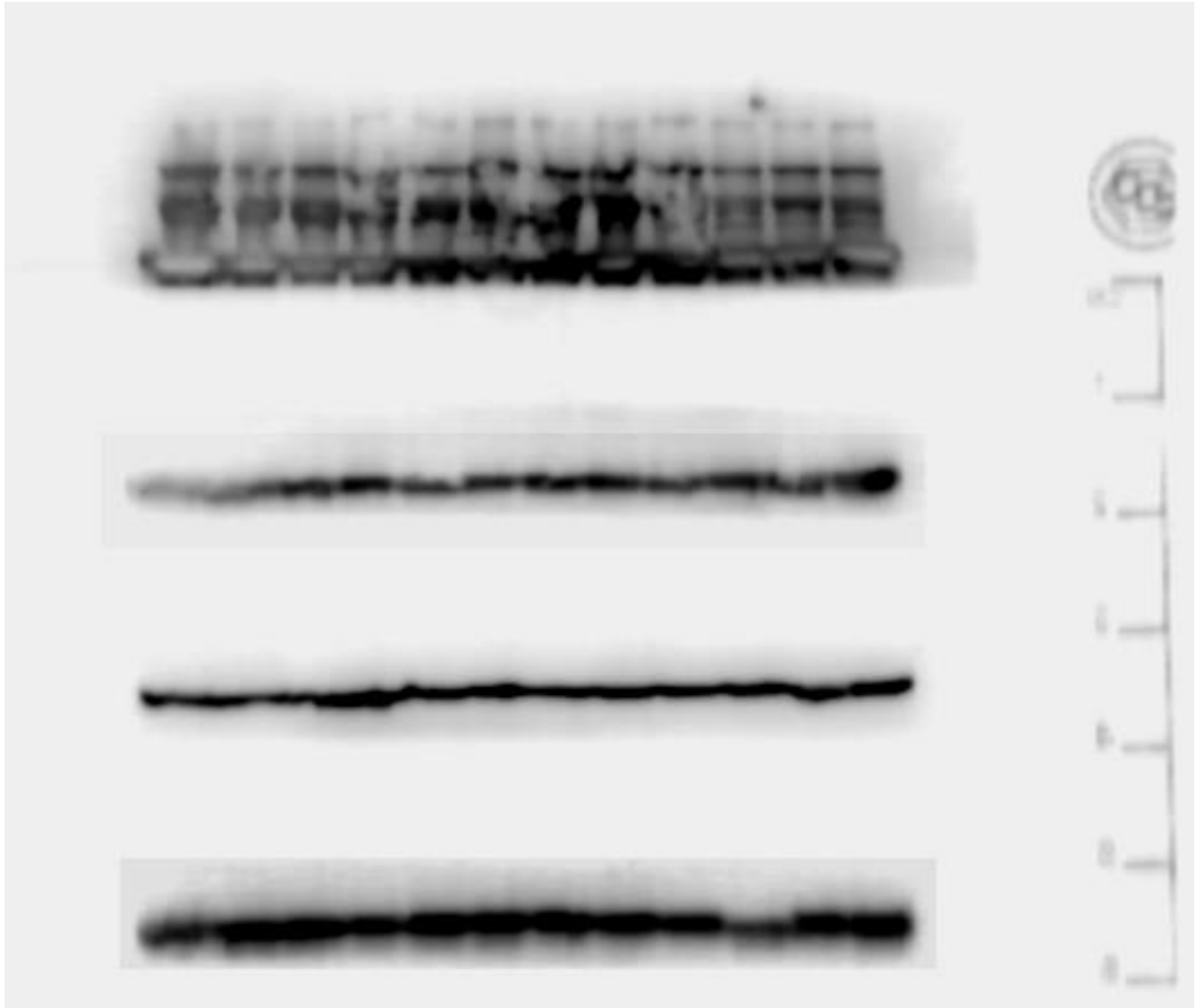
IRb
AKT
Actin
S6

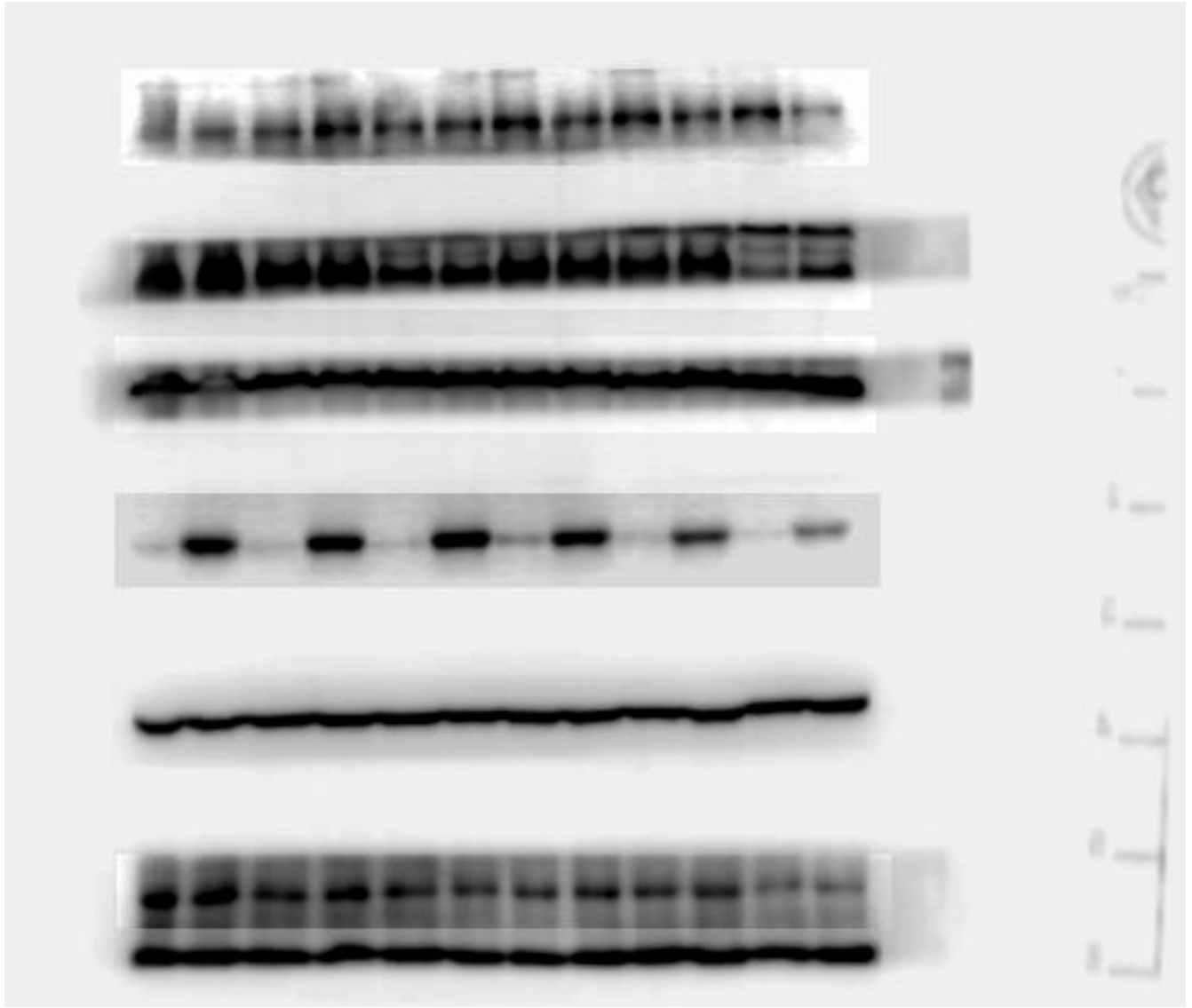
TLR4
PGC1a
p-AKTser – FIG4A
Actin
SDHb

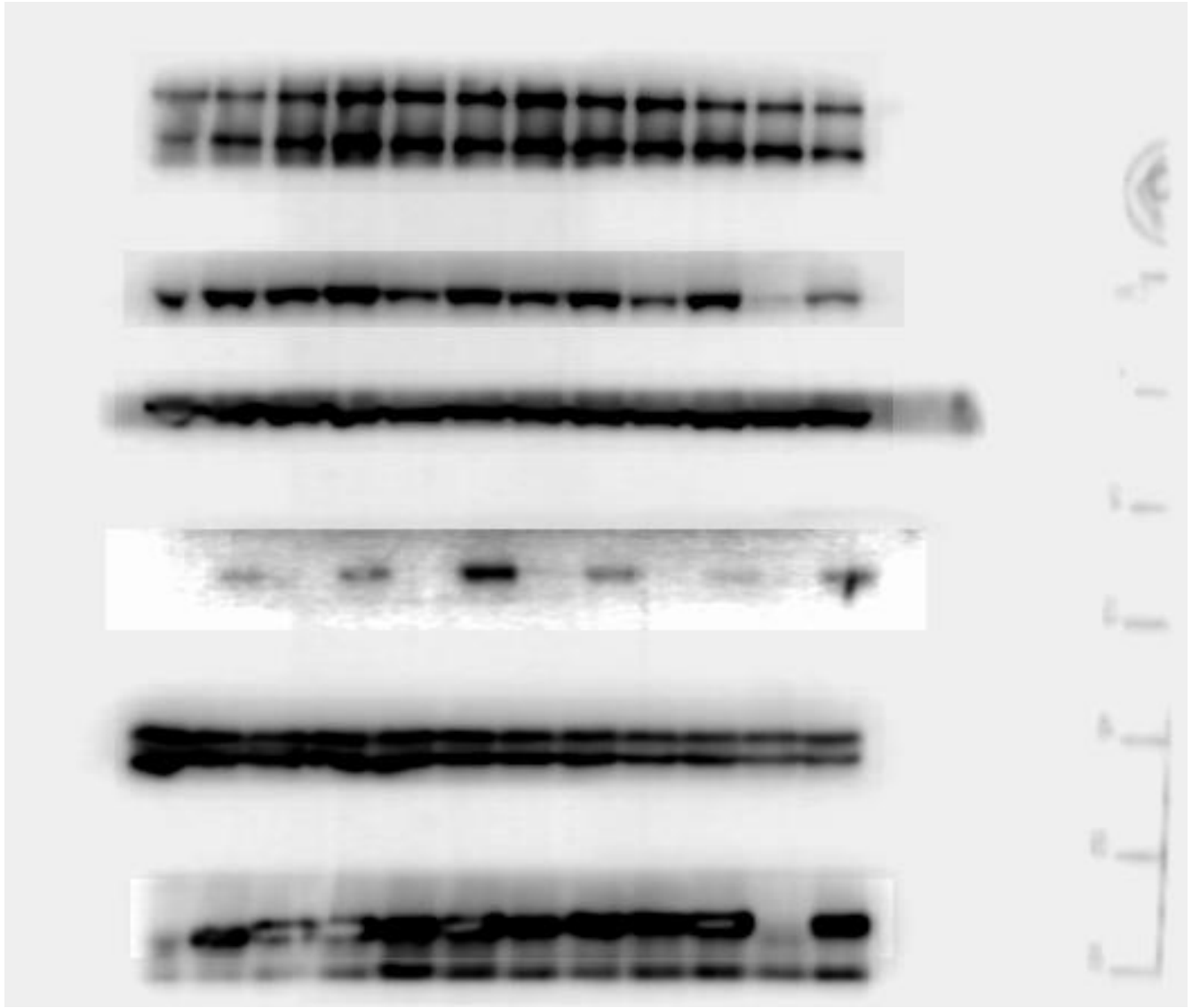
p-ACC
p-ACLy
PGC1a
p-AKTthr
p-ERK
p-S6

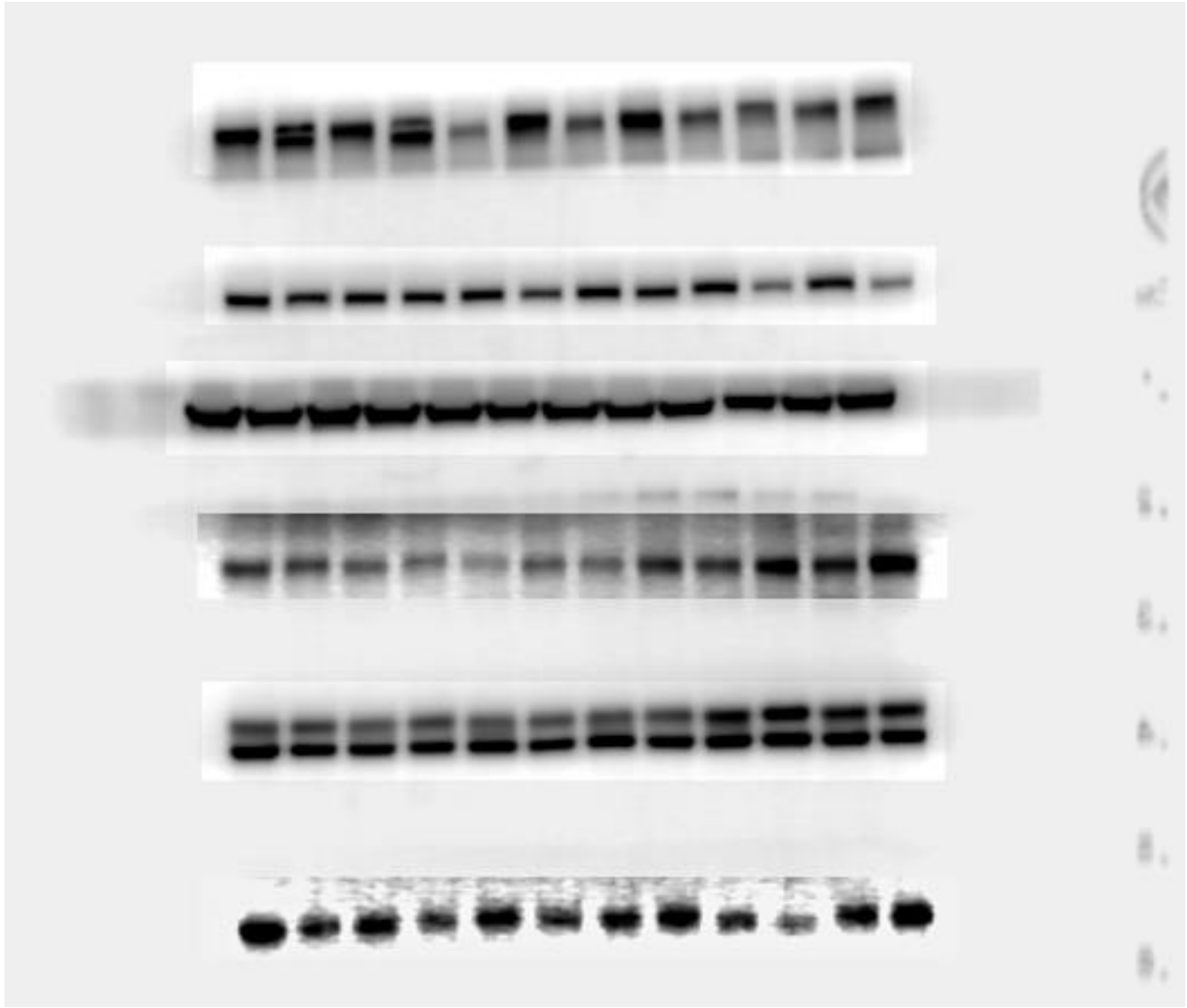
mTOR
ACLy
PGC1a
p70S6K
ERK
S6

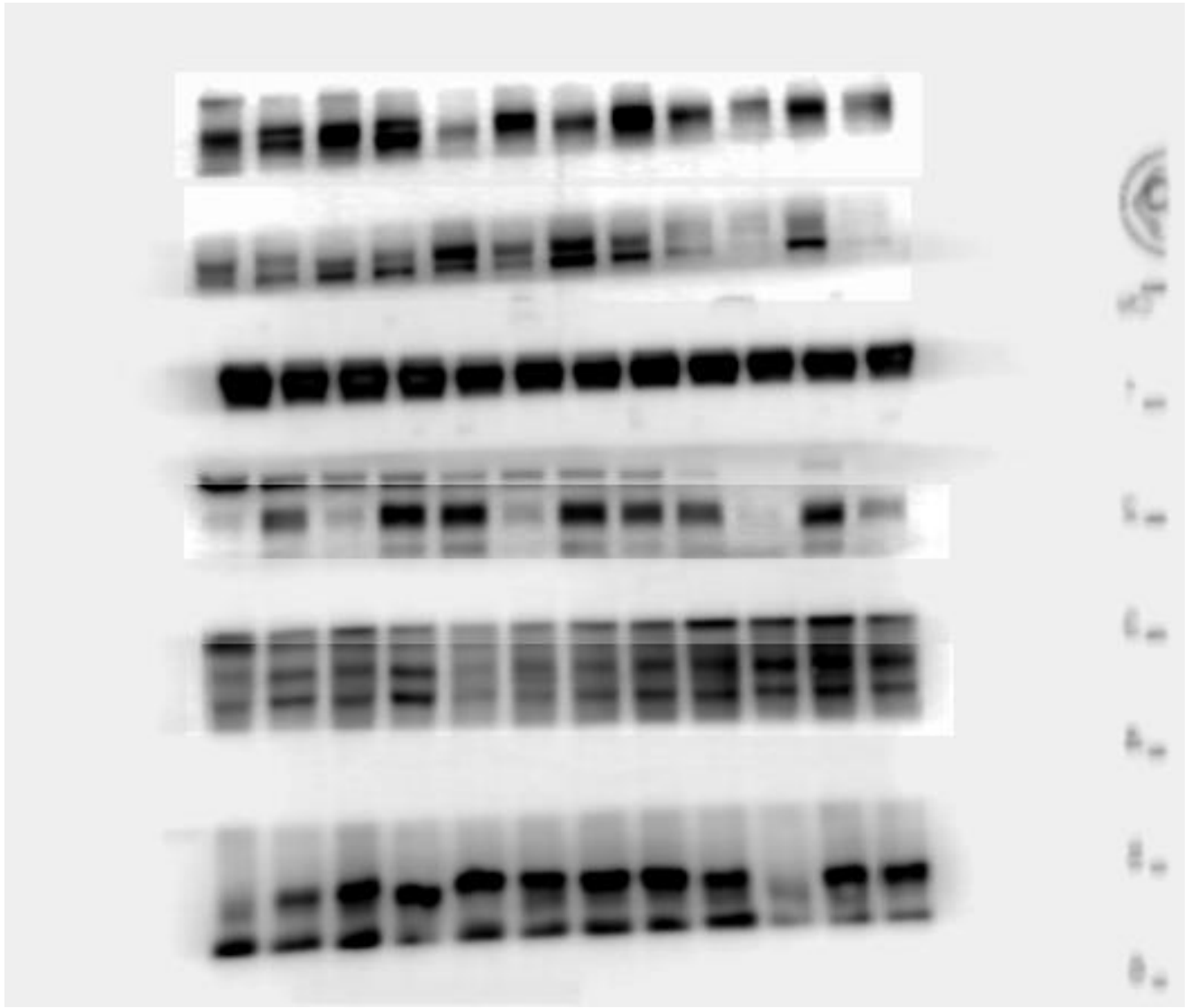
p-mTOR
p-ACLy
IRb
p-p70S6K
p-ERK
p-S6

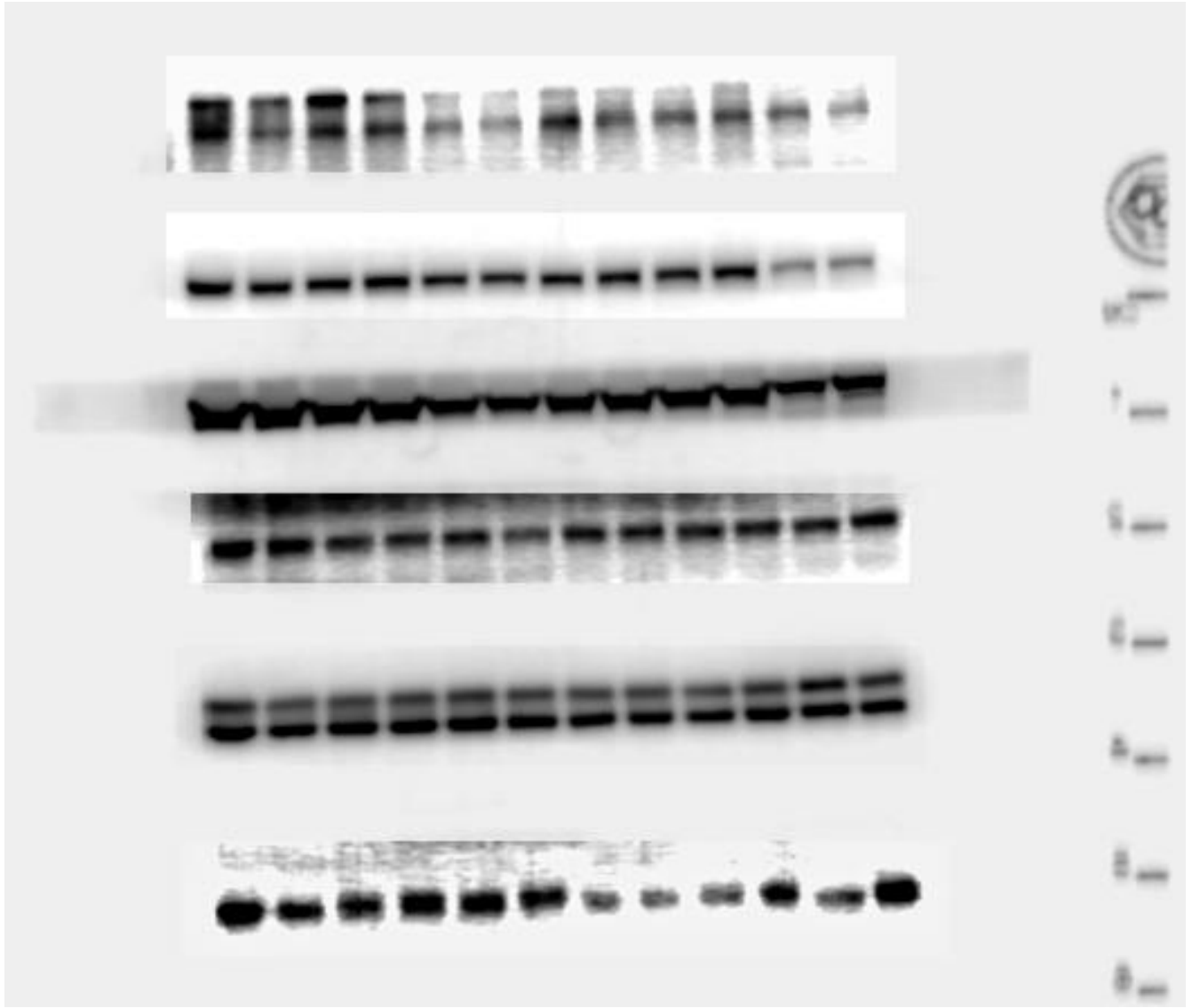
ACC
ACLy
PGC1a
p70S6K – FIG4A
ERK
S6

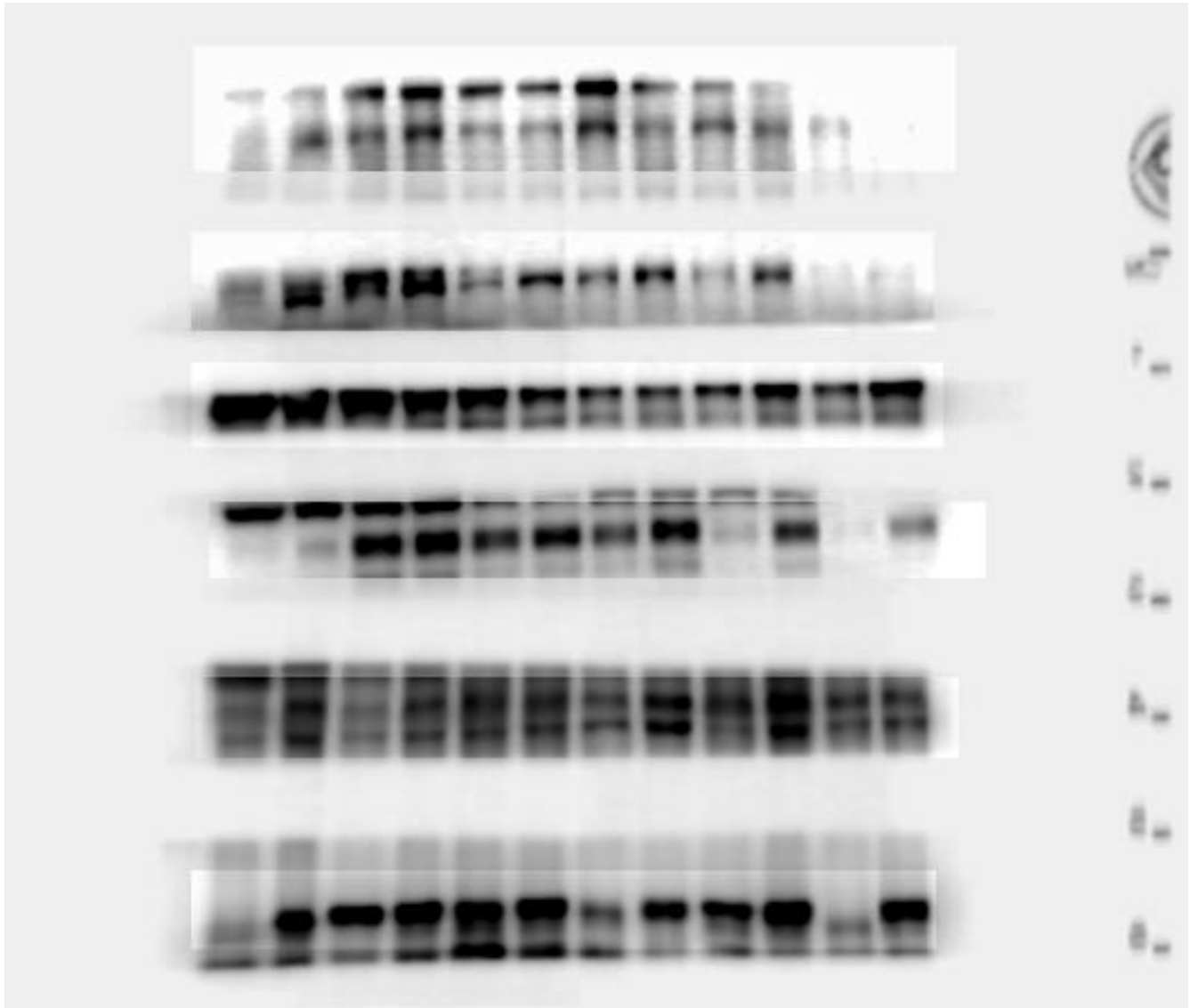
p-ACC
p-ACLy
IR
p-p70S6K – FIG4A
p-ERK
p-S6

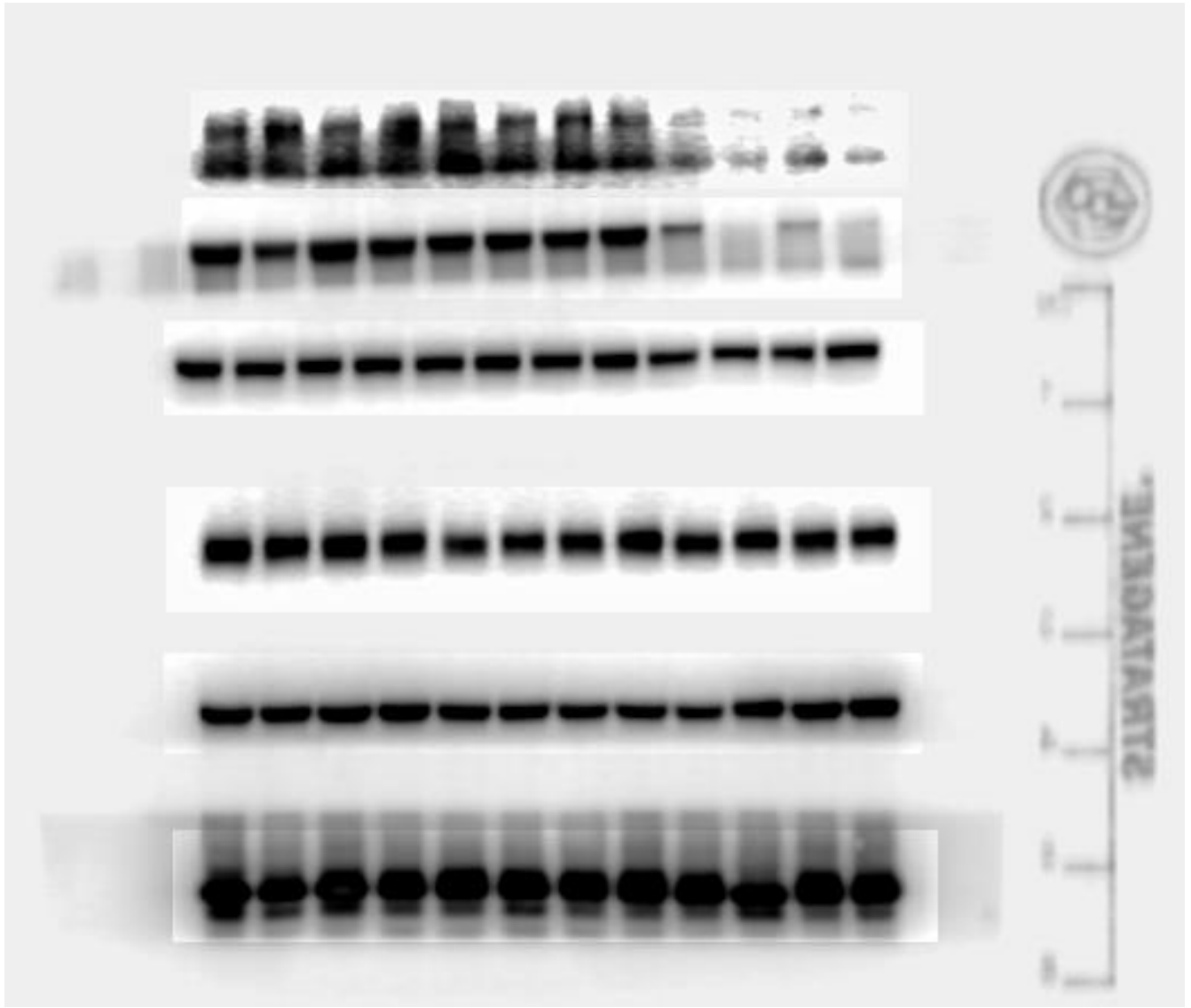
p-ACC
iNOS
eEF2
AKT
Actin
S6

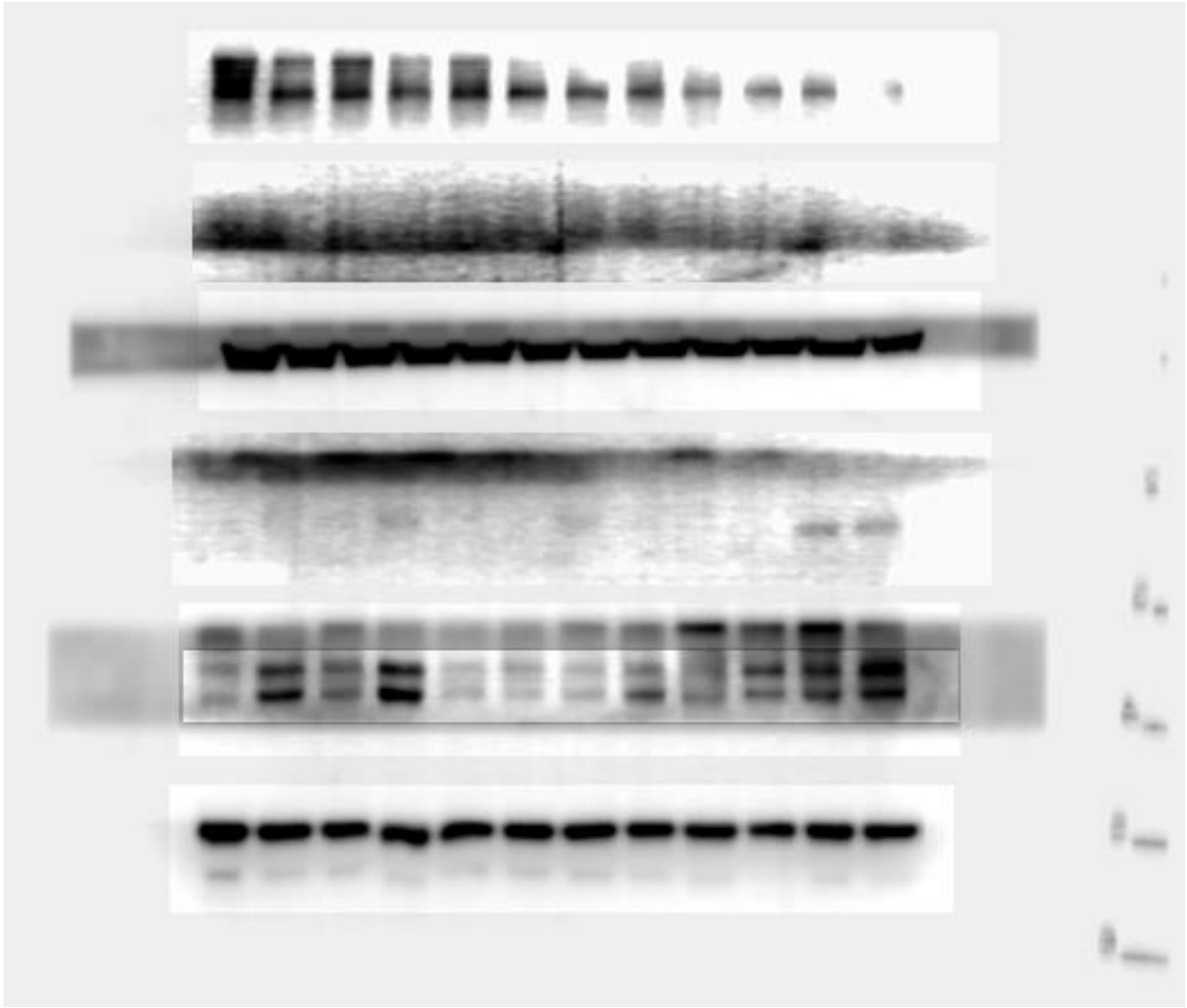
ACC
TLR4
HSP90
p-AKTthr
p-ERK
GAPDH – FIG4B

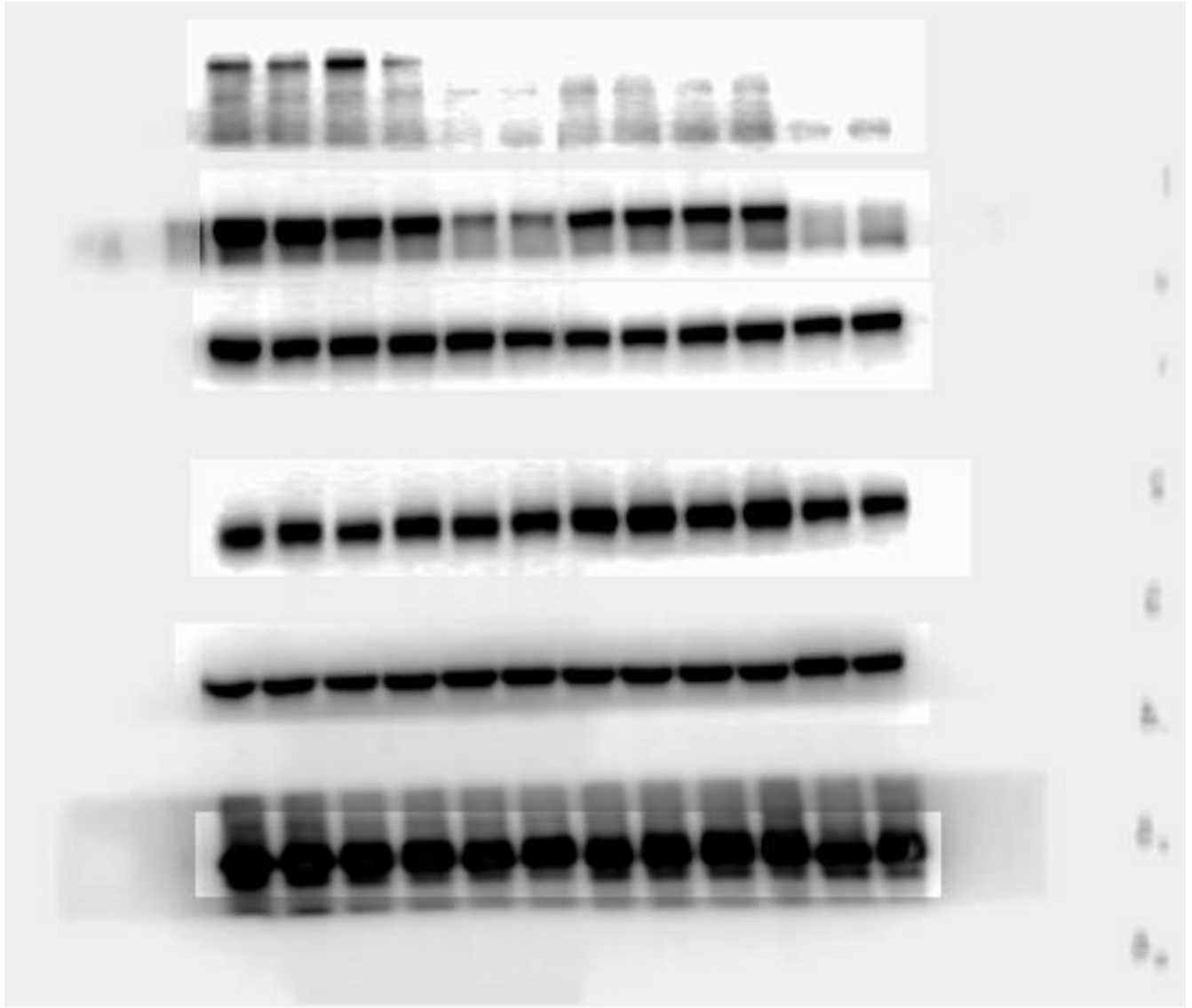
p-ACC
iNOS – FIG5B
eEF2 – FIG5B
AKT
Actin – FIG4A
S6

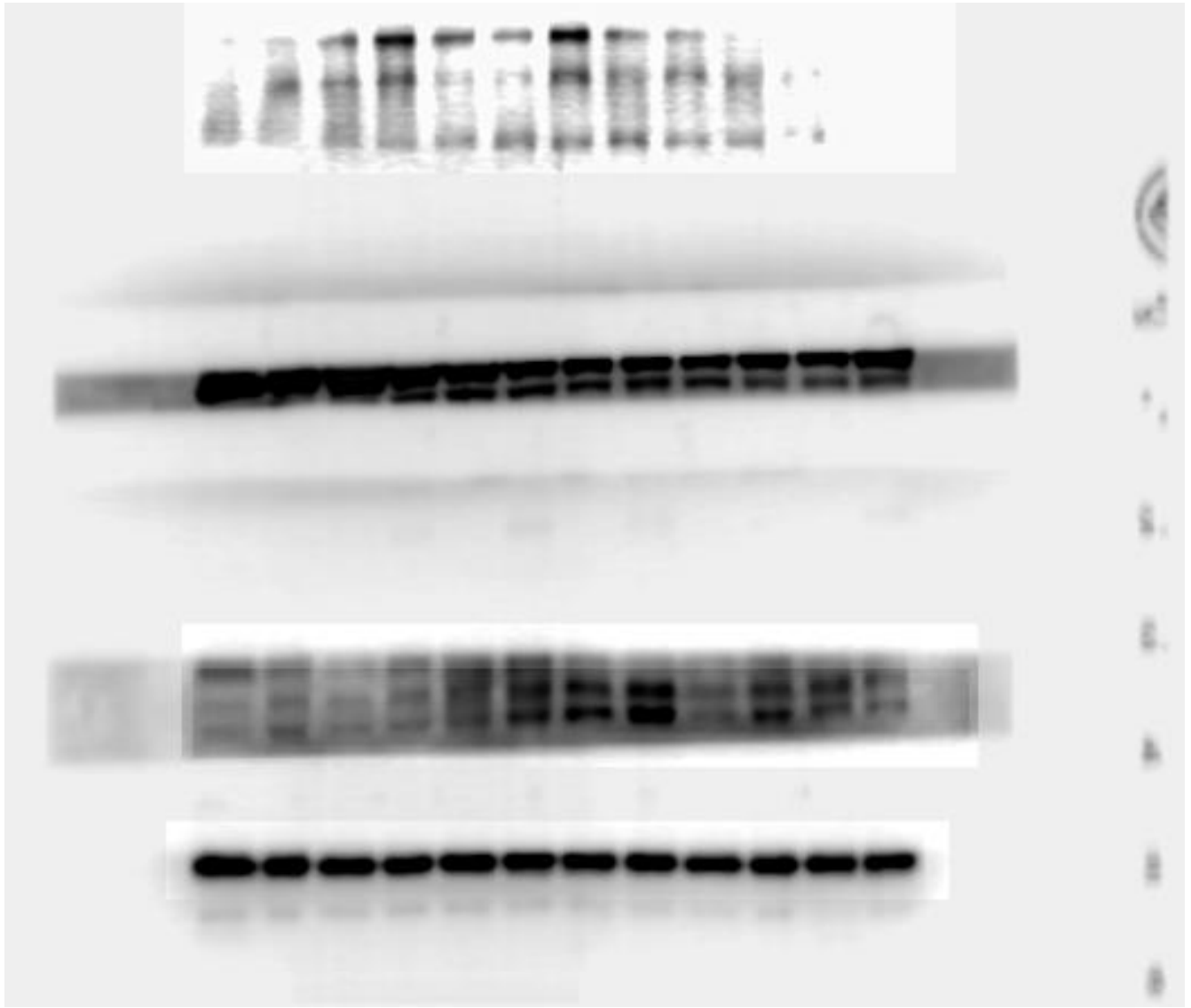
ACC
TLR4
HSP90
p-AKTthr
p-ERK
GAPDH

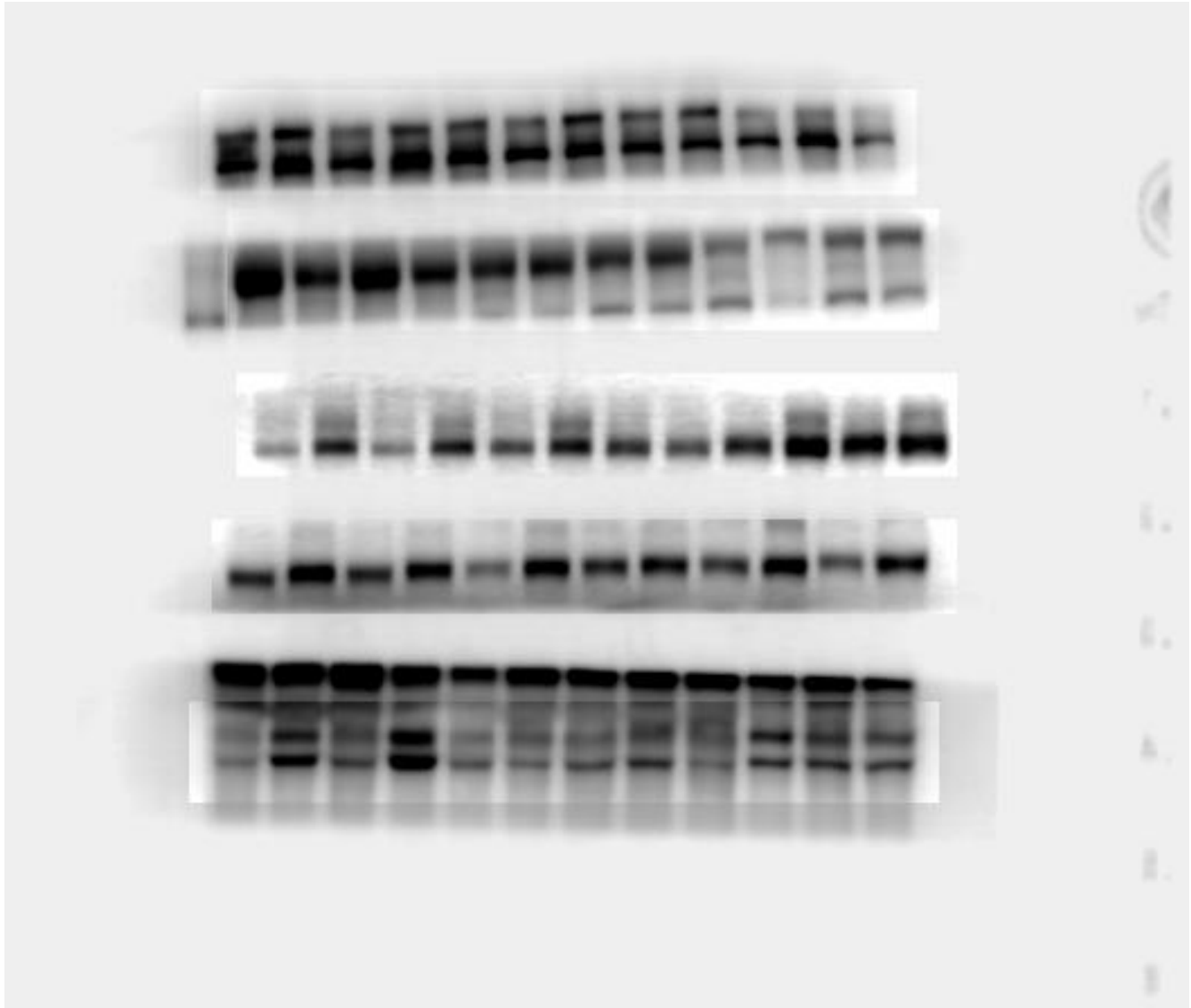

p-ACC – FIG4C

iNOS

p-PKC – FIG4B

P70S6K

p-ERK

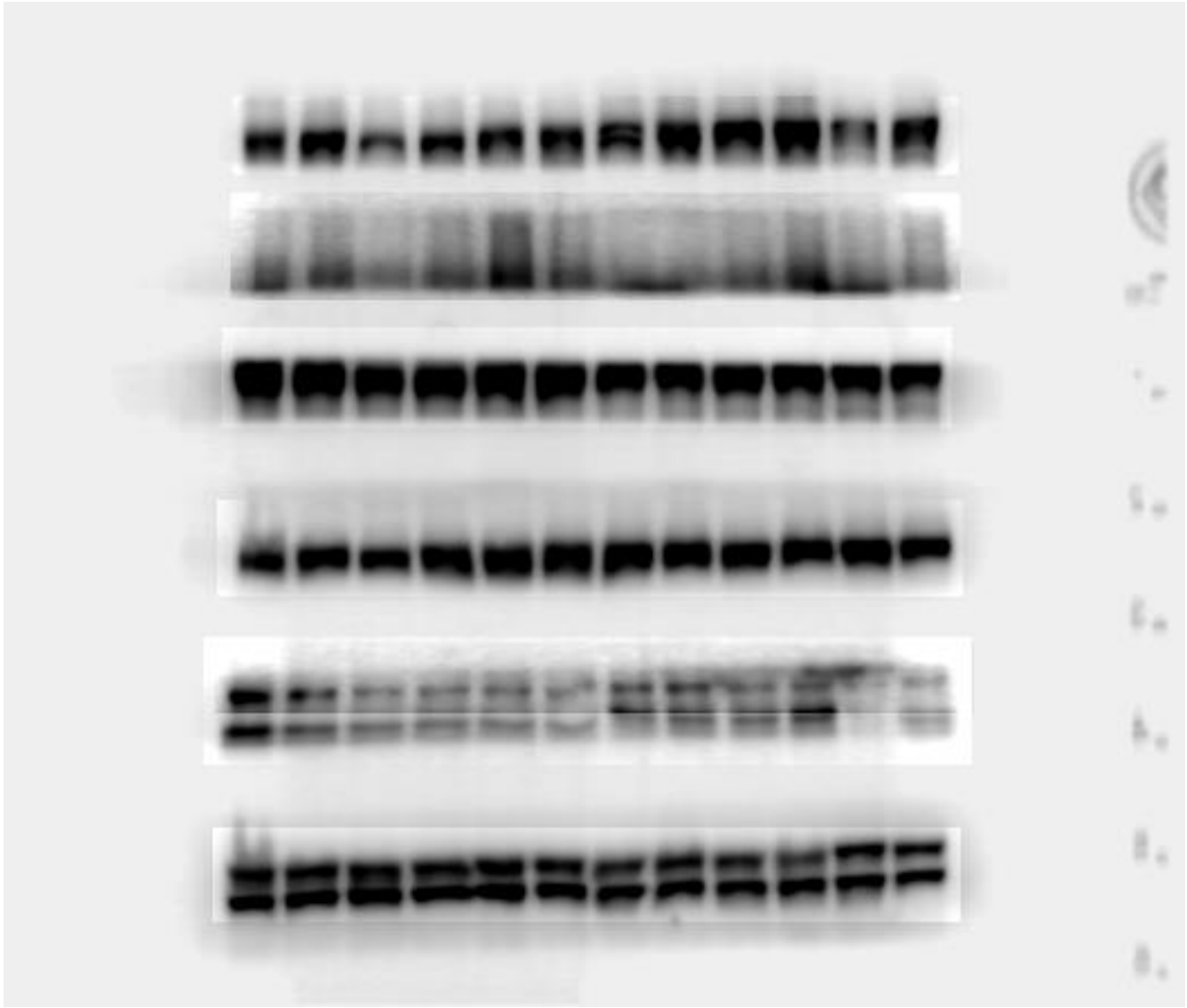
p-mTOR – FIG4A
TLR4
IRb – FIG4A
AKT
p-ERK
ARG1

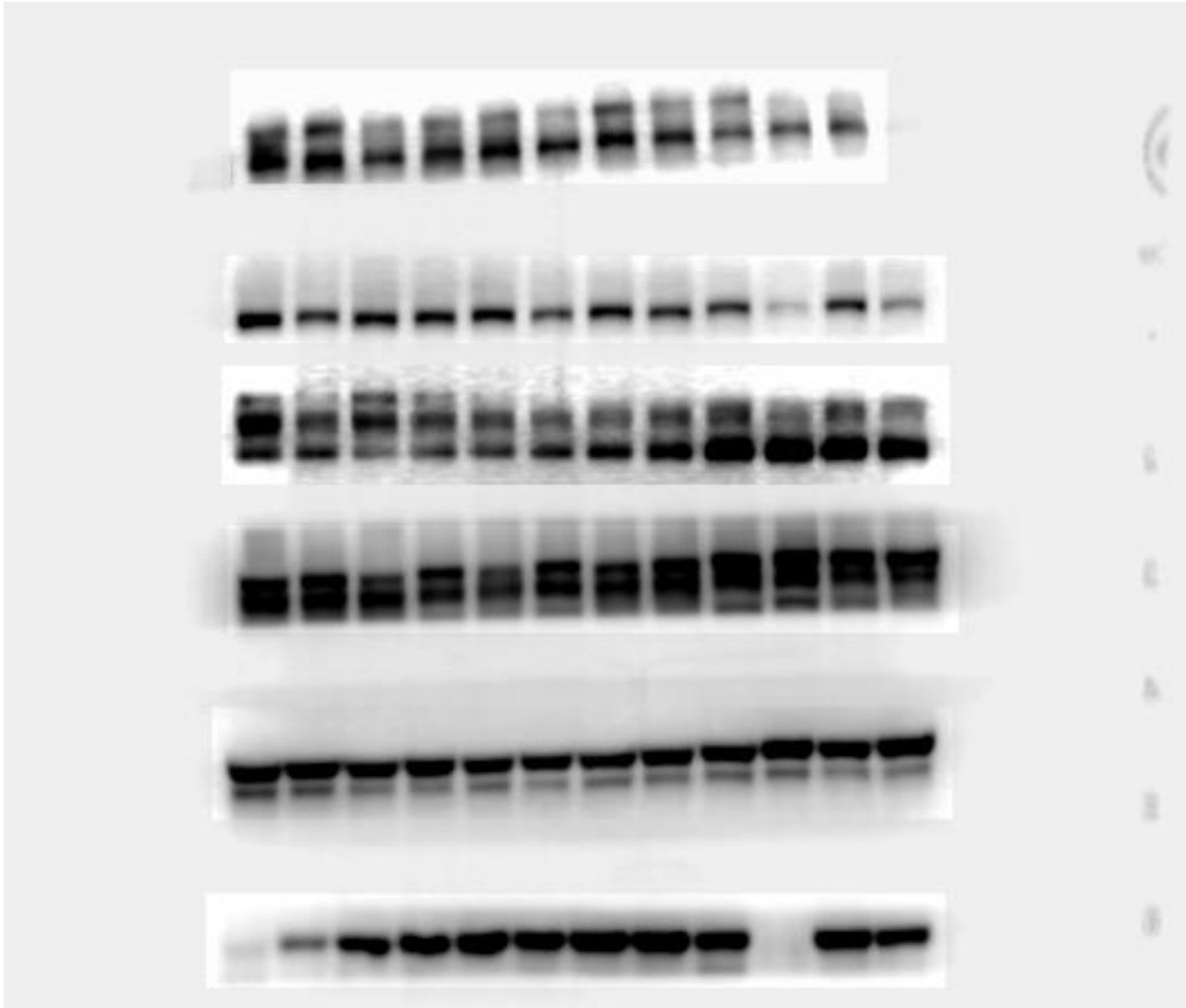
ACC
ACLy
PKC
NFKB
Actin
p-S6

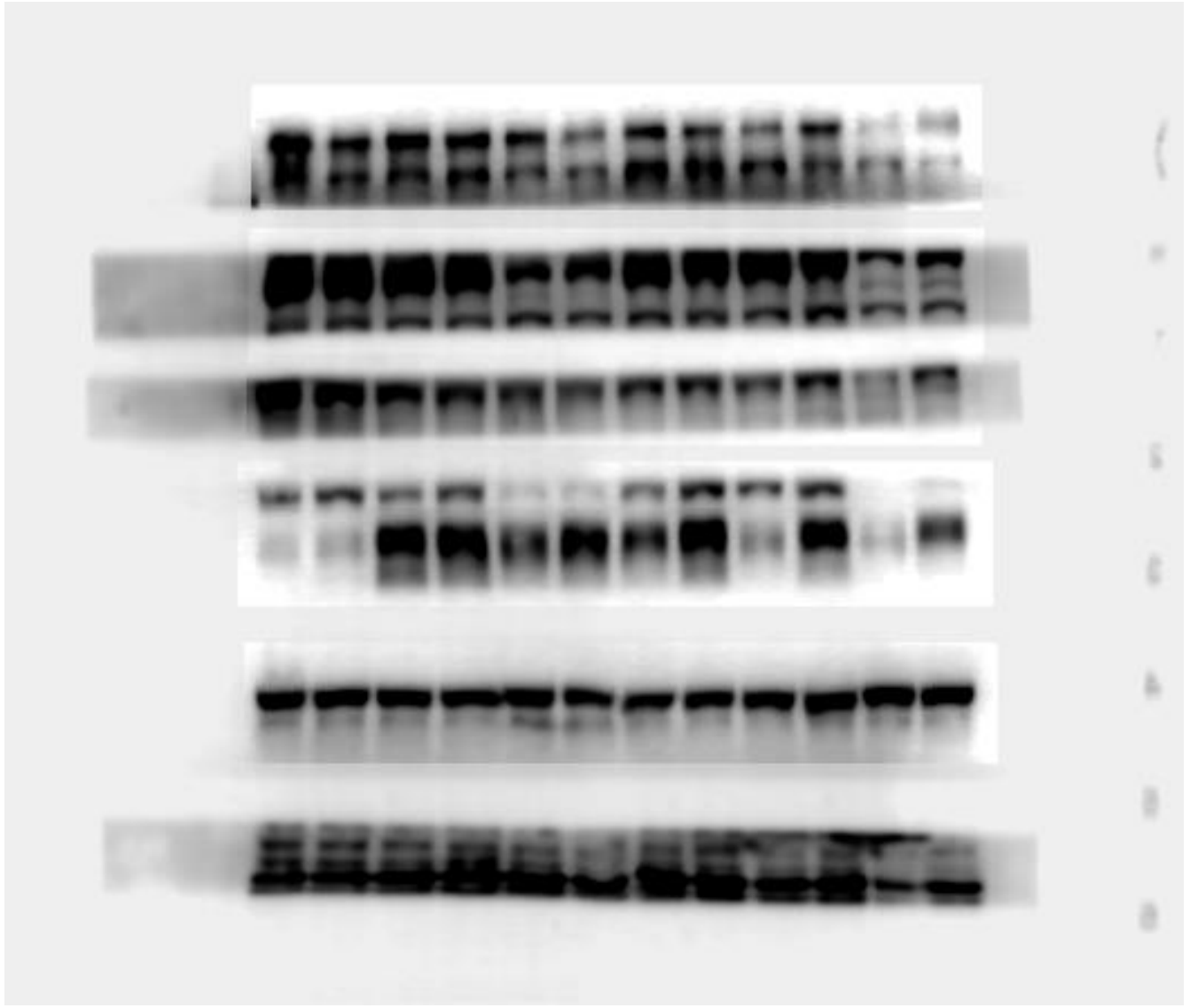
ACC
TLR4
p-IKK – FIG5B
p-p70S6K
Actin
ARG1

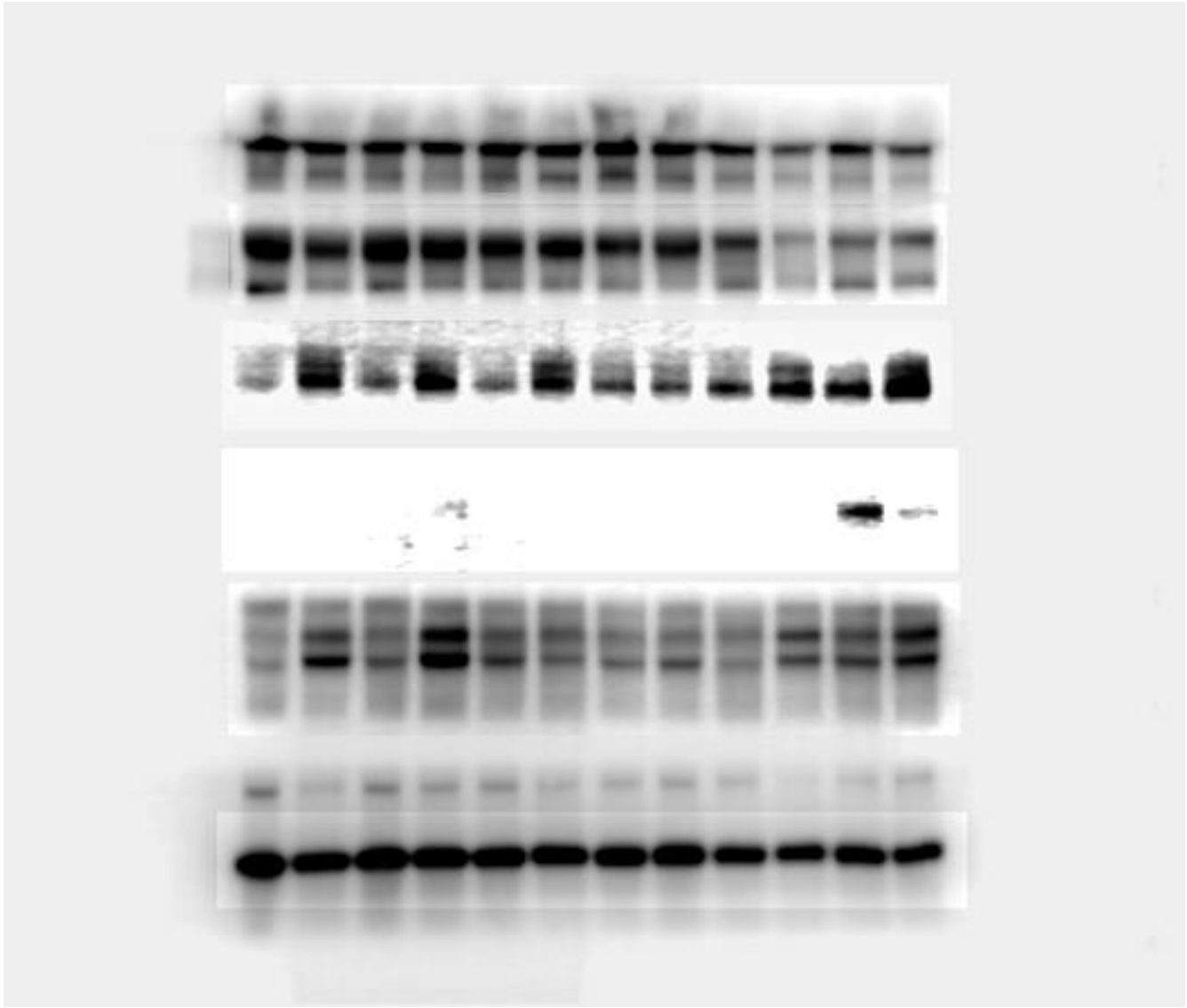
p-ACC
iNOS
p-PKC
p-AKTthr
p-ERK
SDHb

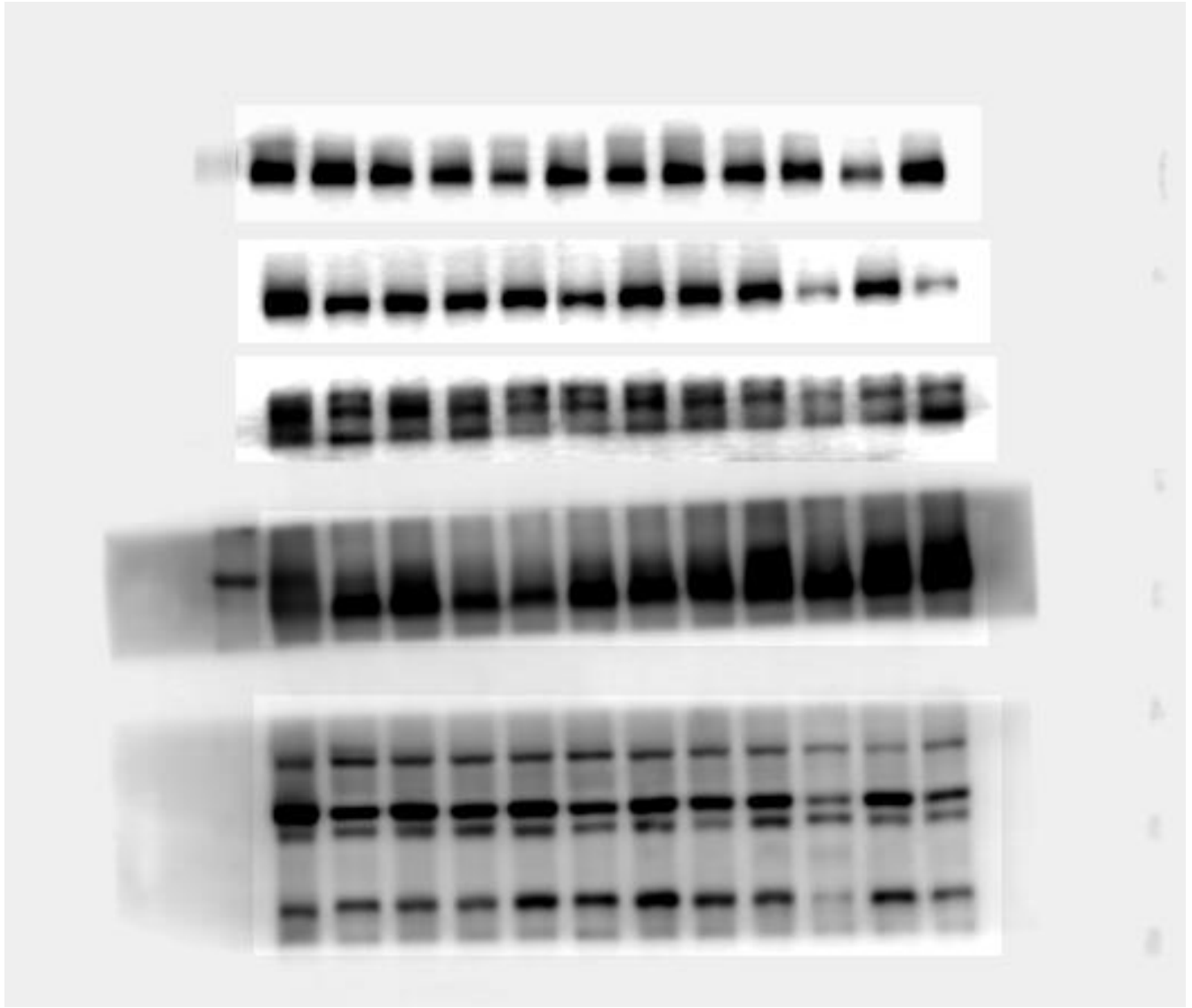
mTOR
ACLy
PKC – FIG4B
p-NFKB
SCD1

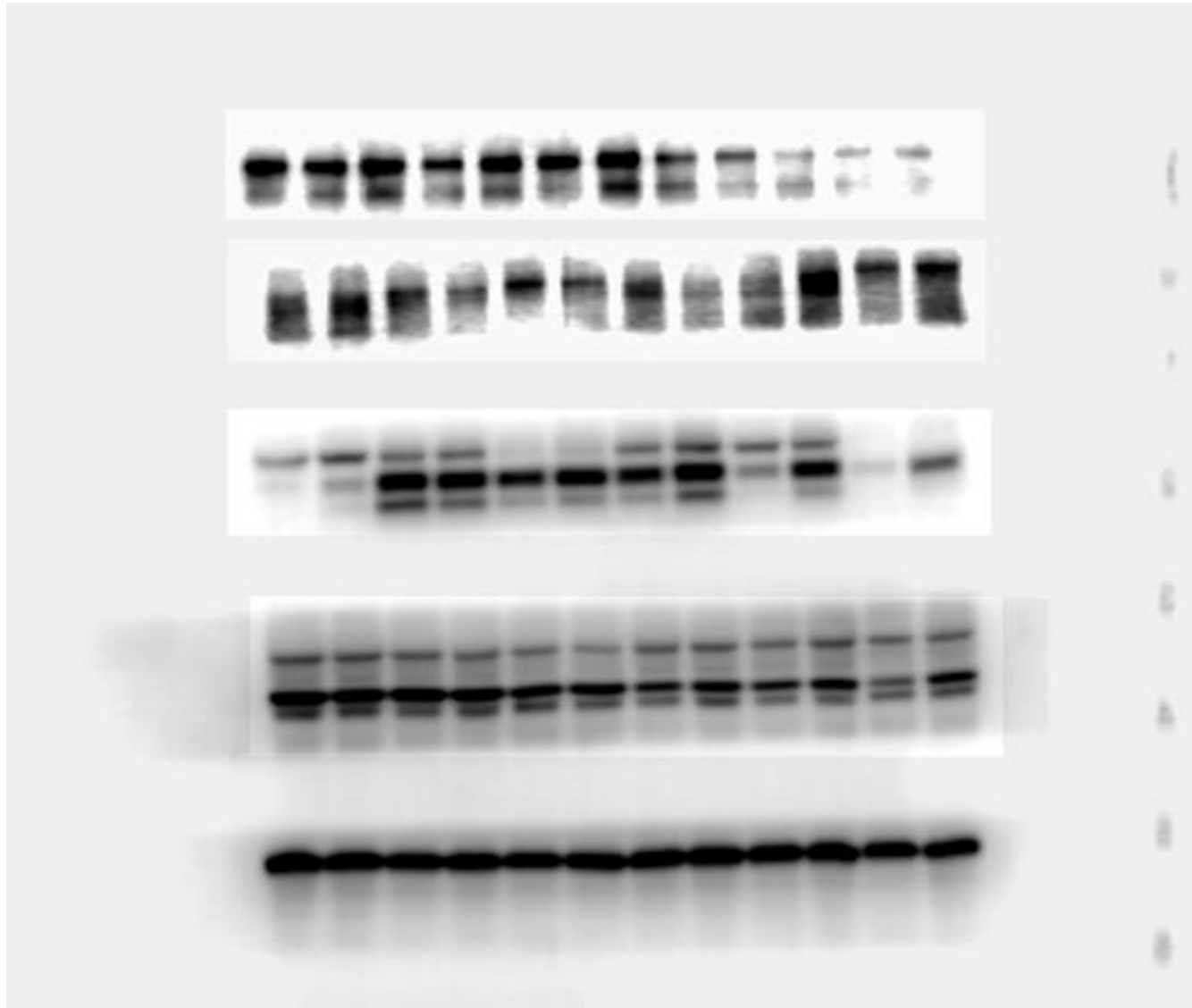
ACC
IKK
p-p70S6K
SCD1
SDHb

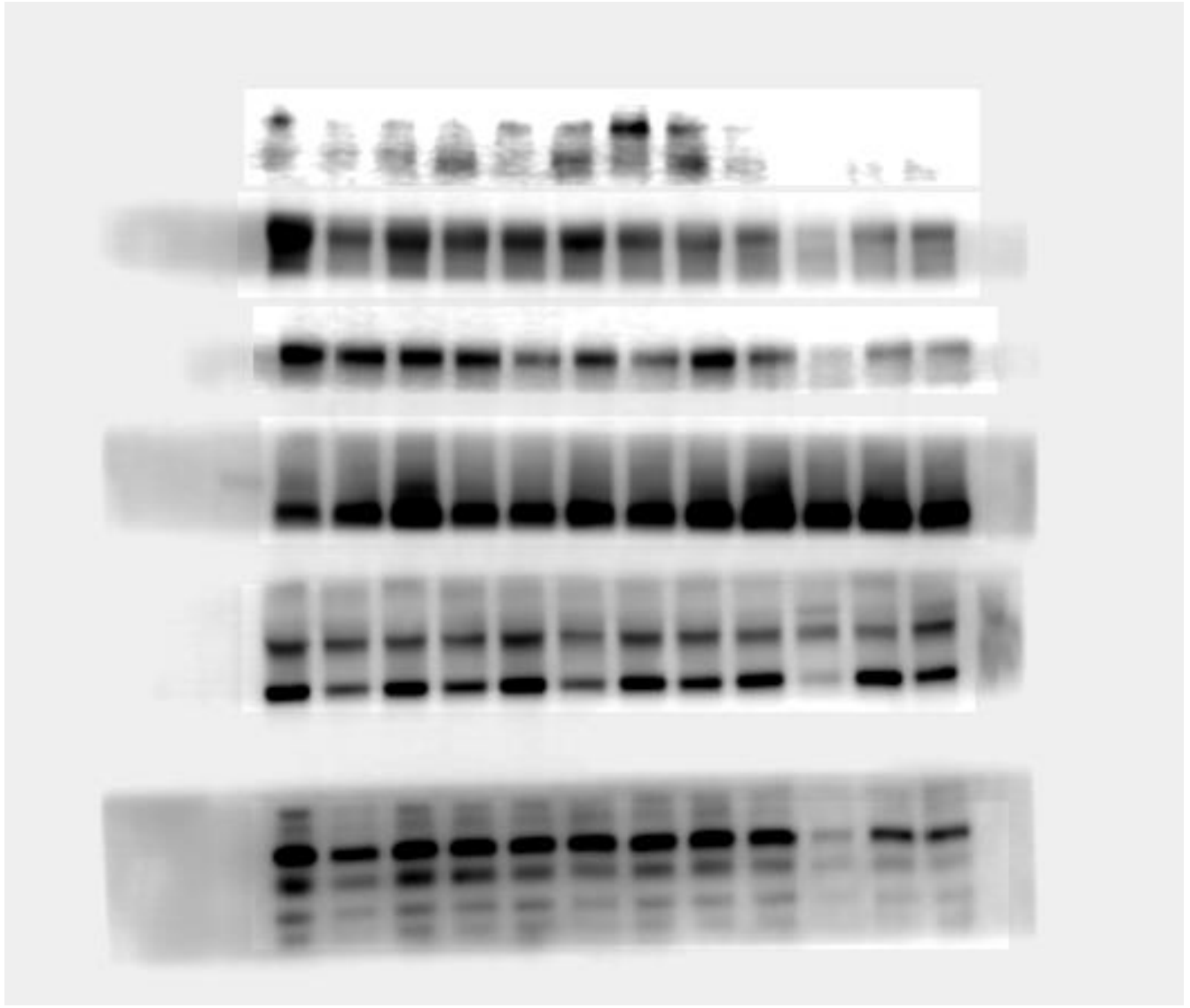
p-mTOR
p-PI3K
pIKK
p-NFKB
SCD1 – FIG4C
ARG1

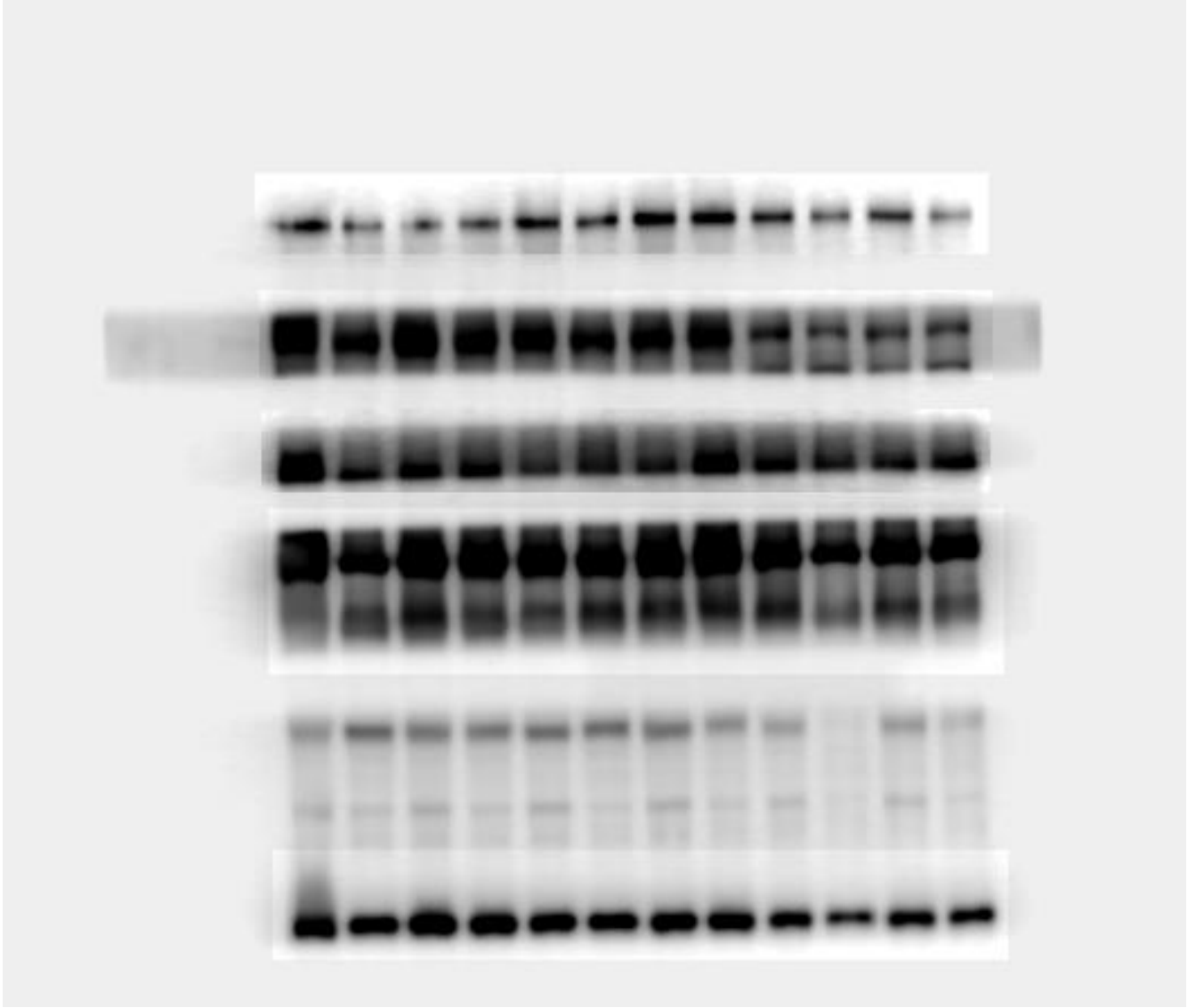
p-ACC
TLR4
IKK – FIG5B
SDHA
SDHB

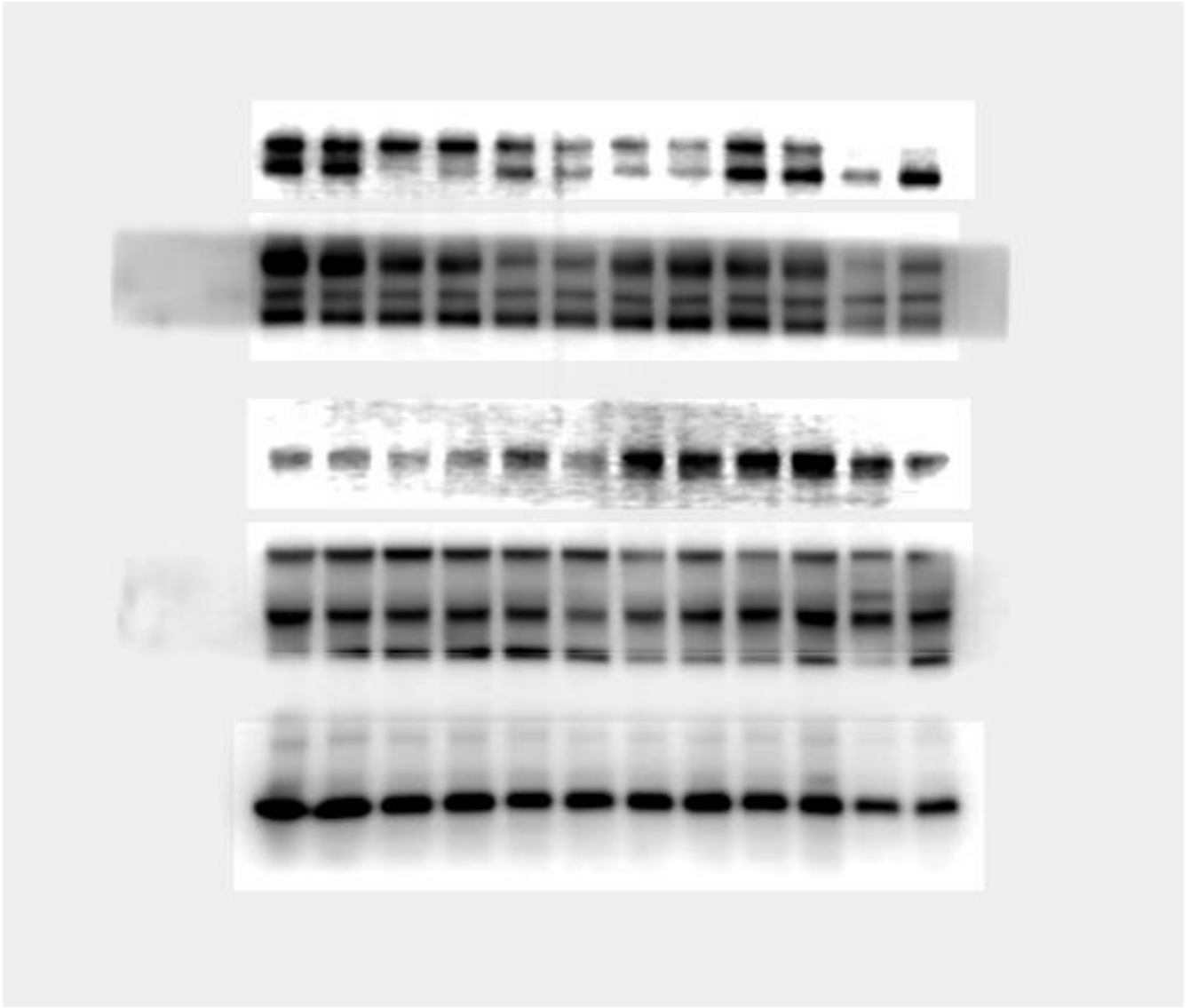
mTOR
TLR4 – FIG5B
p-70S6K
SCD1
SDHB

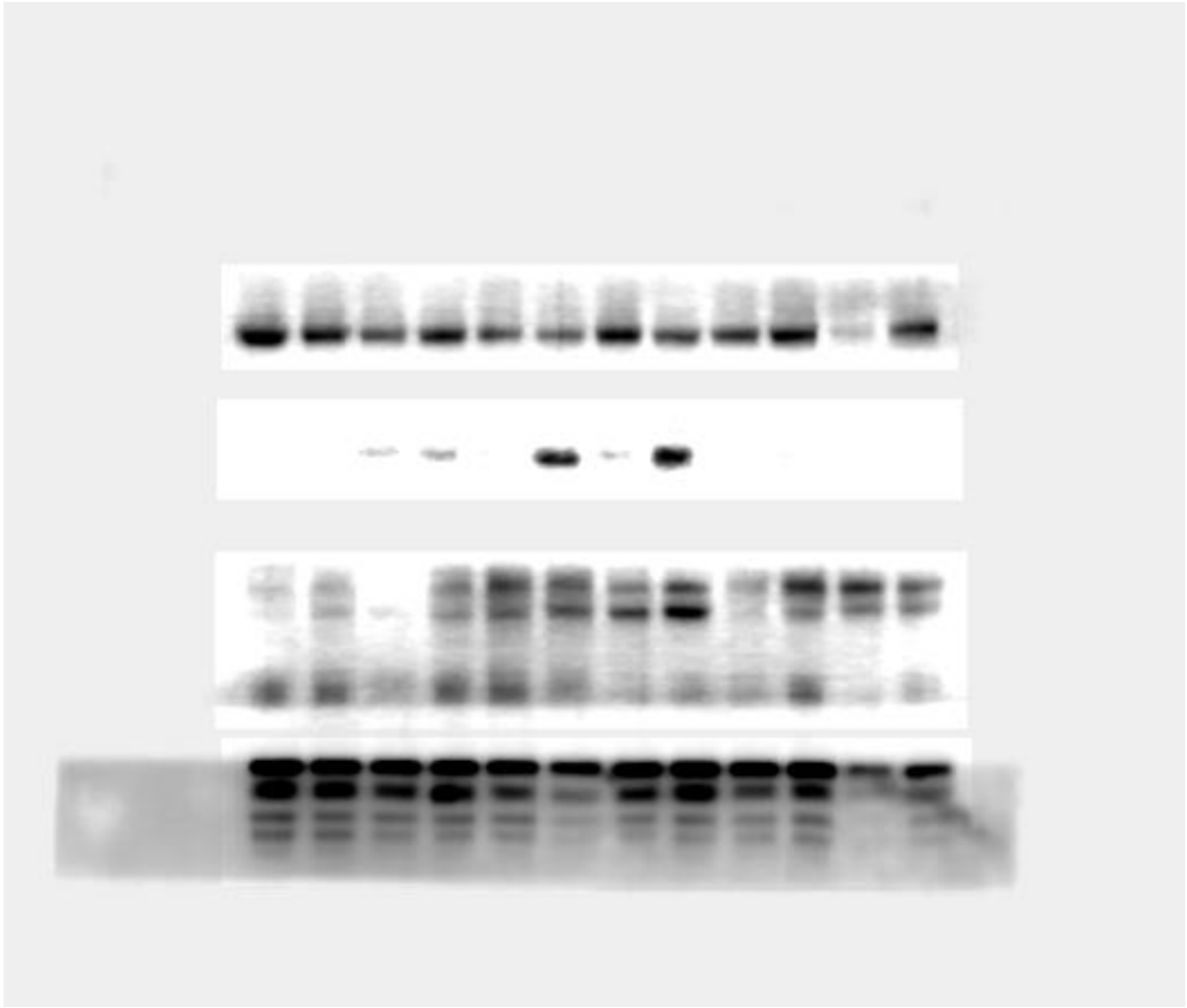
p-IKK
p-AKTthr
p-ERK
ARG1

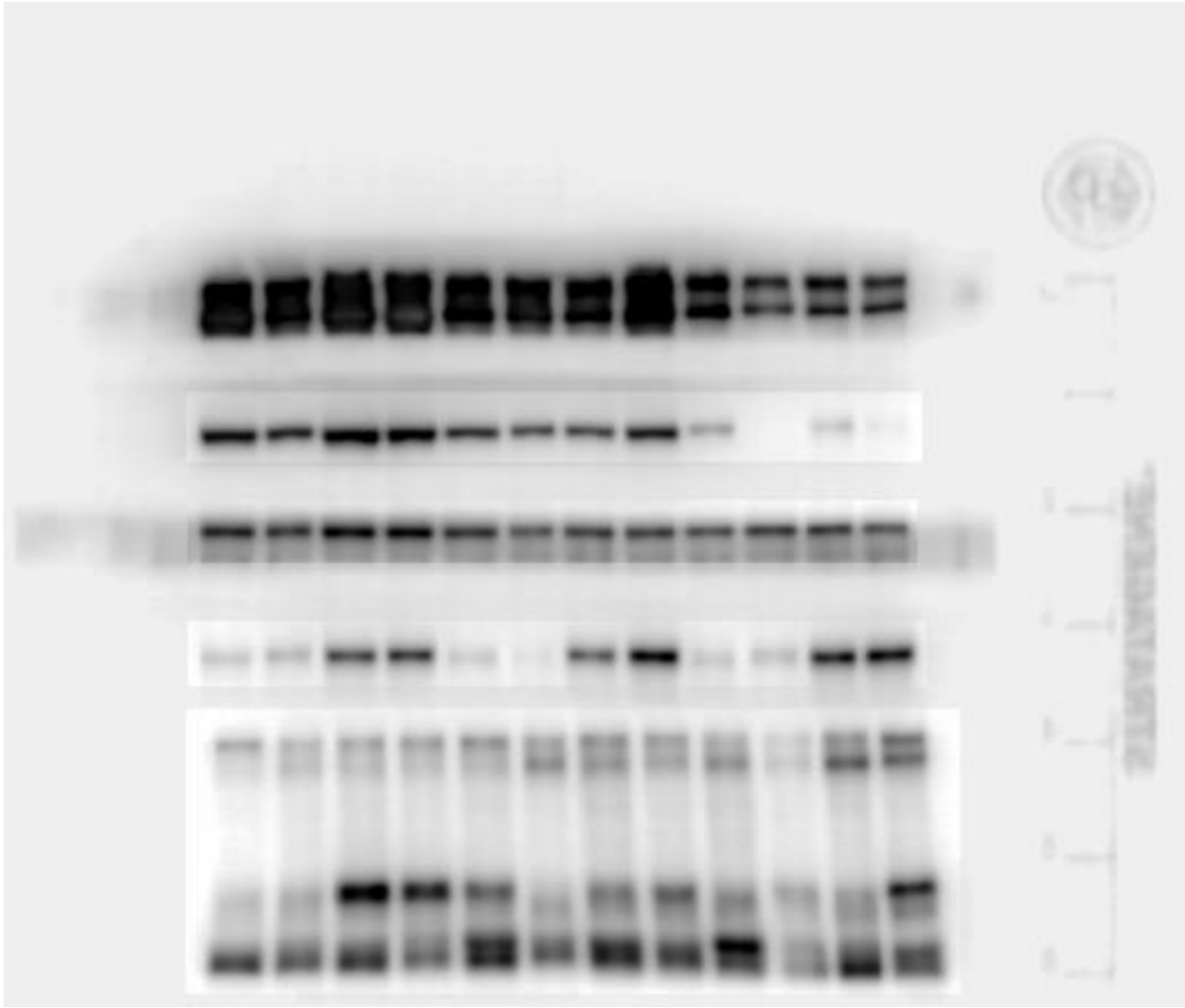
p-ACC
p-ACLy
HSP90
p-AKTthr
p-S6

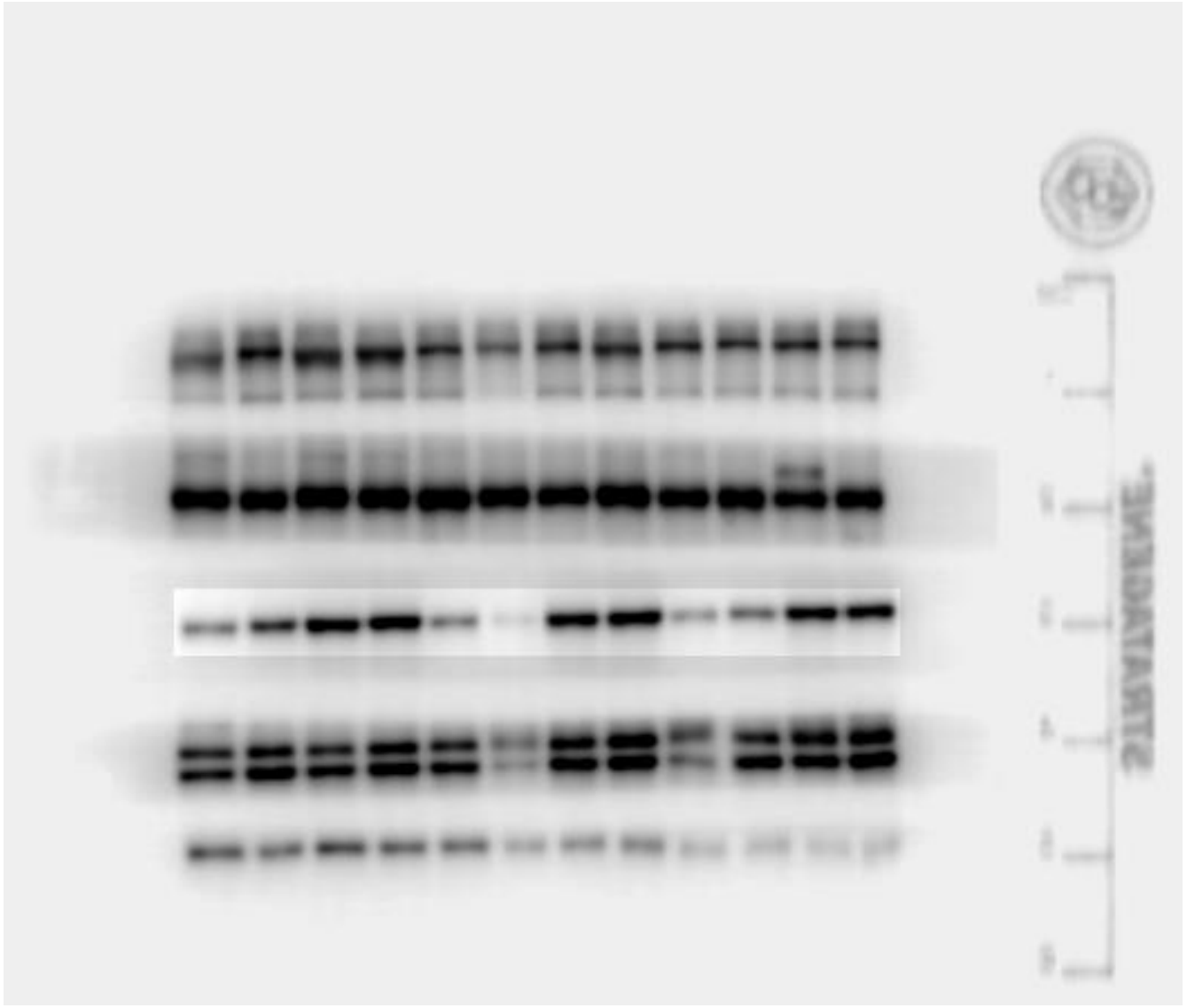
p-mTOR
IRb
p-AKTser
p-ERK
GAPDH

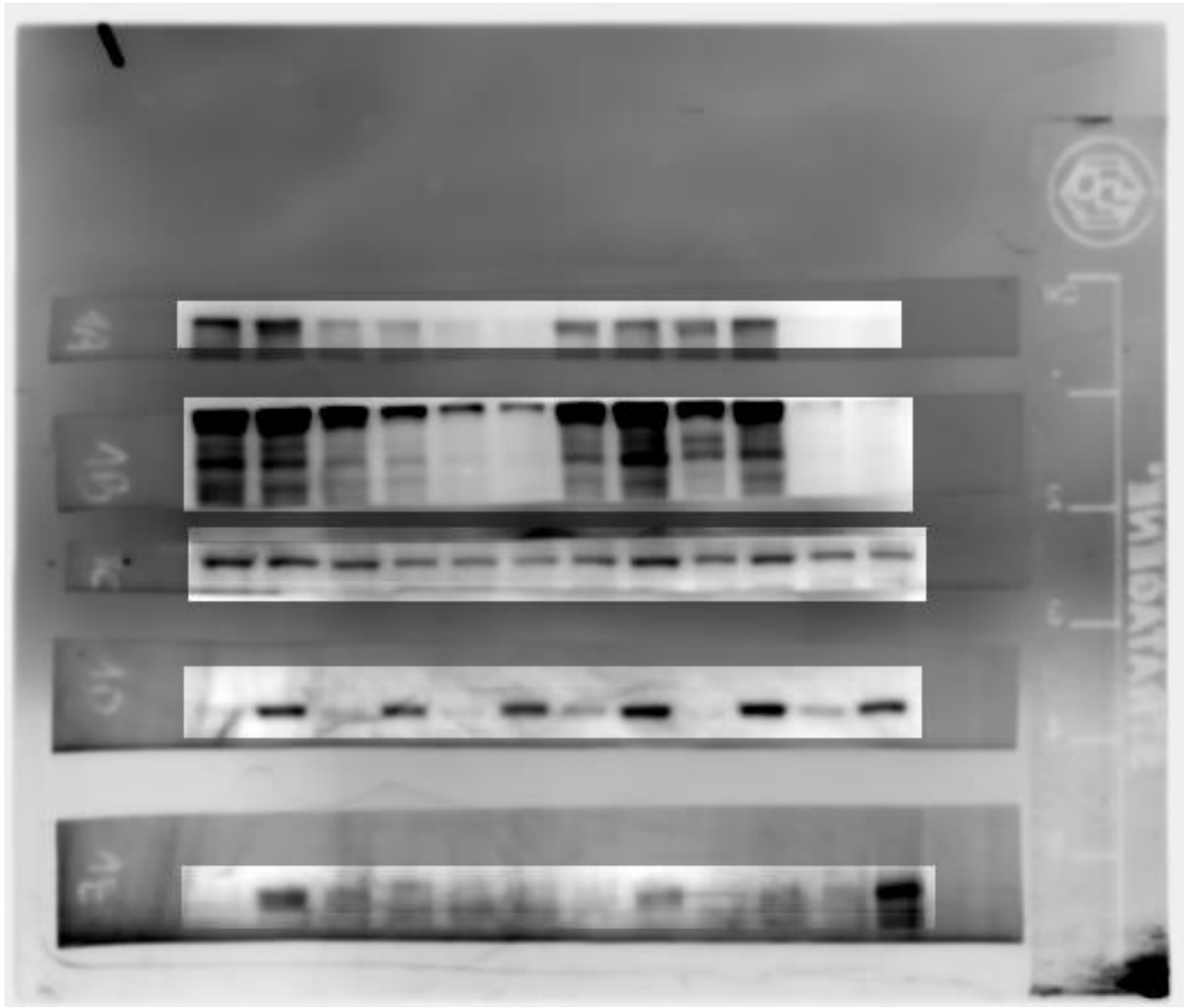
p-ACC
p-ACLy
HSP90
p-AKTser
p-S6

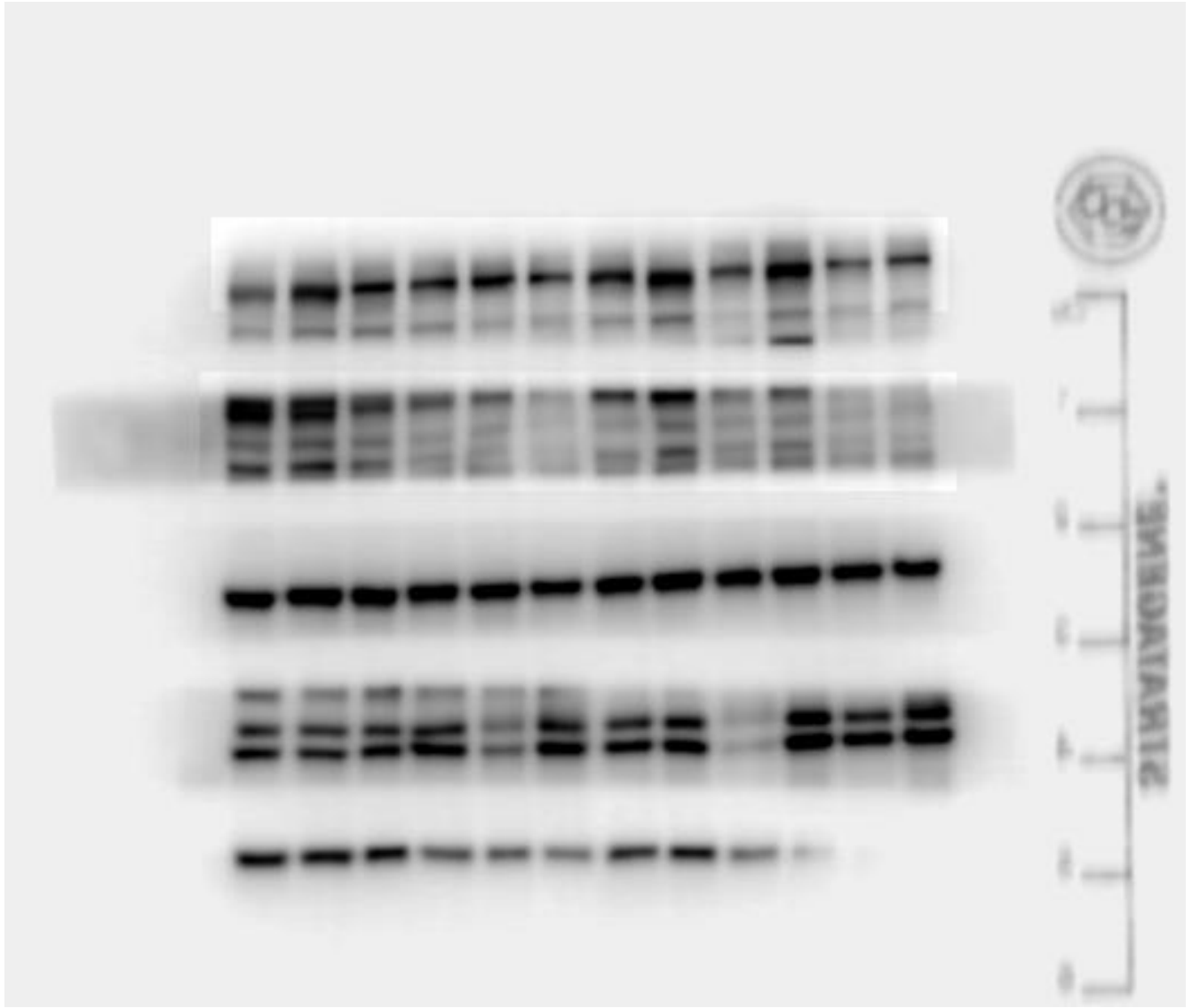

p-mTOR – FIG6G

p-PI3K – FIG6G

AKT – FIG6G

p-ERK

GAPDH

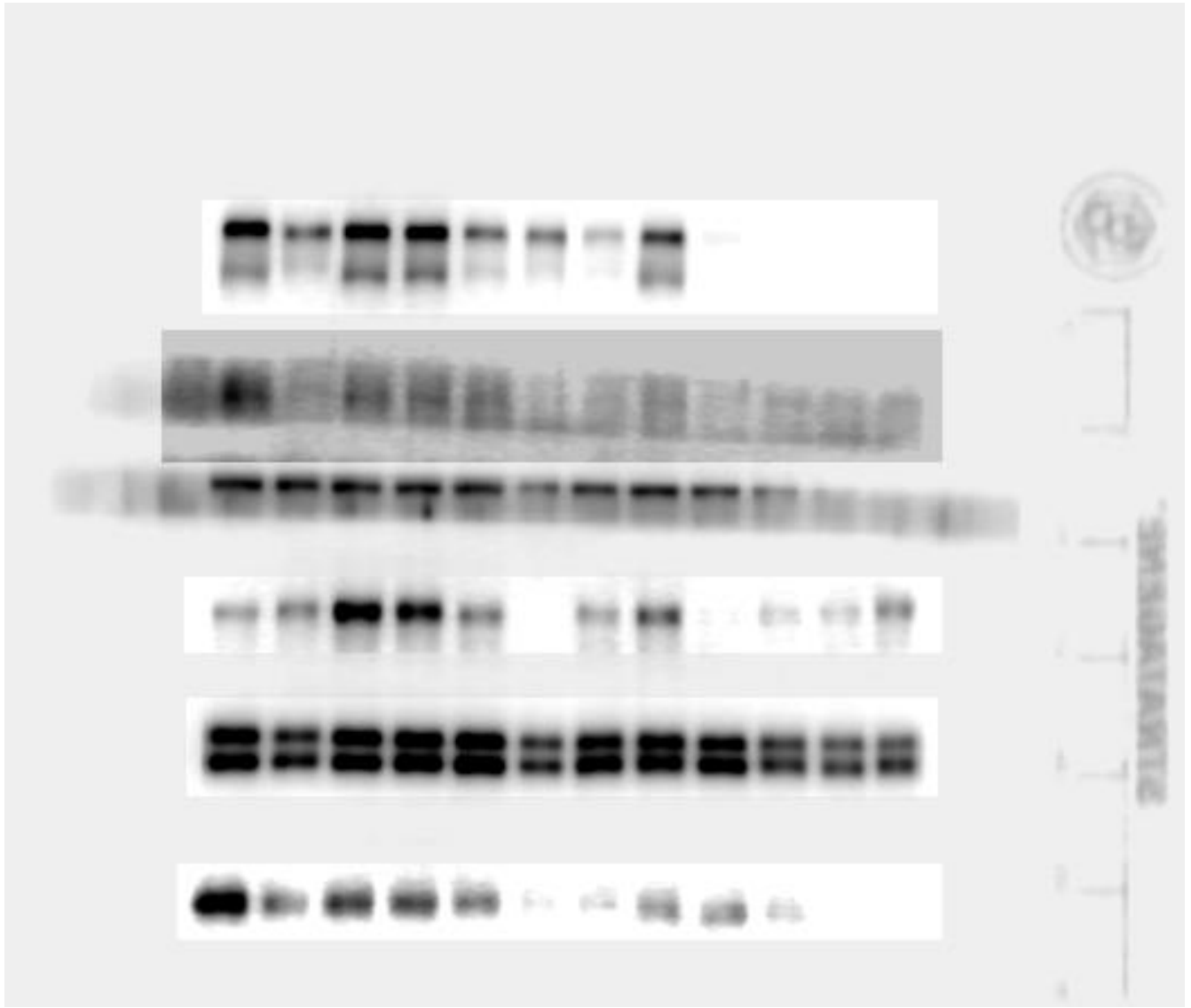
p-ACC
PGC1a
HSP90
p-p70S6K
ERK
S6

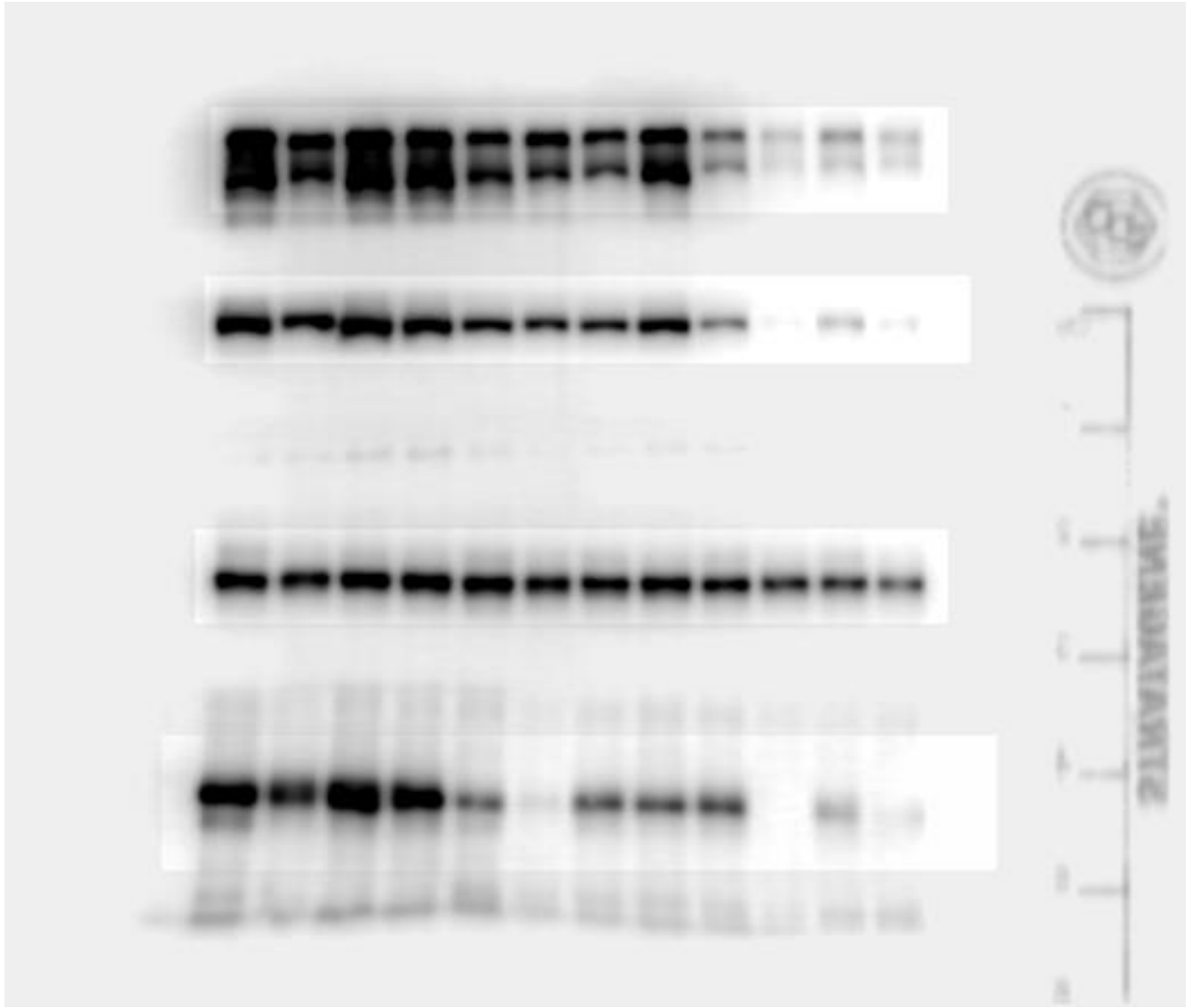
ACC
ACLy
eEF2
AKT
SCD1

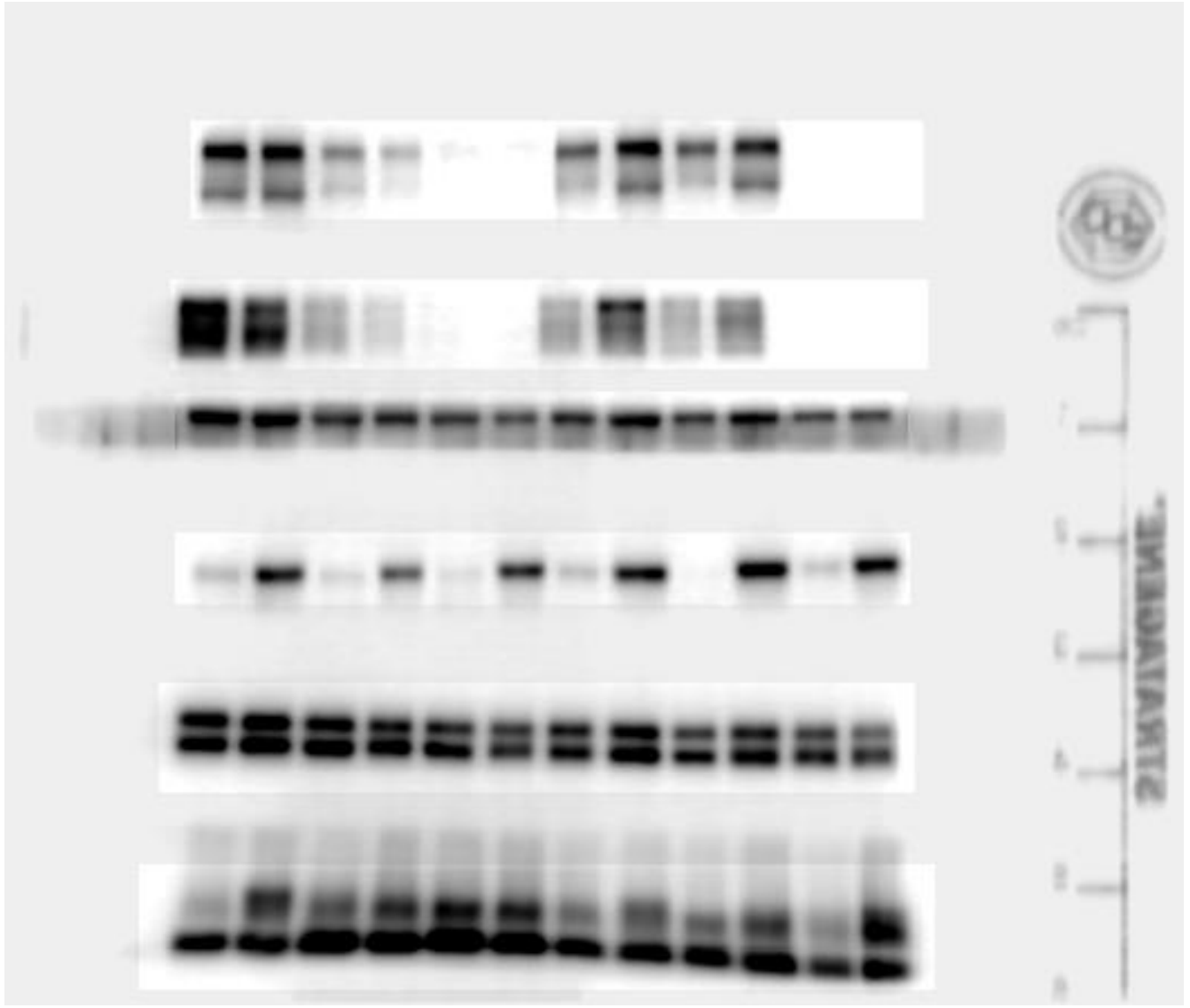
p-ACC
p-ACLy
HSP90
p-AKTThr – FIG6G
ERK
p-S6

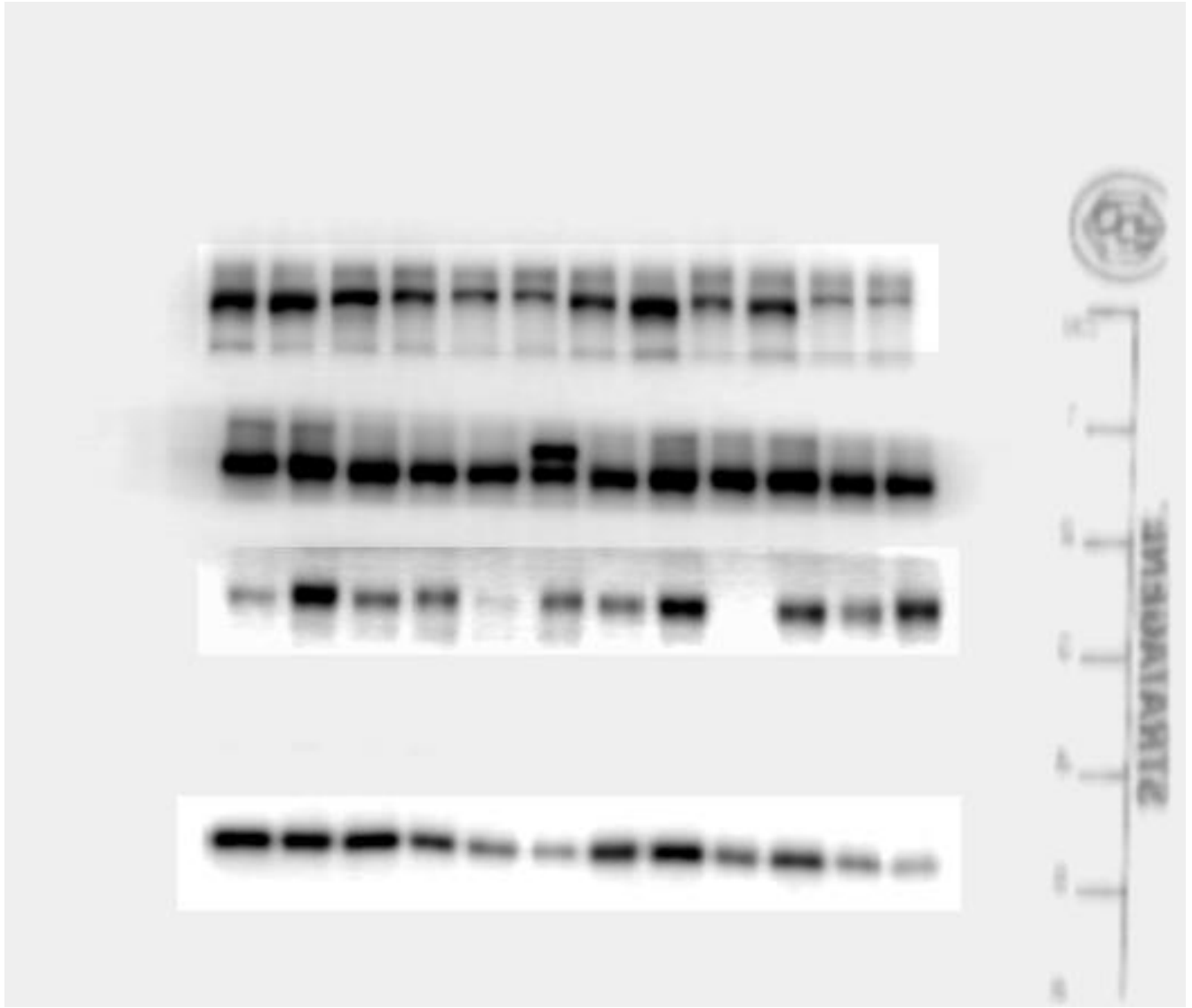
mTOR
IRb – FIG6G
p-p70S6K
Actin
GAPDH

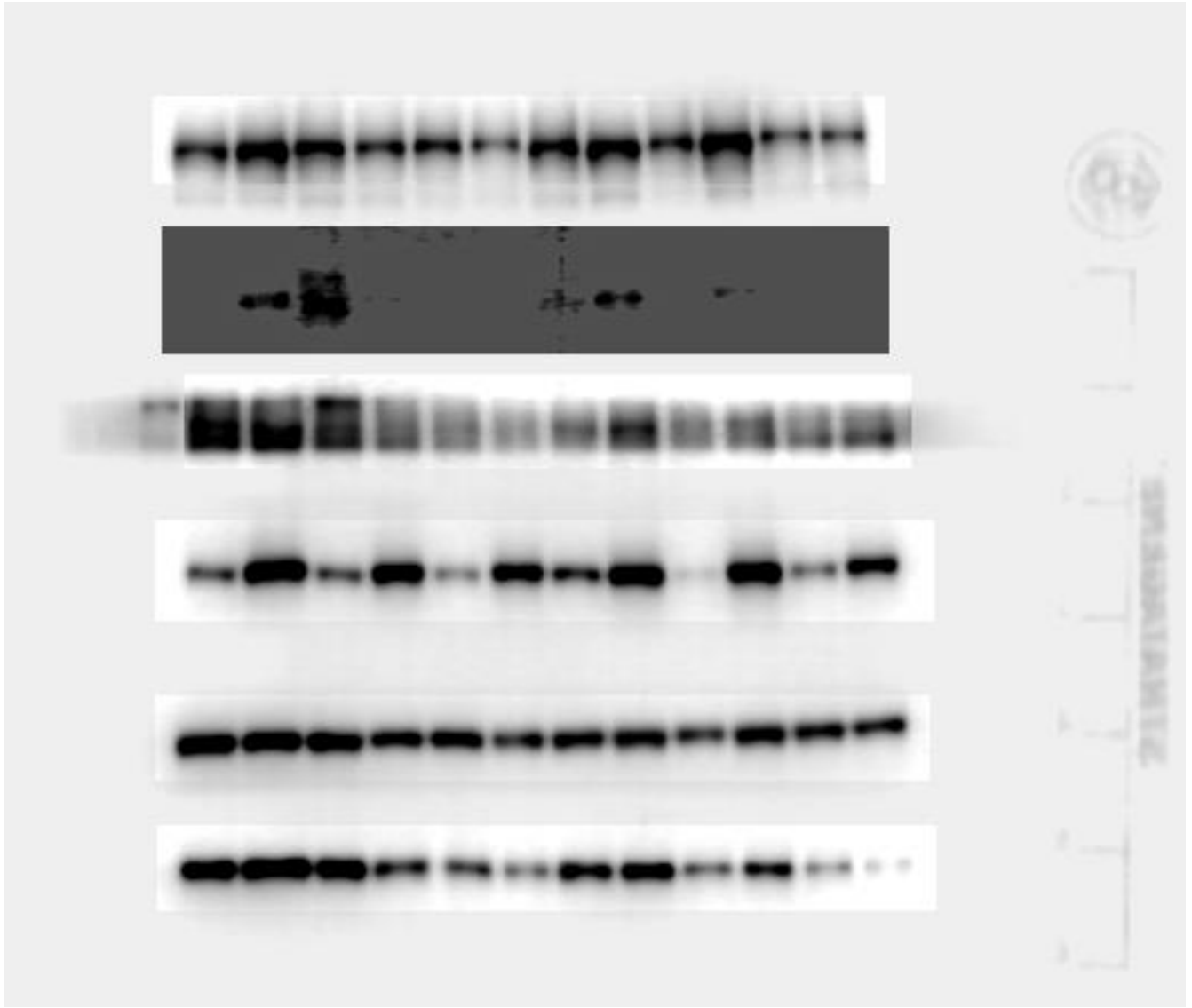
mTOR
IRE1
p-PI3K
pAKTser
Actin
GAPDH

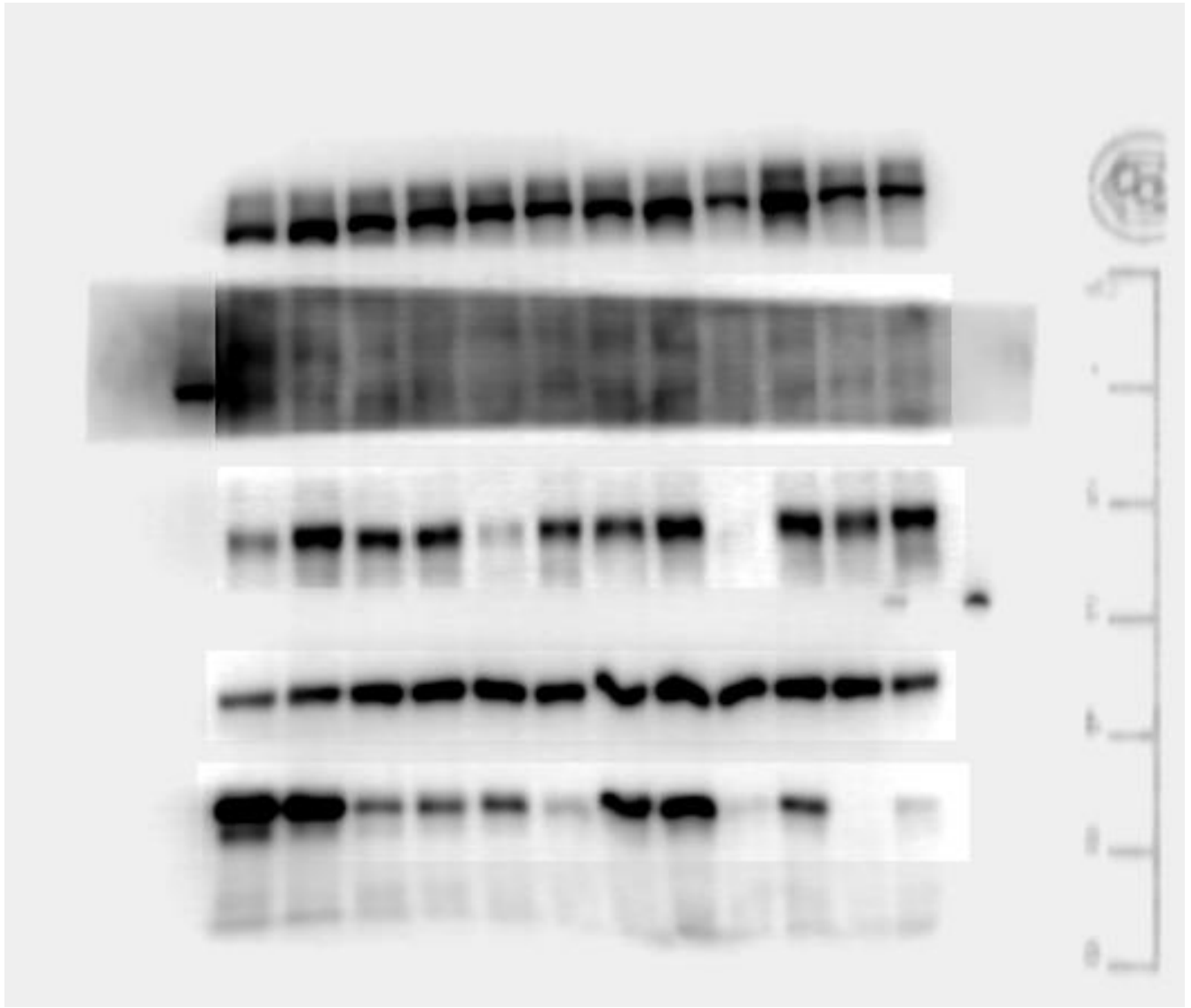
p-mTOR
PGC1a
p70S6K
Actin
SCD1

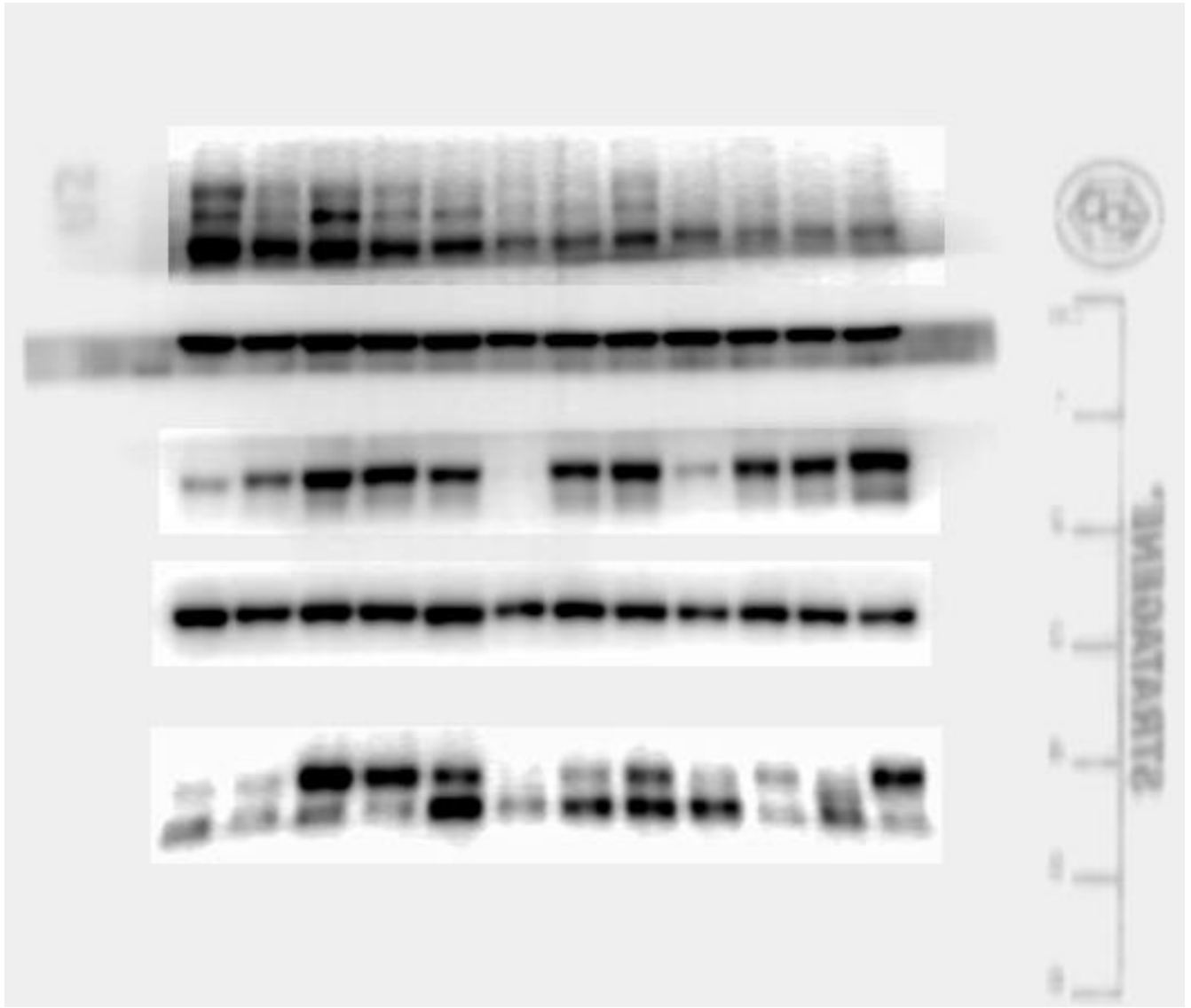
iNOS
HSP90
p-p70S6K
Actin
p-S6

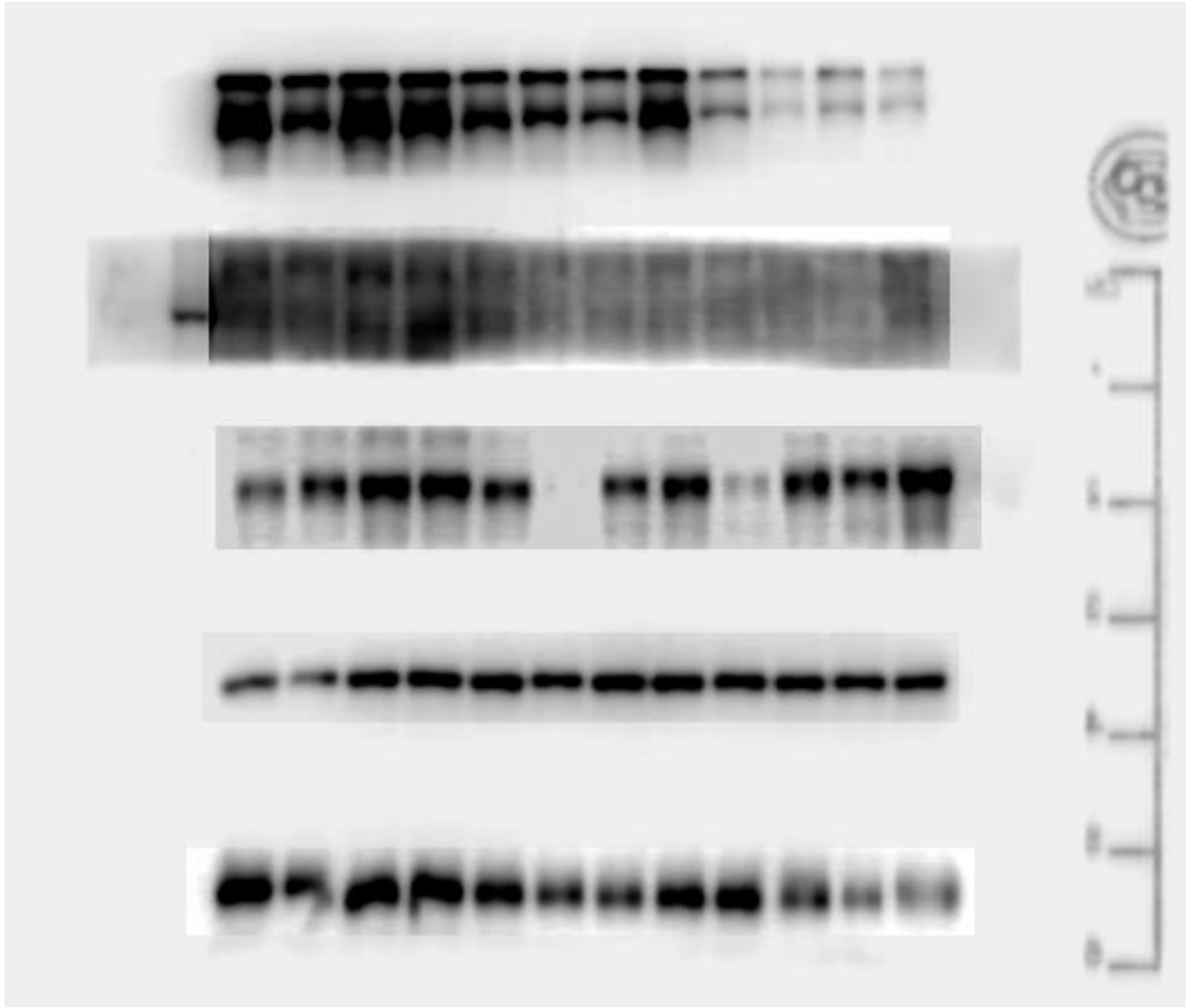
ACC
PGC1a
p70S6K
Actin
GAPDH

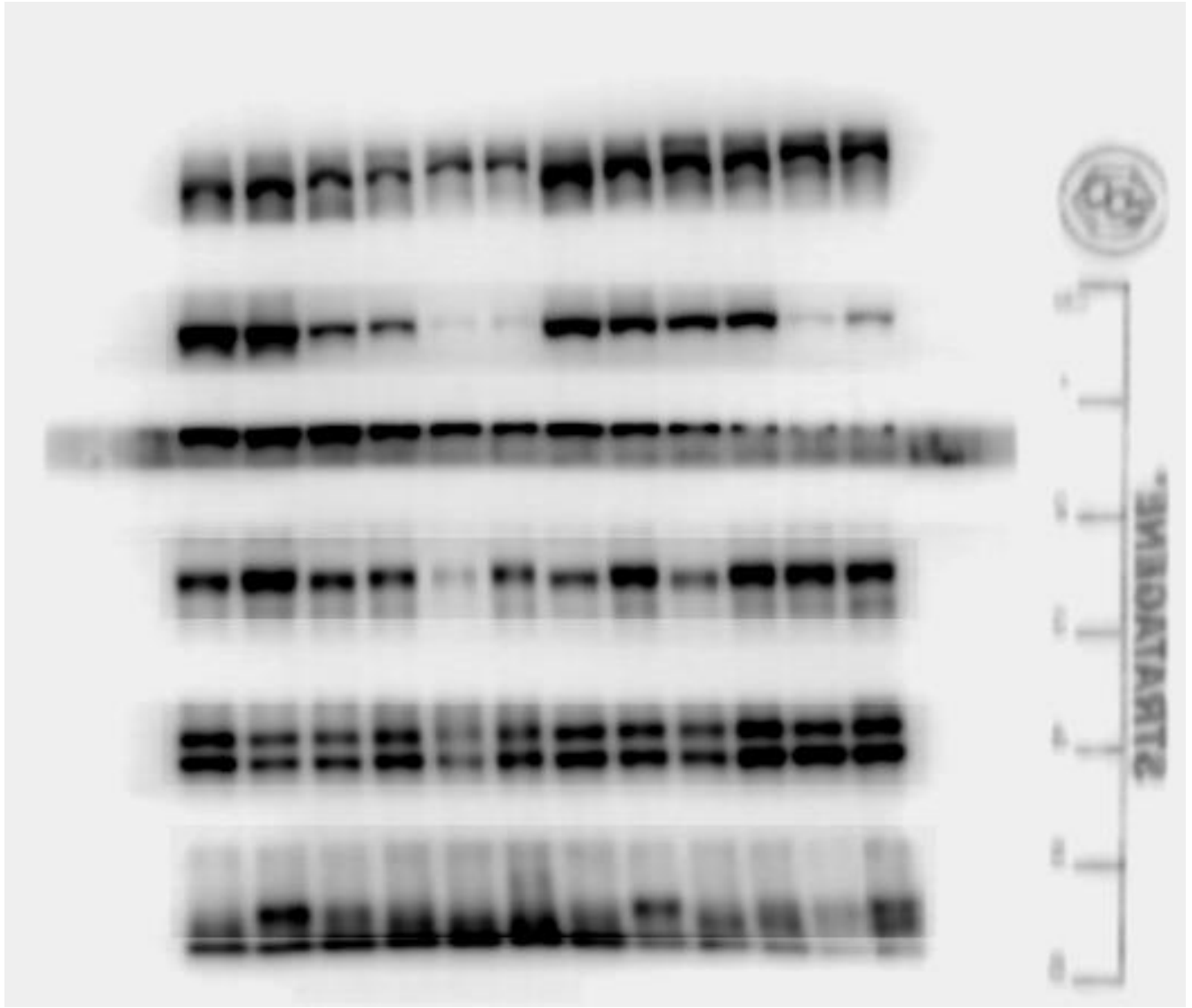
mTOR
ACLy – FIG6A
HSP90
p-p70S6K
p-ERK
p-S6

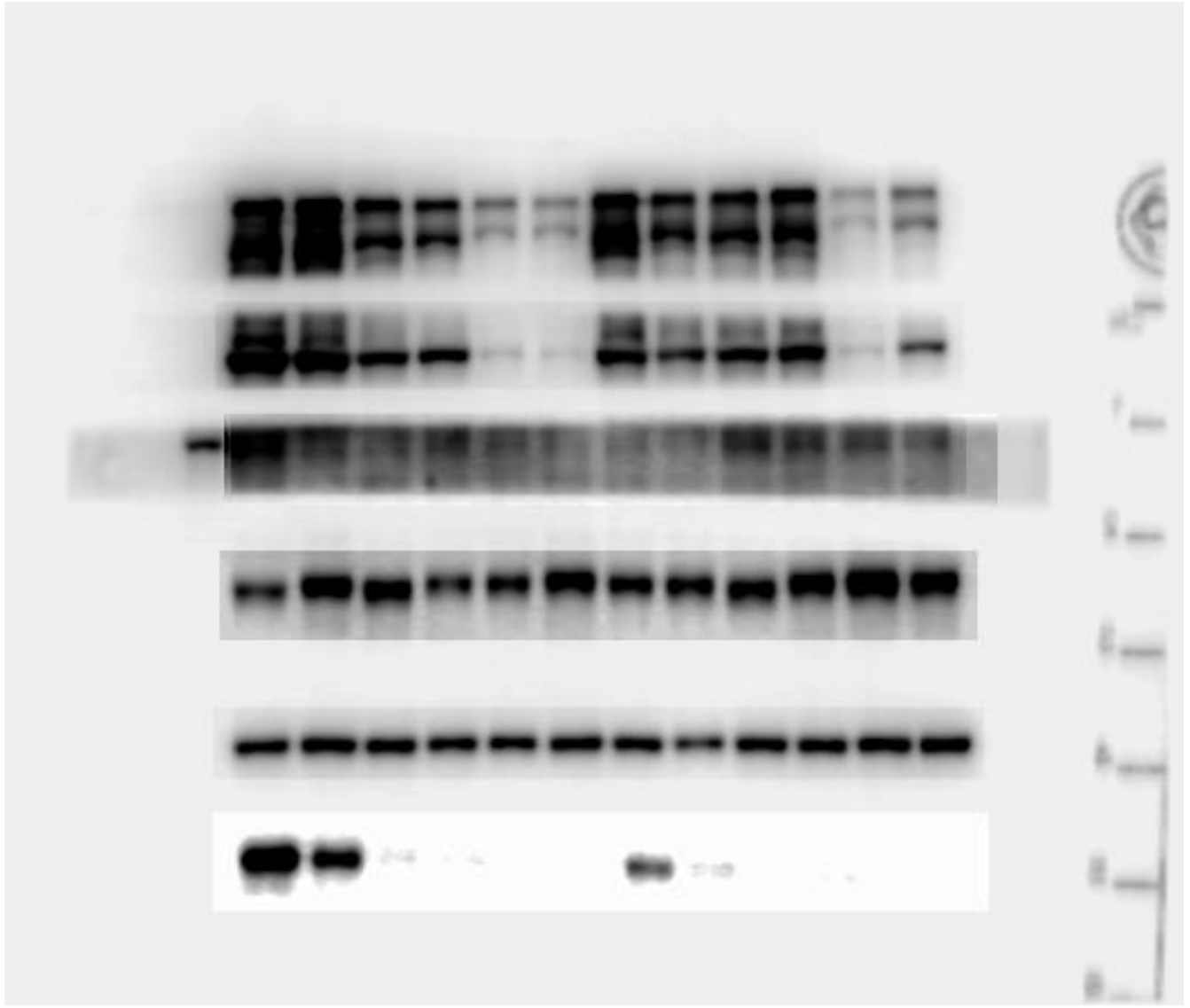
p-ACC – FIG6A
p-ACLy – FIG6A
PGC1a
p70S6K – FIG6G
Actin – FIG5H
SCD1

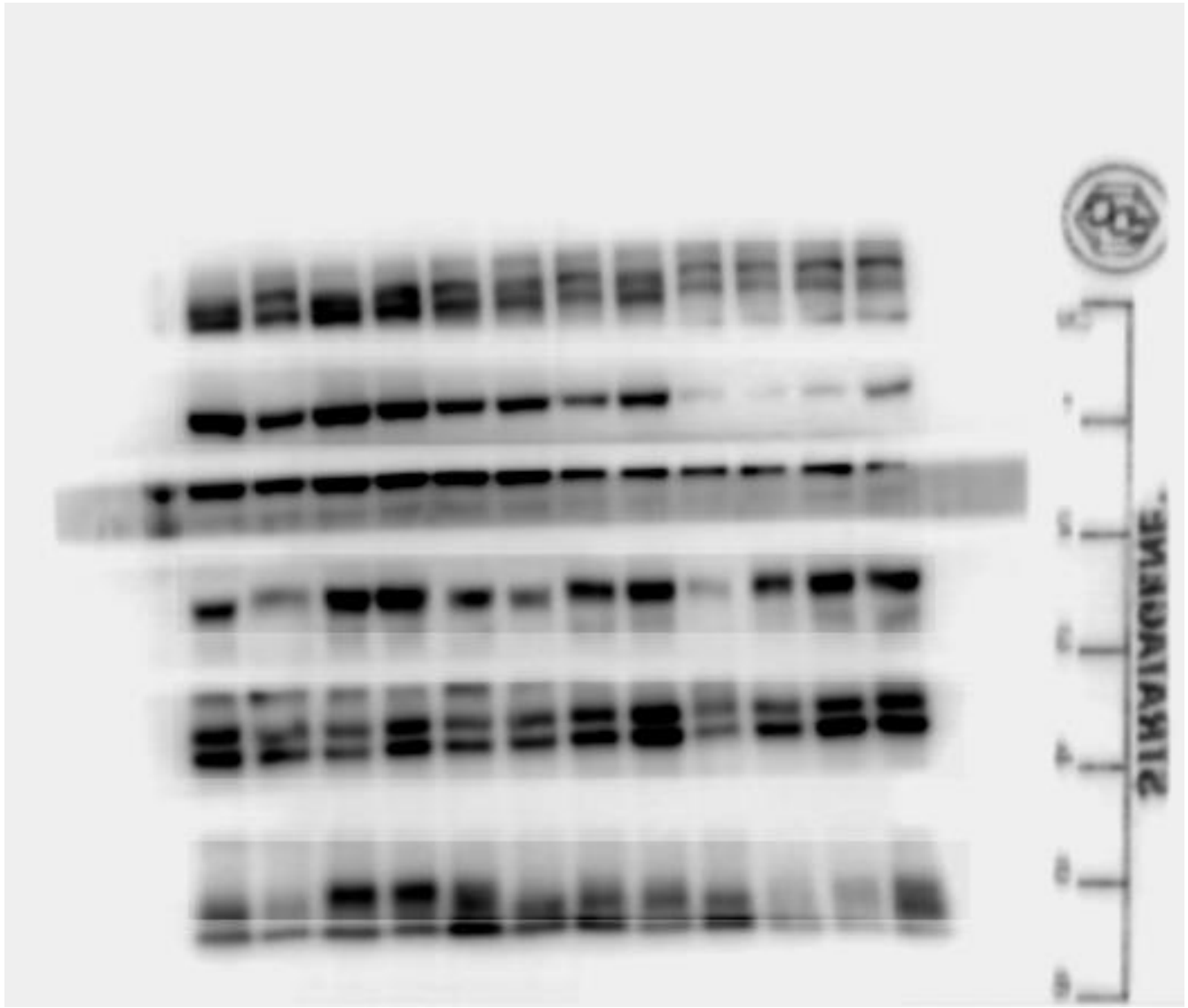
mTOR
ACLy
HSP90
p-p70S6K
p-ERK
p-S6

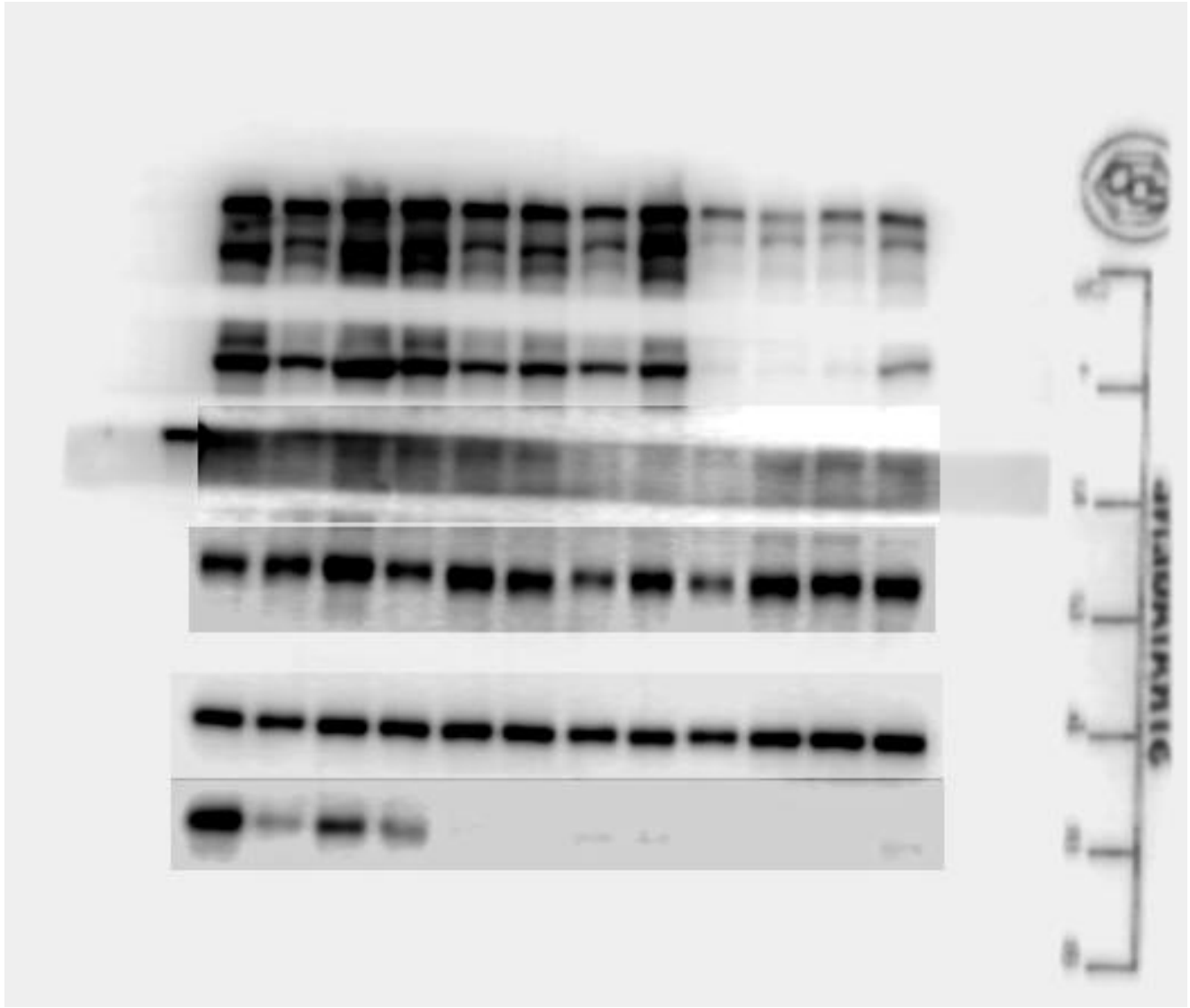
pACC
p-ACLy
PGC1a
p70S6K
Actin
SCD1

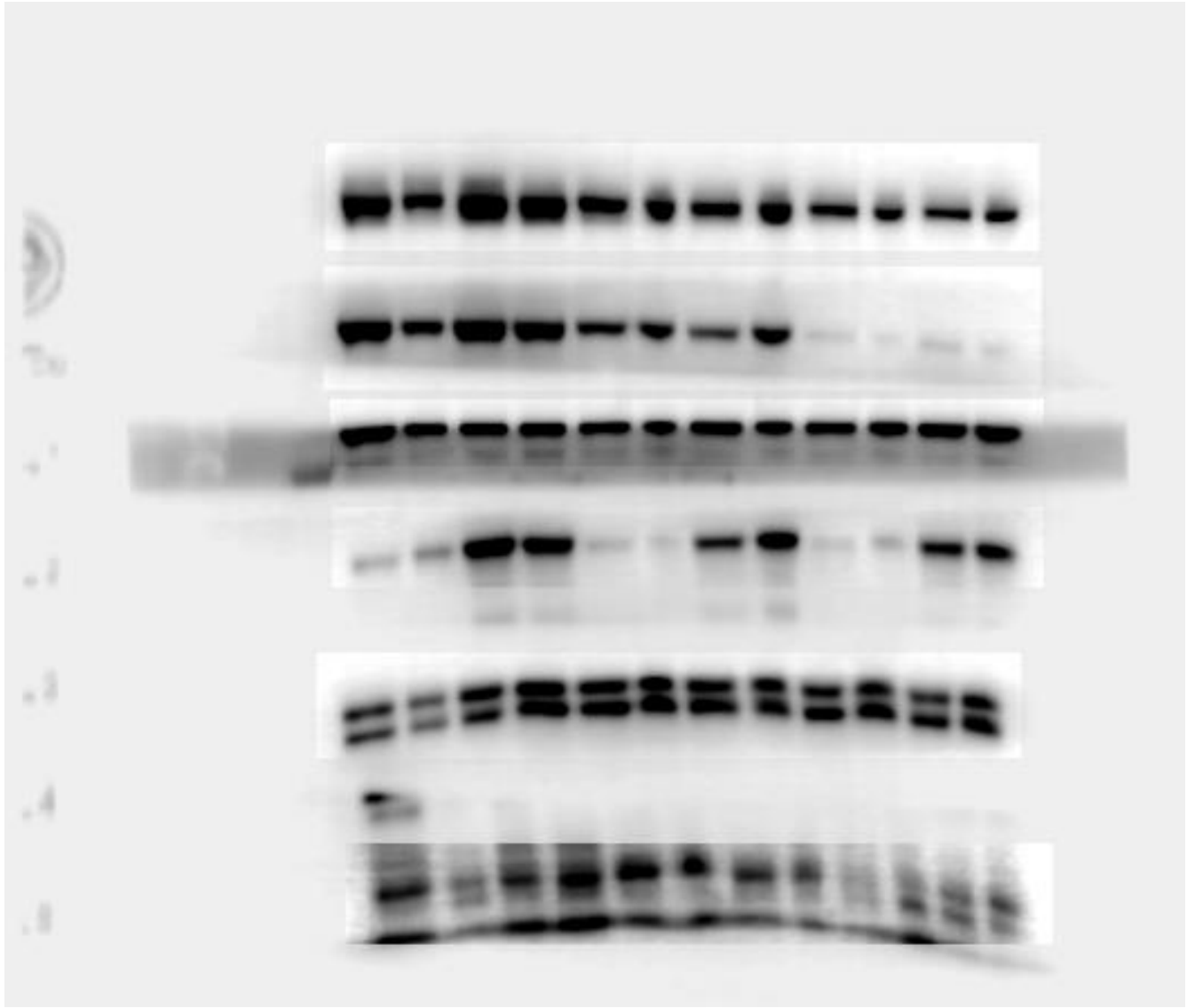
mTOR
ACLy
HSP90
pAKTthr
ERK
SCD1

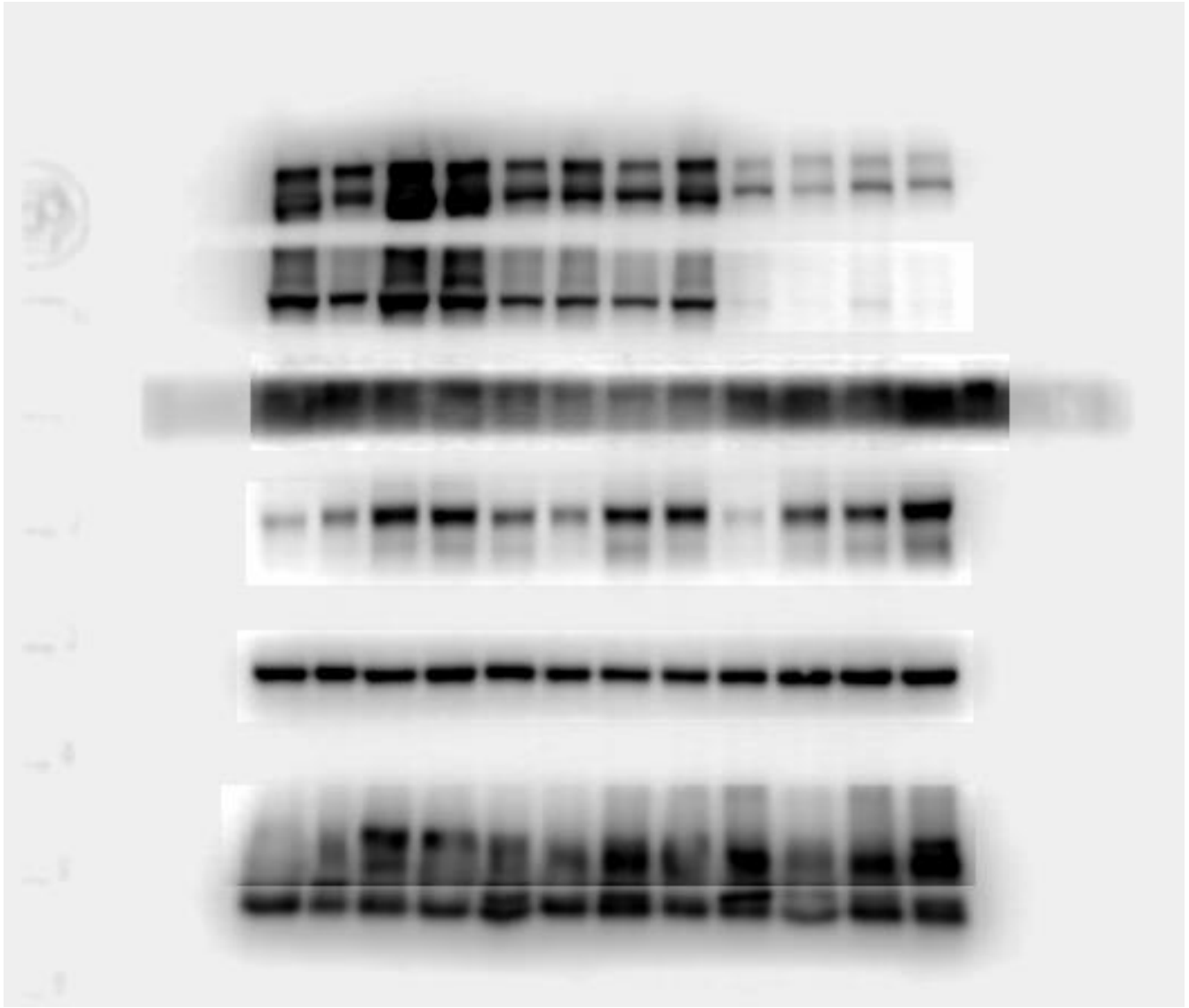
p-ACC
p-ACLy
PGC1a
p-p70S6K
Actin – FIG6G
p-S6

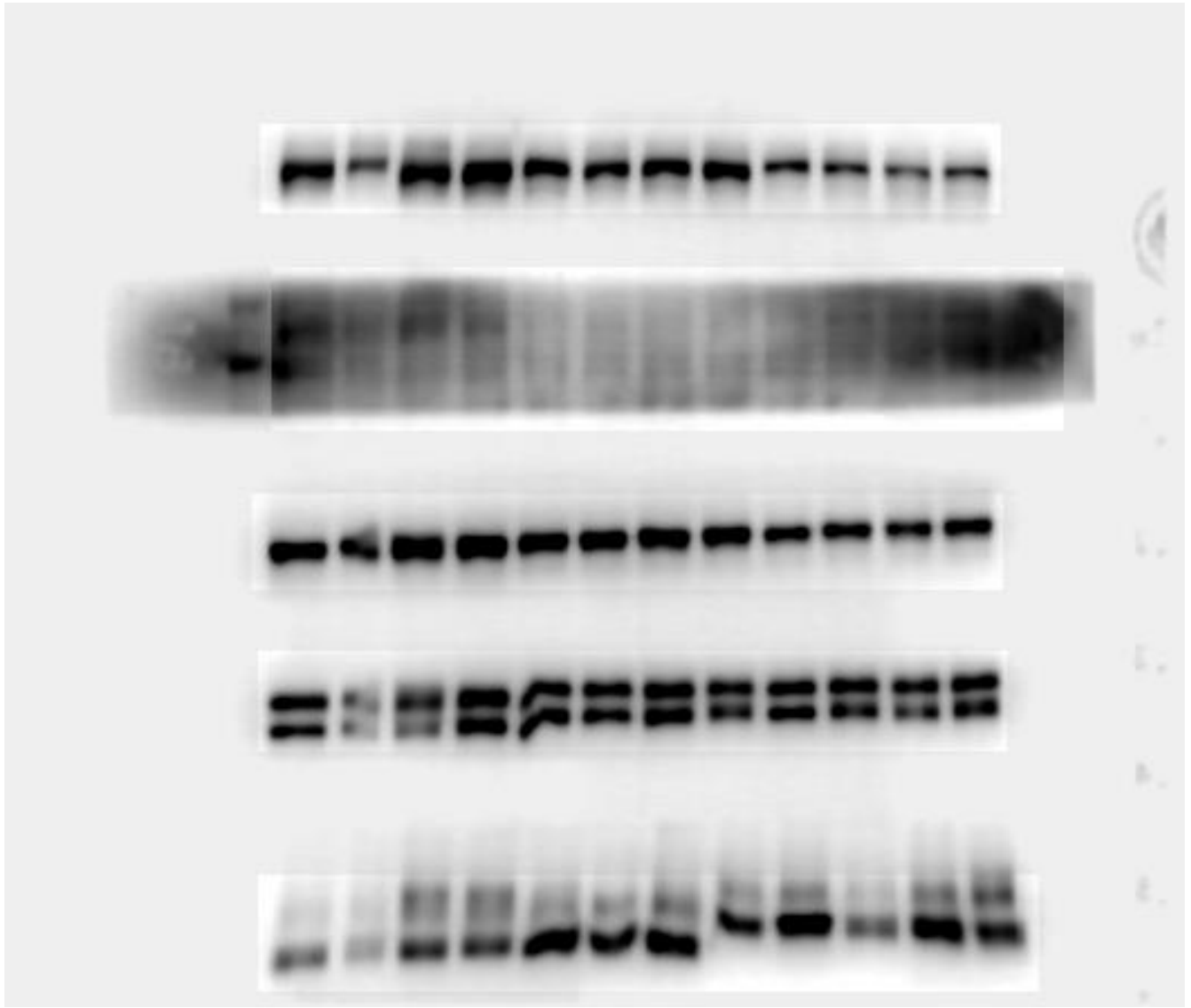
mTOR
PGC1a
AKT
ERK
p-S6

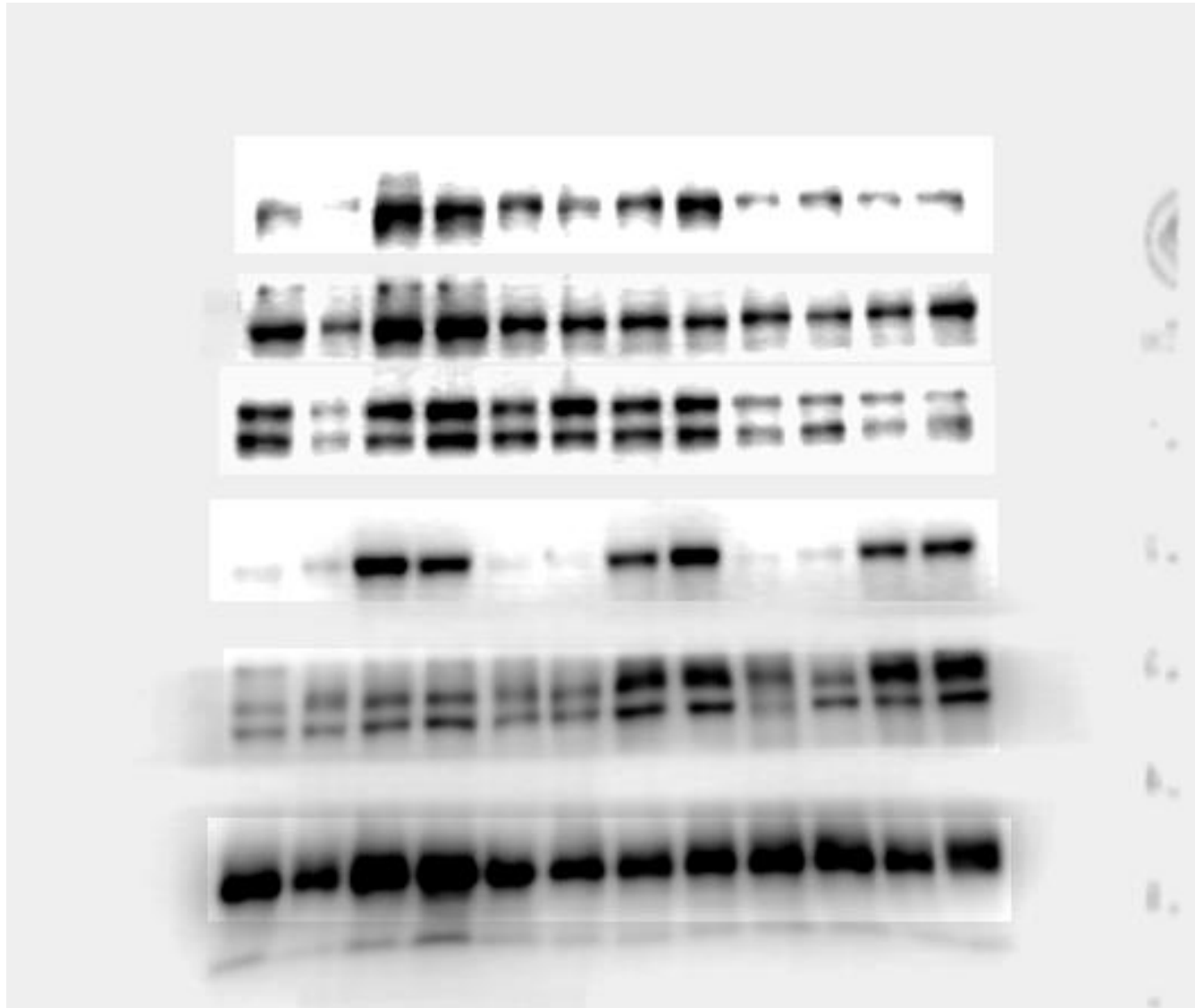
p-mTOR
iNOS
p-PKC
p-AKTthr
p-ERK
S6

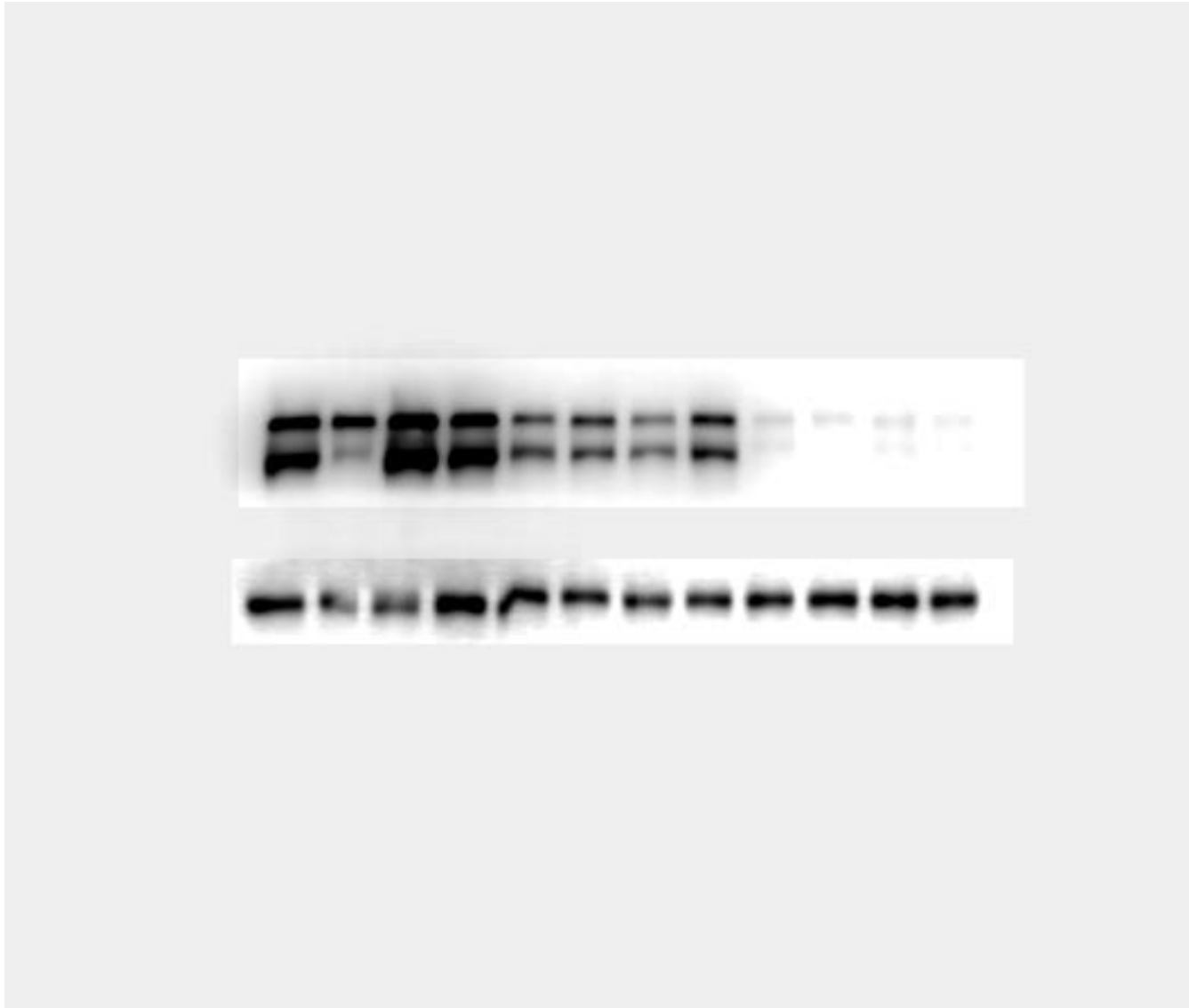
ACC
Actin

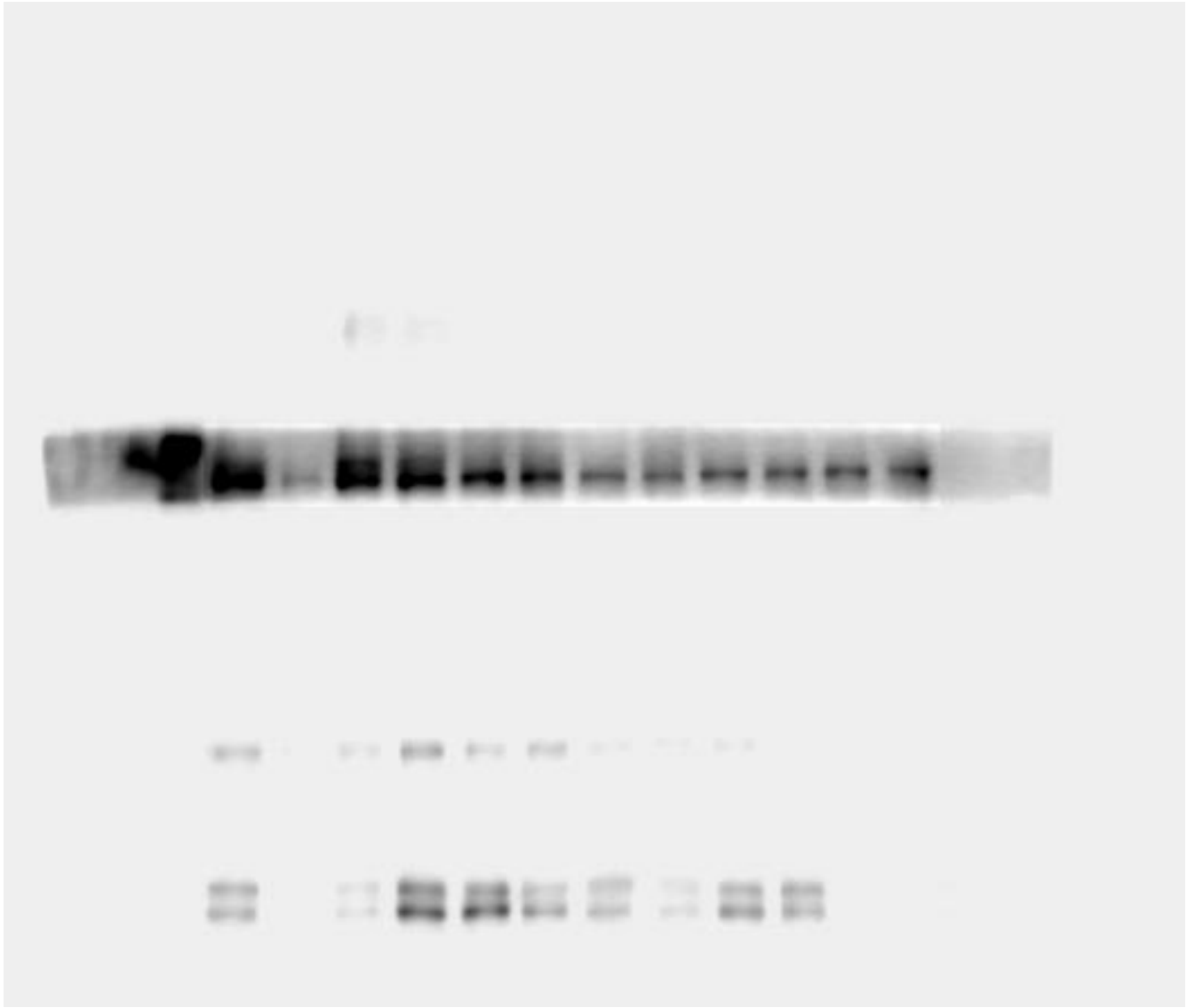
PKC
AKT
ERK

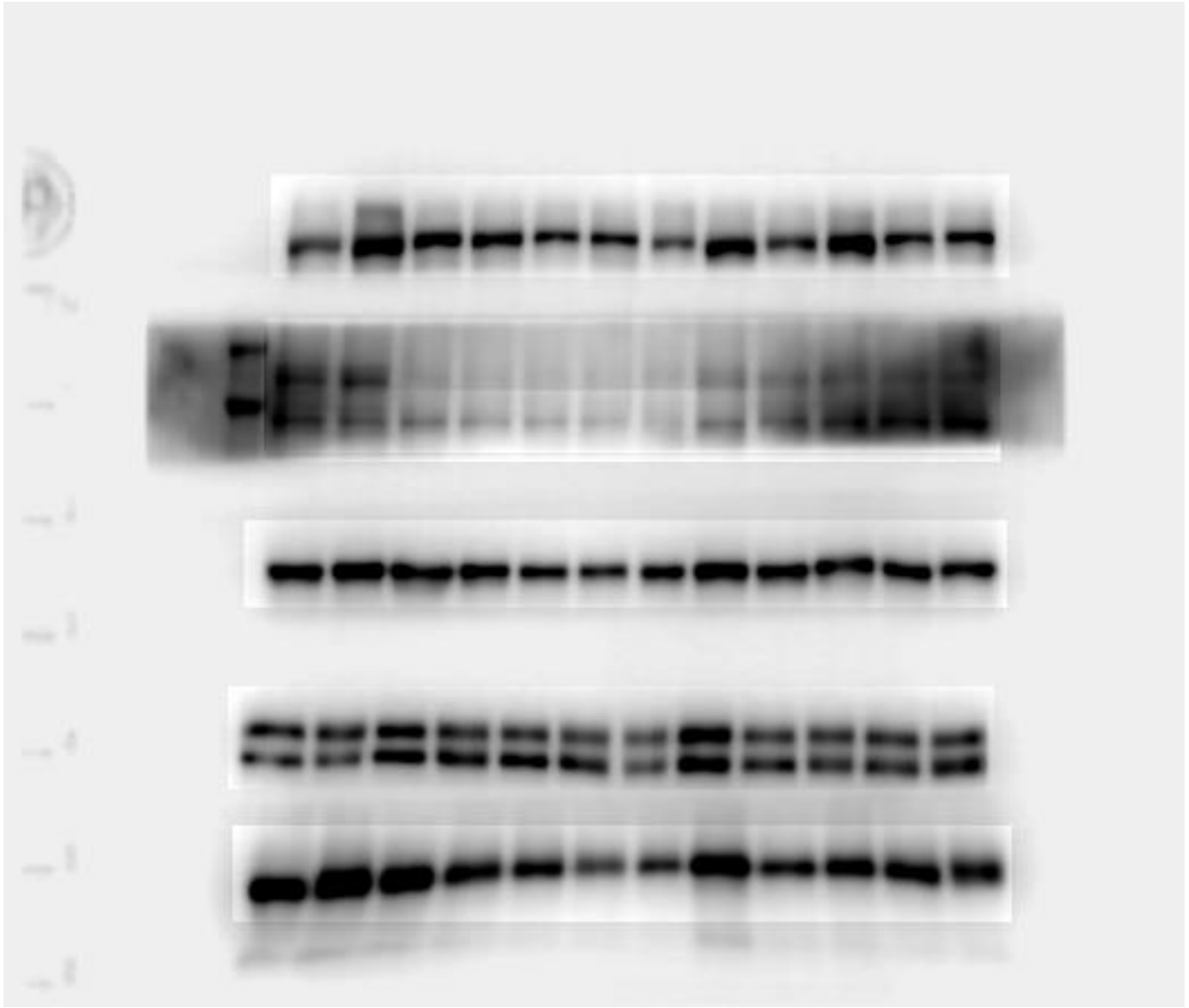
p-mTOR
PGC1a
AKT
ERK
S6

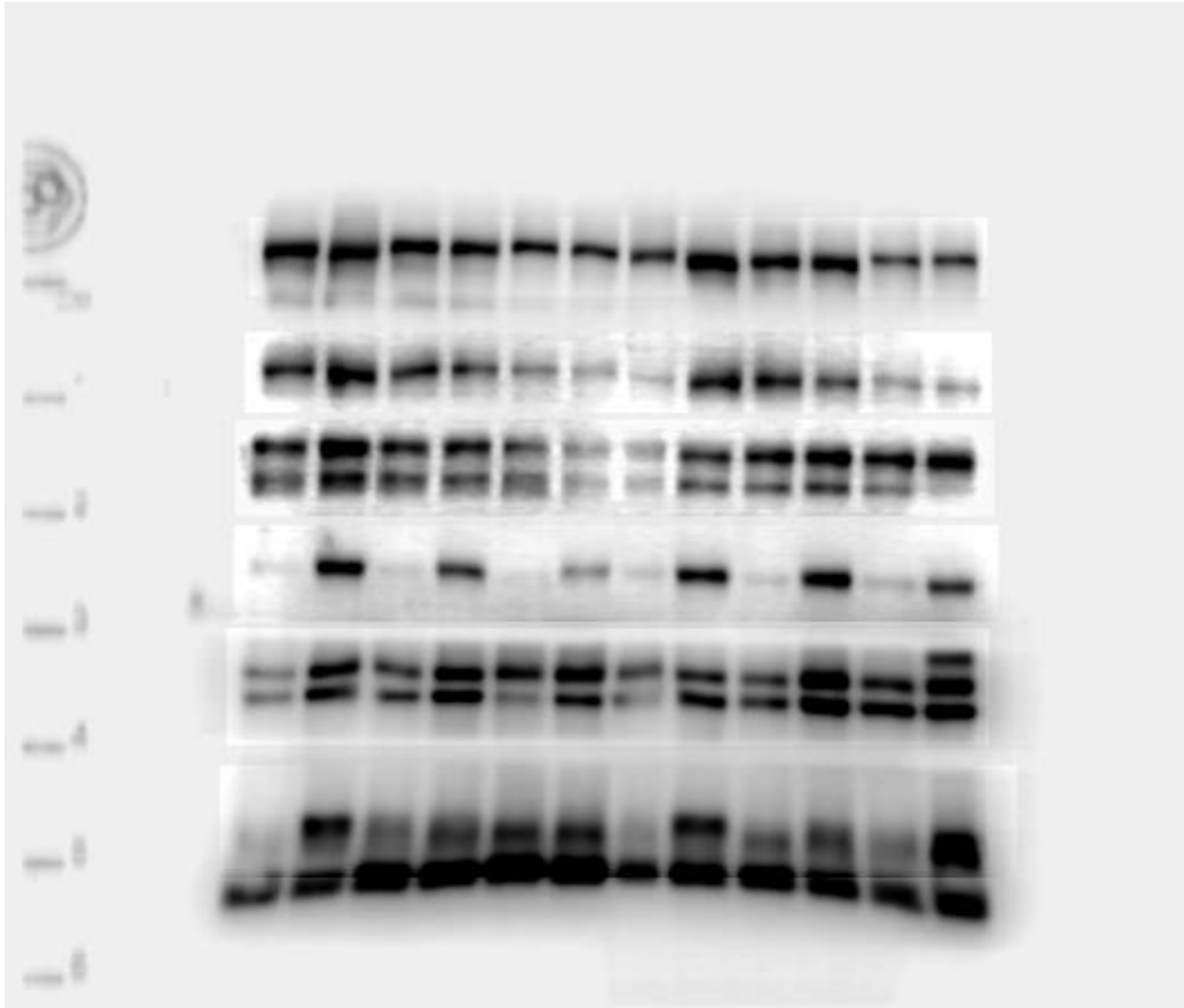

mTOR – FIG6G

iNOS

p-PKC

p-AKTser – FIG6G

p-ERK

p-S6

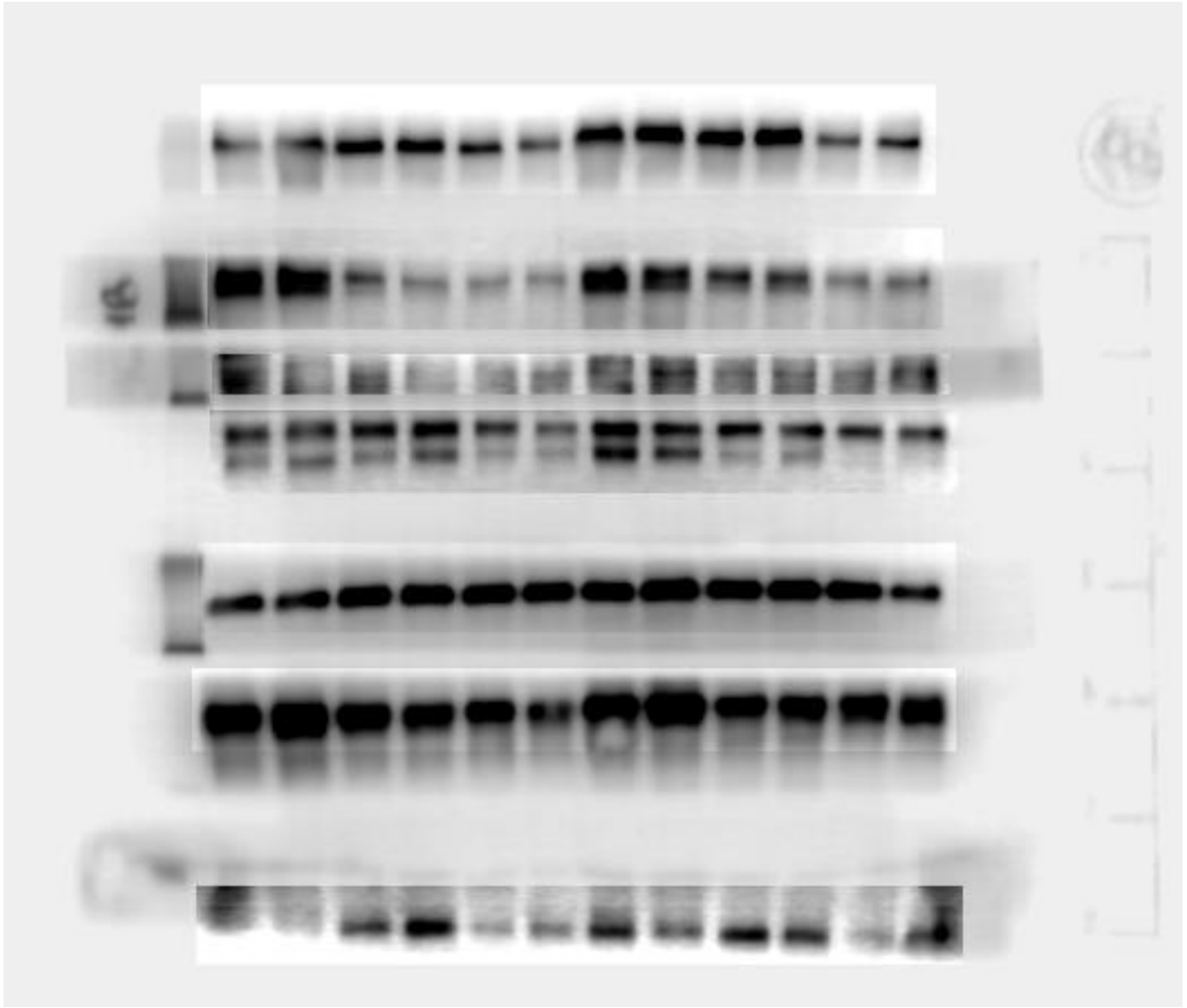

mTOR

iNOS – FIG5H

PGC1a

PPARg – FIG6A

p-CREB

S6

TNFa

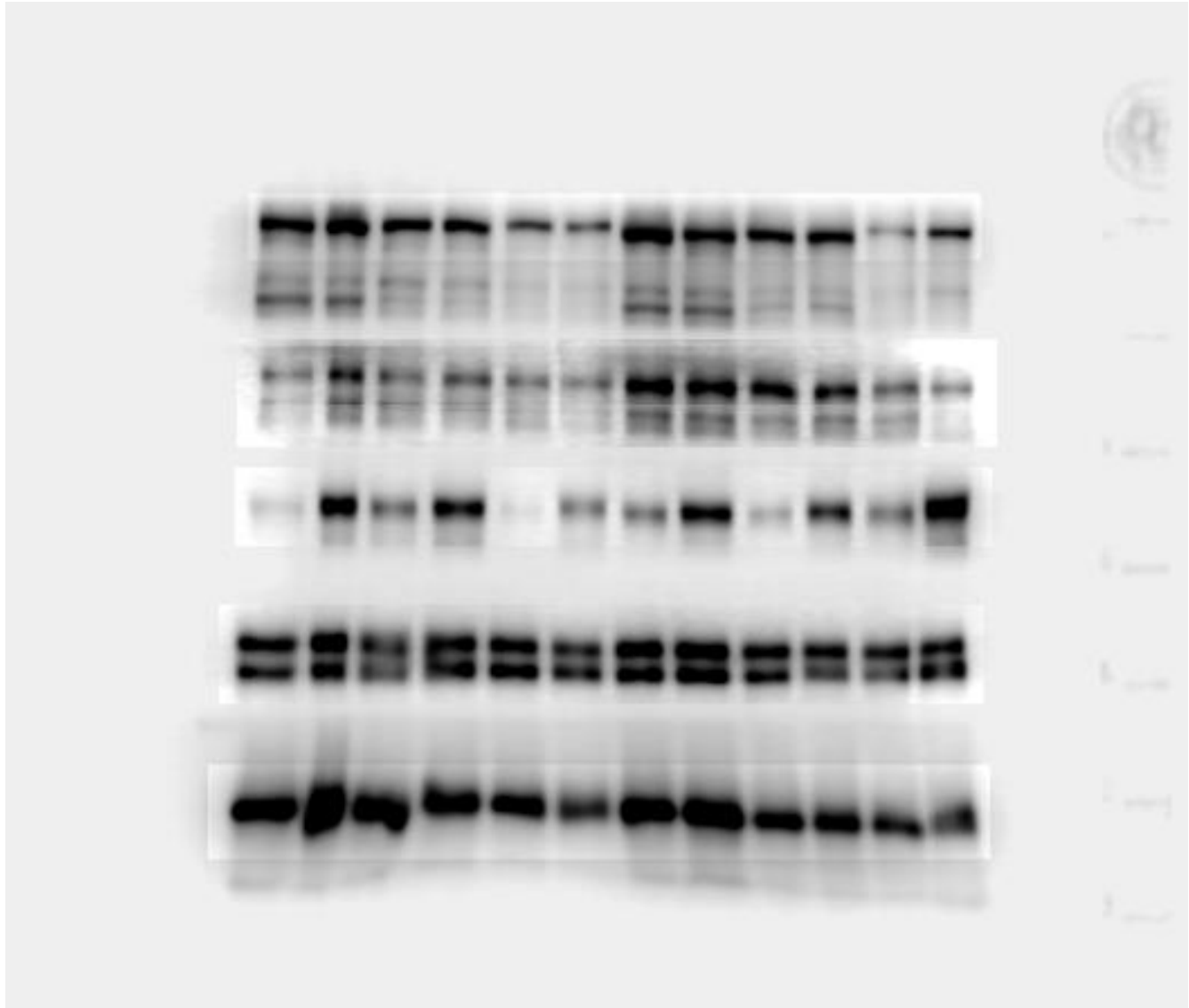
mTOR
p-PKC
p-P70S6k – FIG6G
ERK
S6

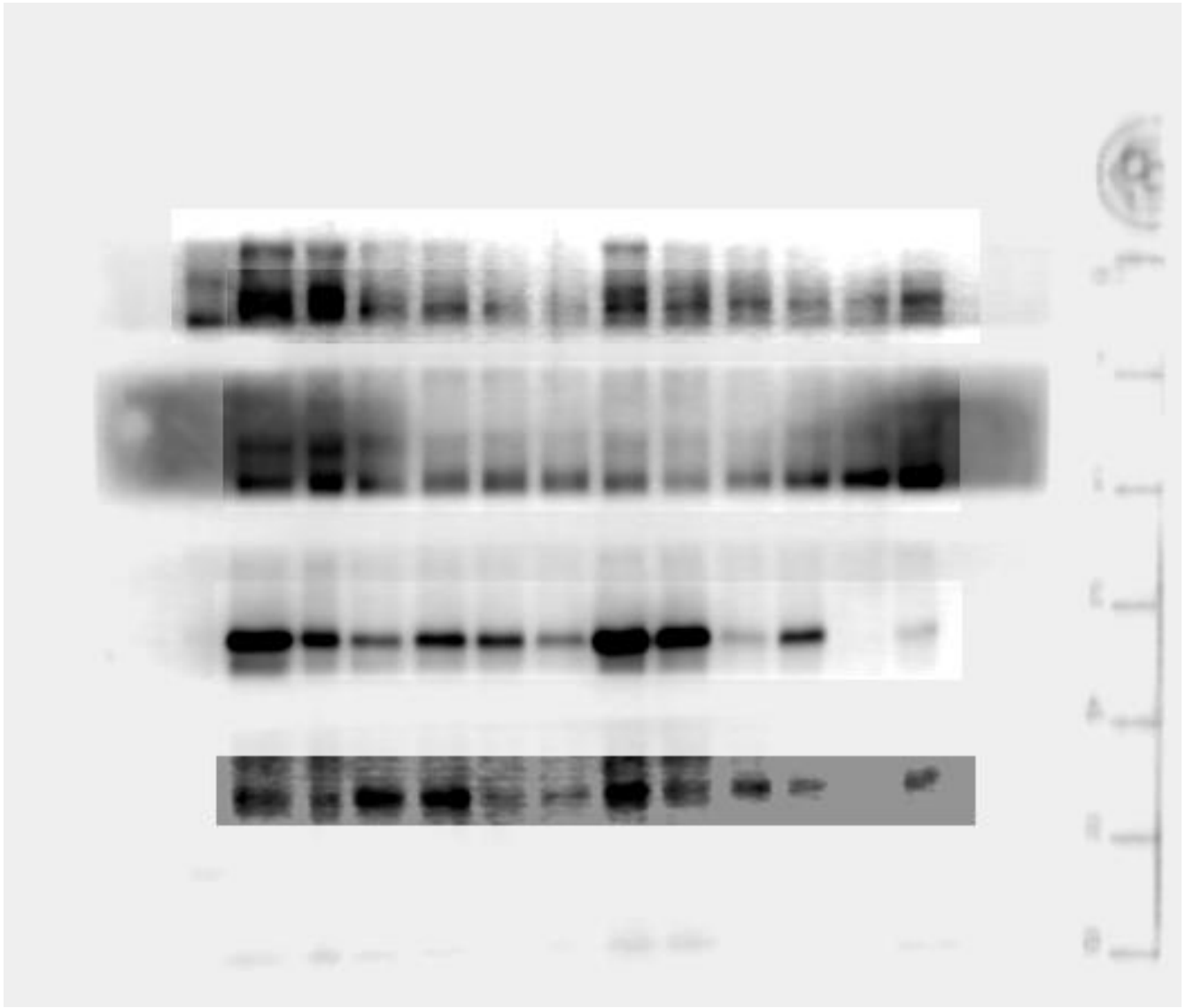

TLR4

PGC1a

SCD1 – FIG6A

TNFa

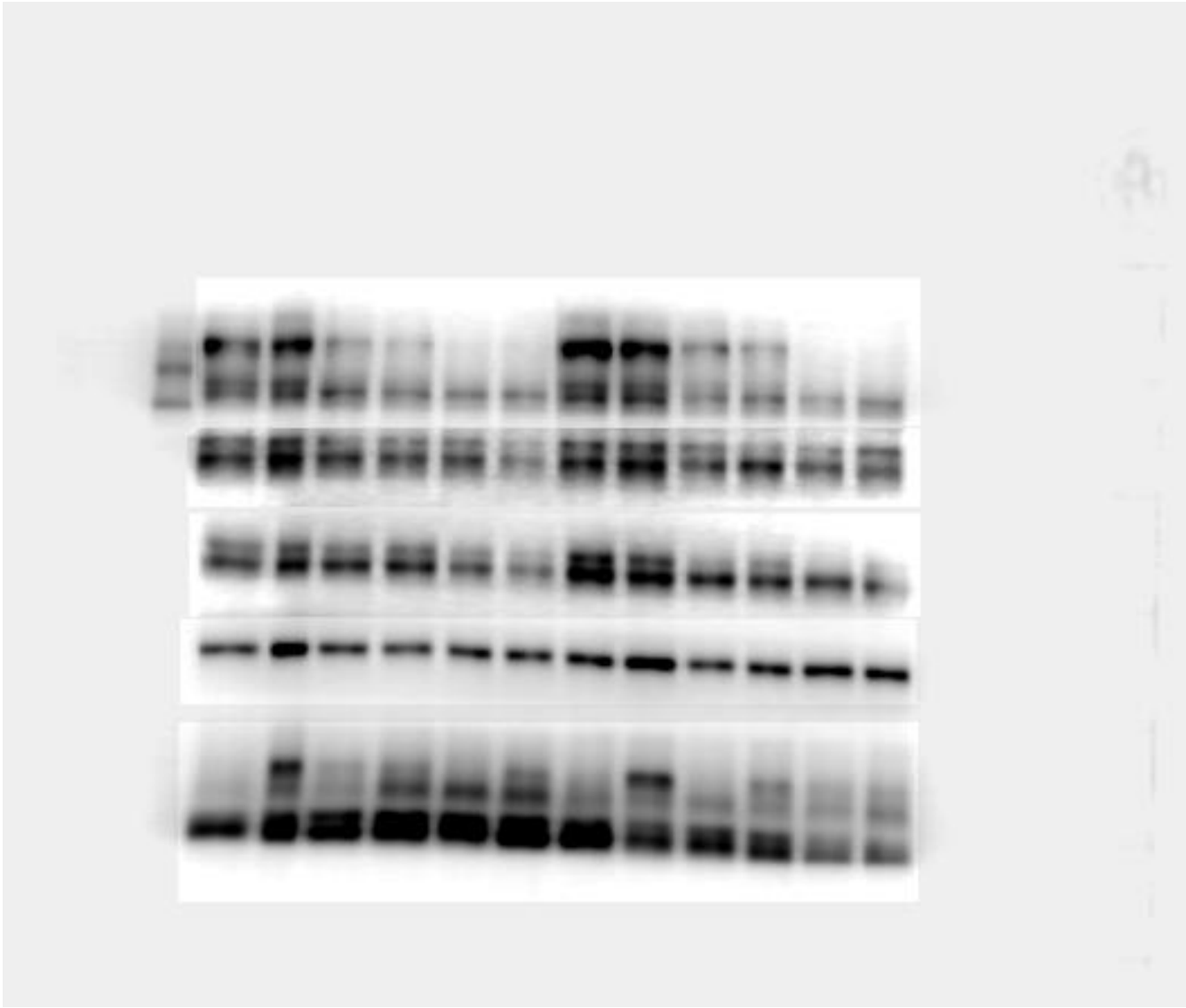

TLR4 – FIG5H

p-PKC

PPARg

Actin

p-S6

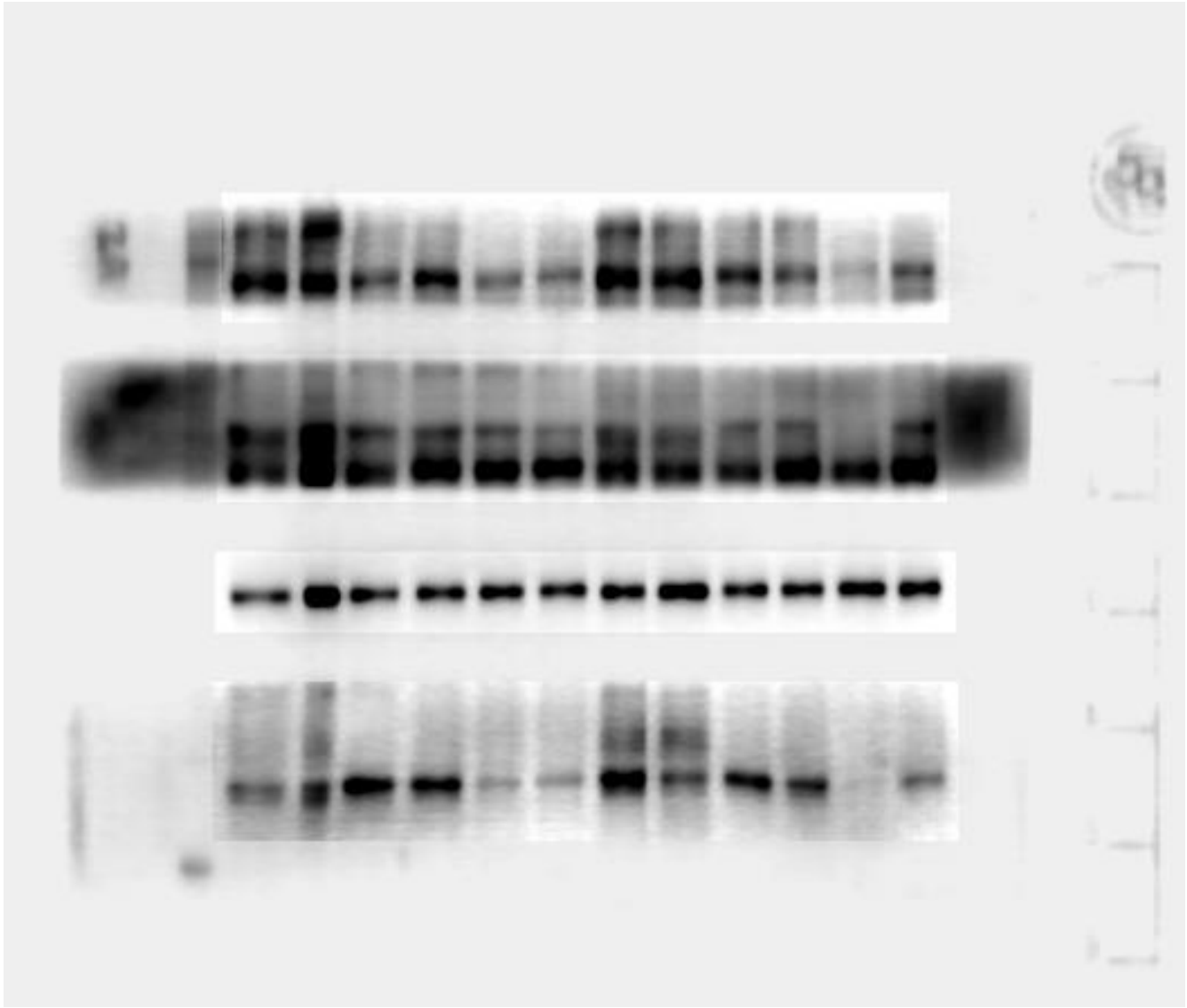
iNOS
PGC1a – FIG6A
Actin
TNFa – FIG5H

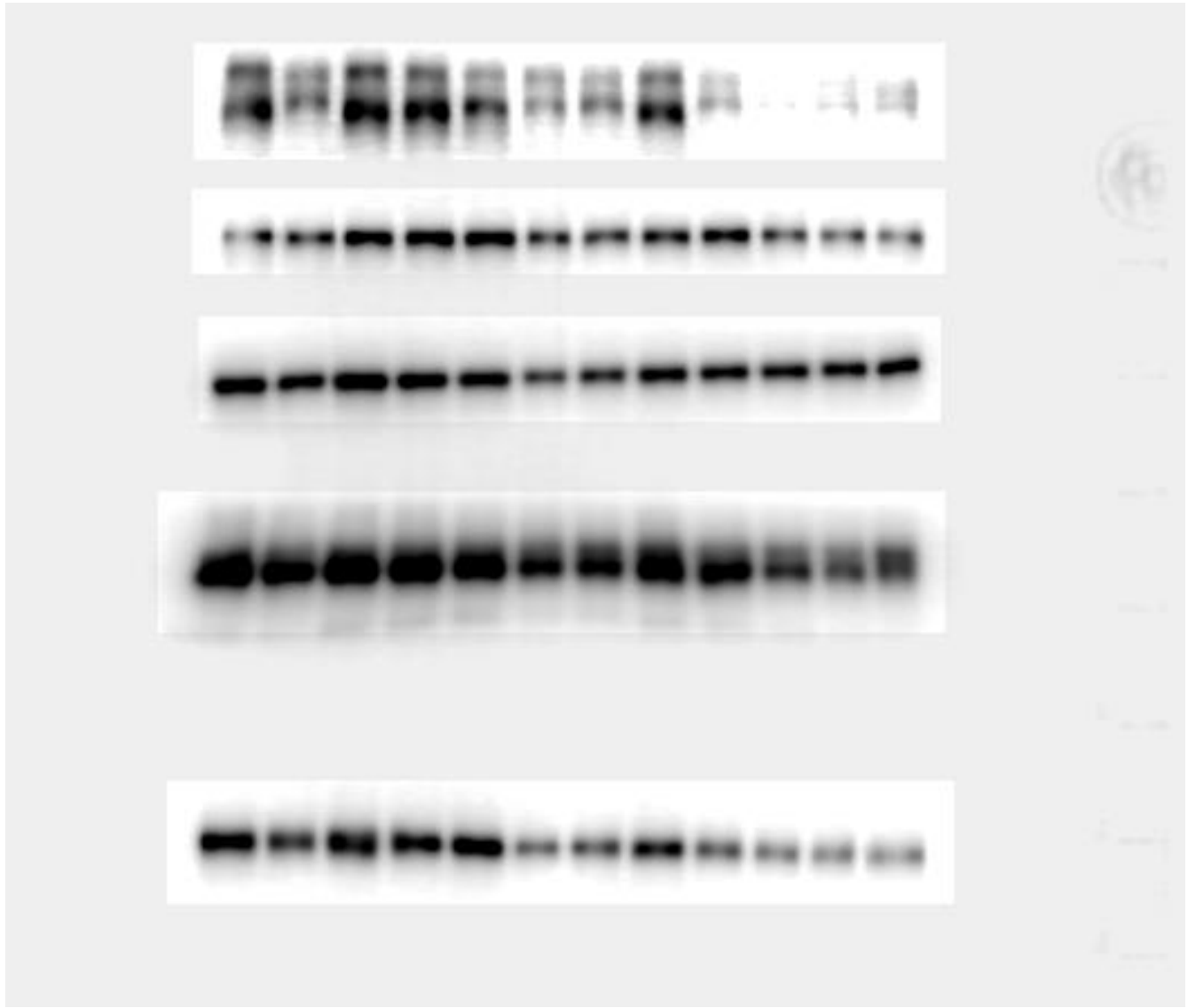
mTOR
eEF2
Actin
S6
GAPDH

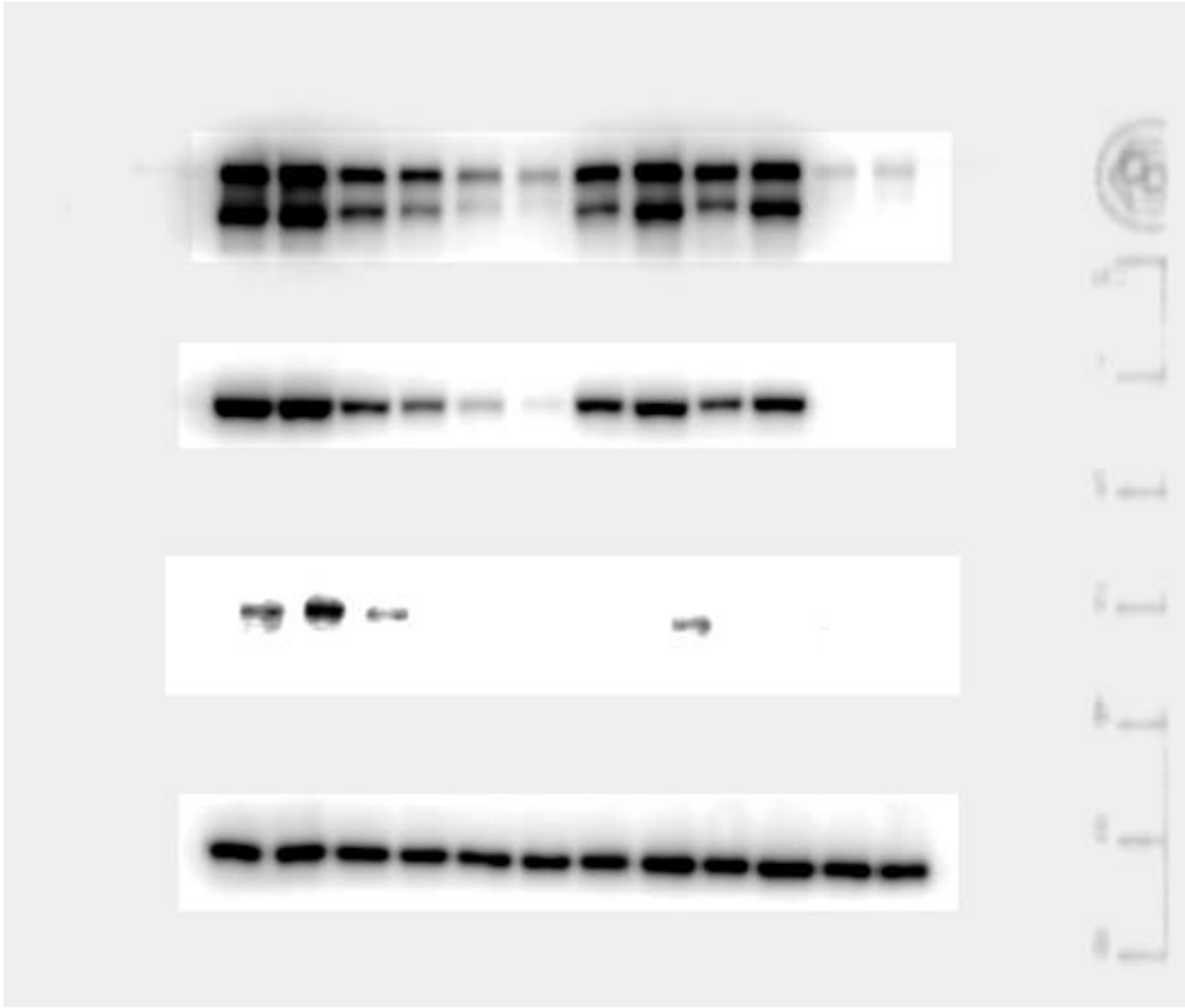

ACC – FIG6A

ACLy

p70S6K

Actin – FIG6A

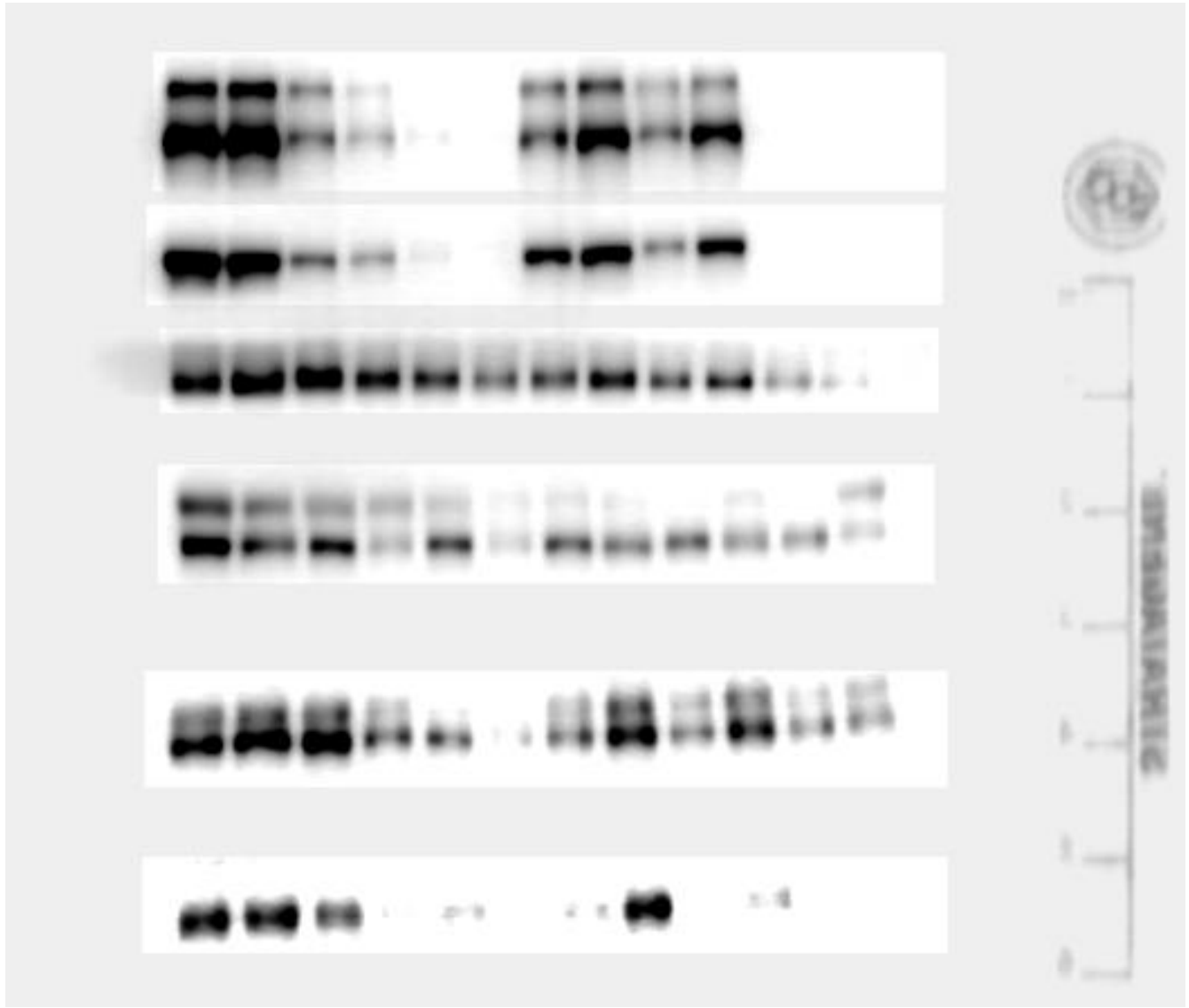
ACC
ACLy
IRb
AKT
ERK
S6

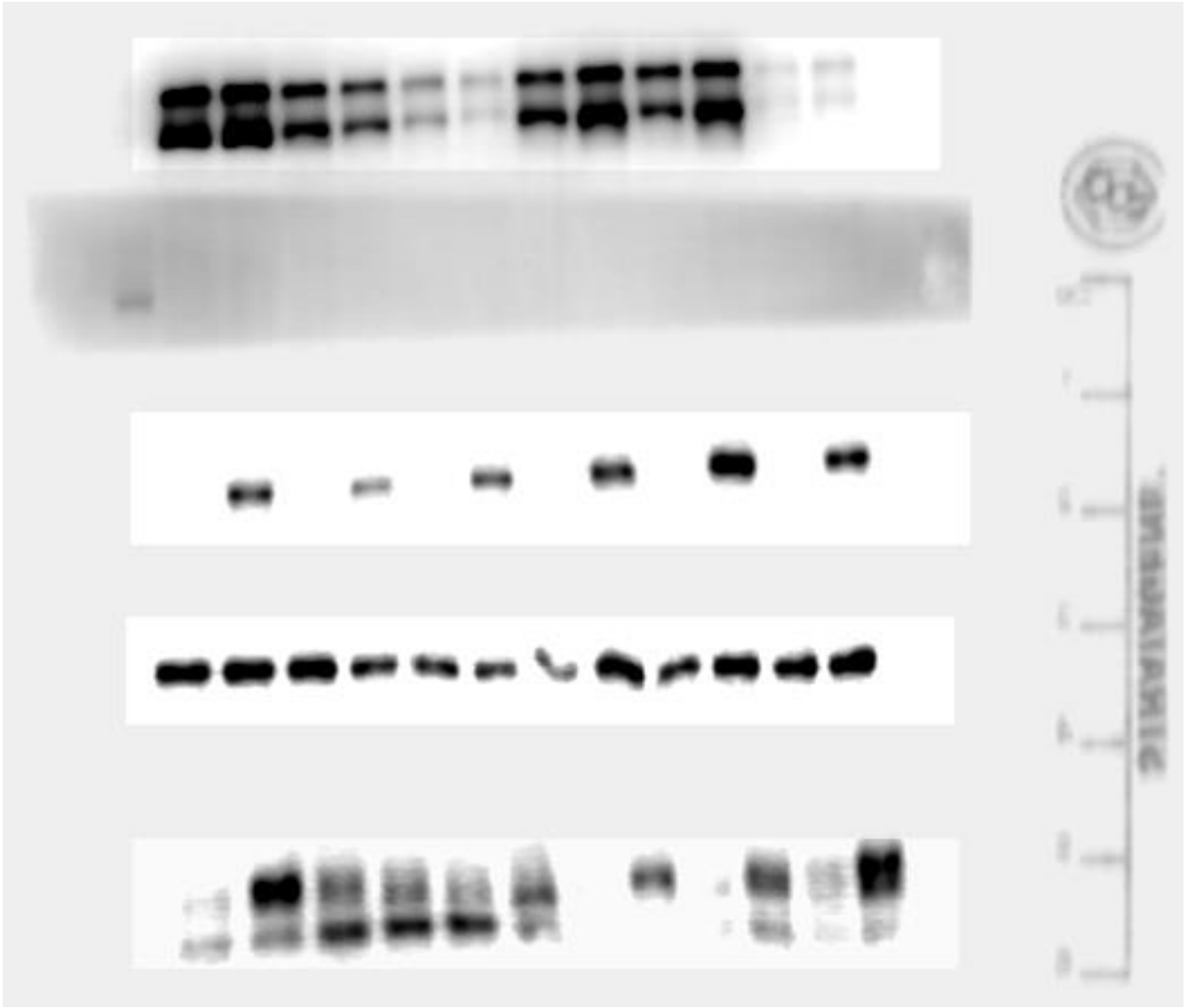
p-ACC
PGC1a
p-AKTthr
Actin
p-S6

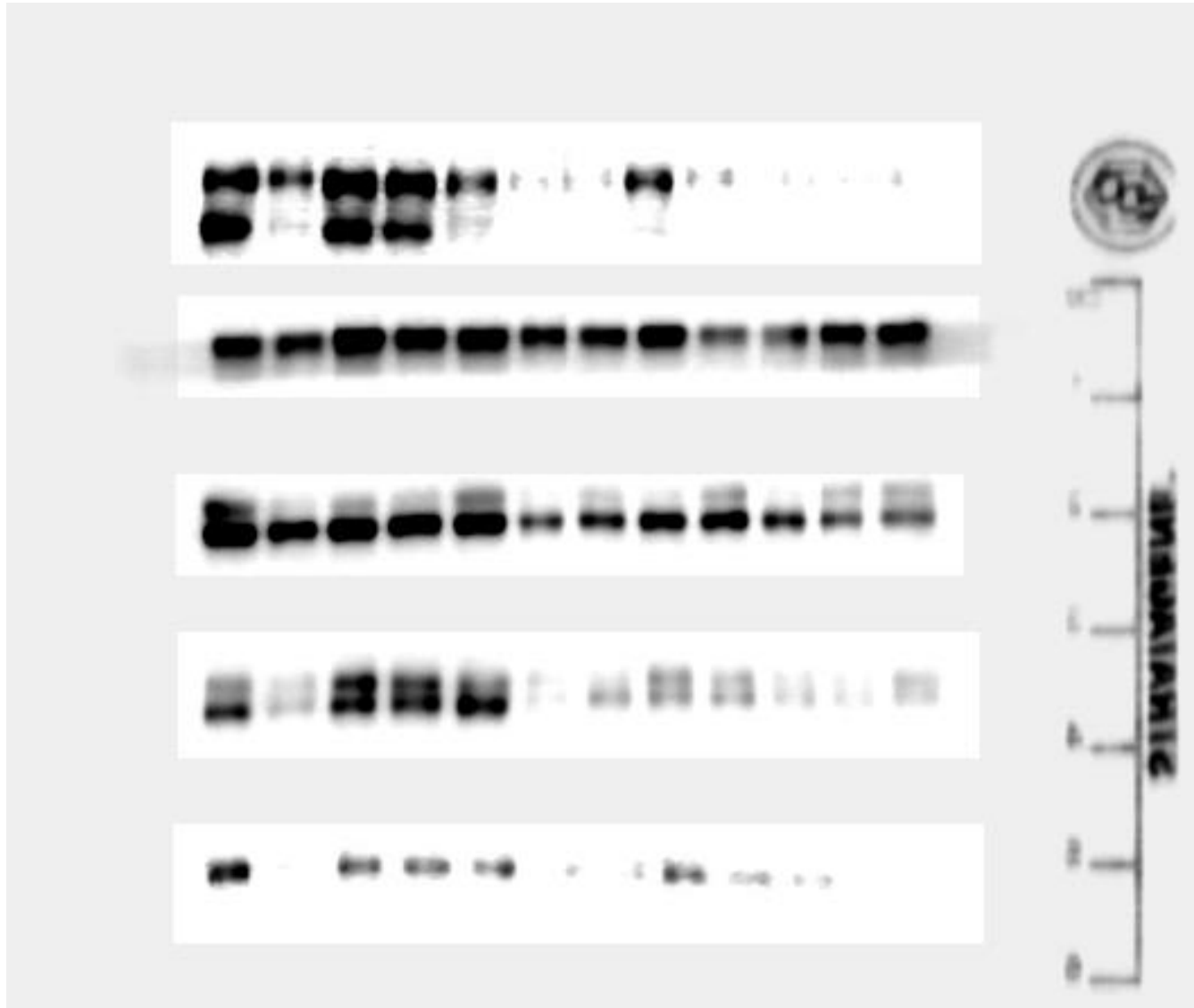
mTOR
IRb
AKT
ERK
S6

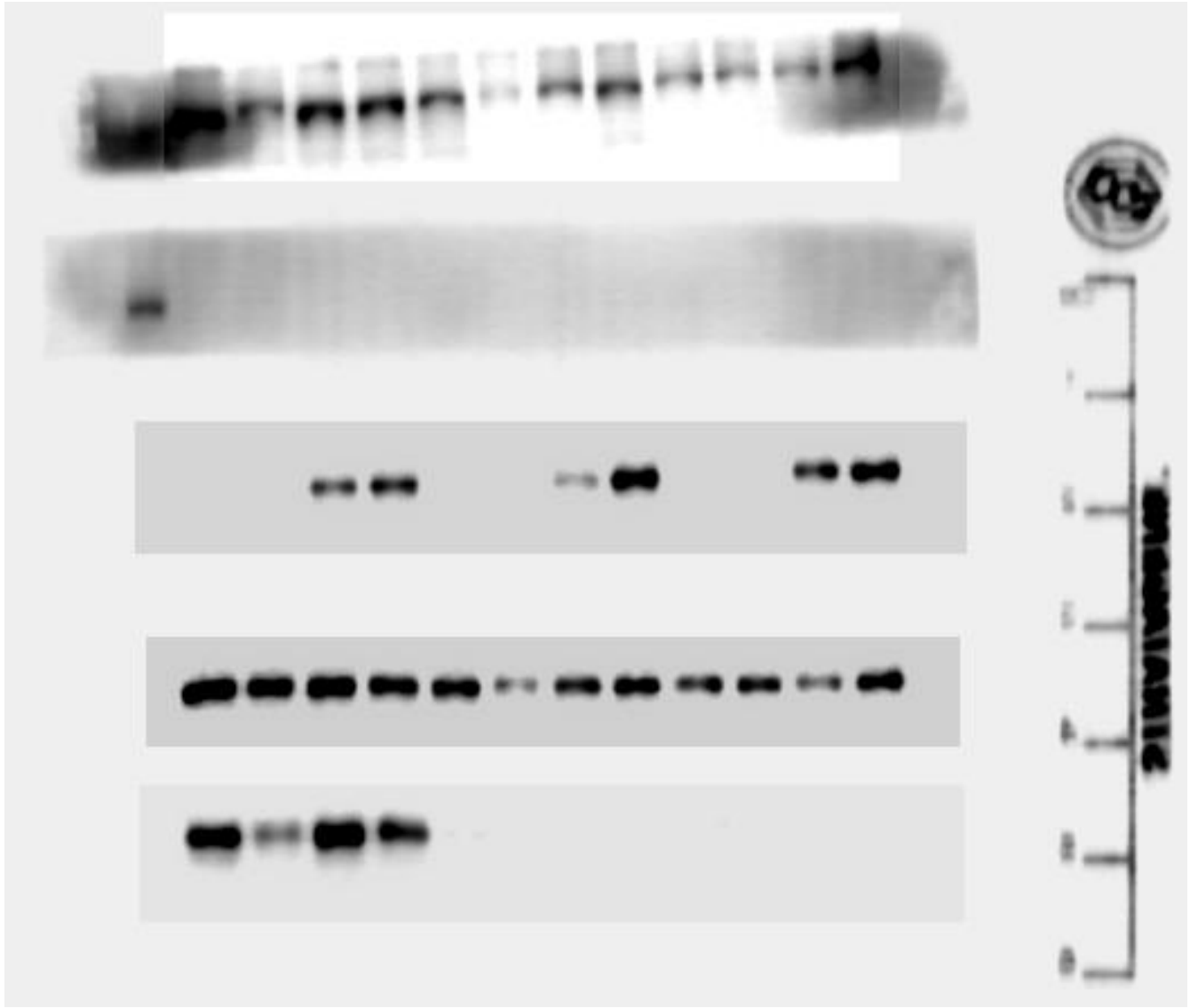
p-mTOR
PGC1a
p-AKTthr
Actin
SCD1

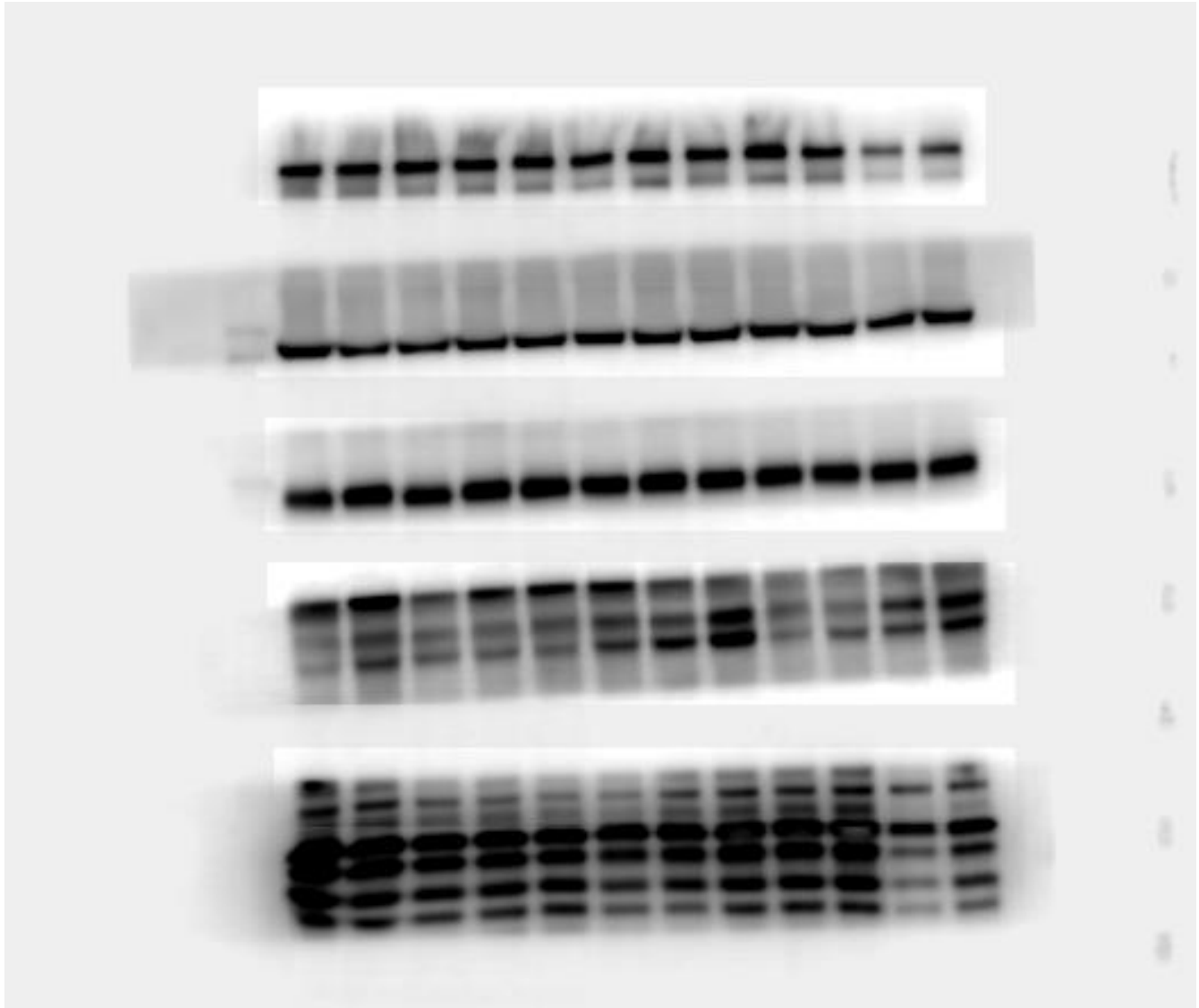
p-ACC
PGC1a
AKT – FIG4A
p-ERK
ARG1

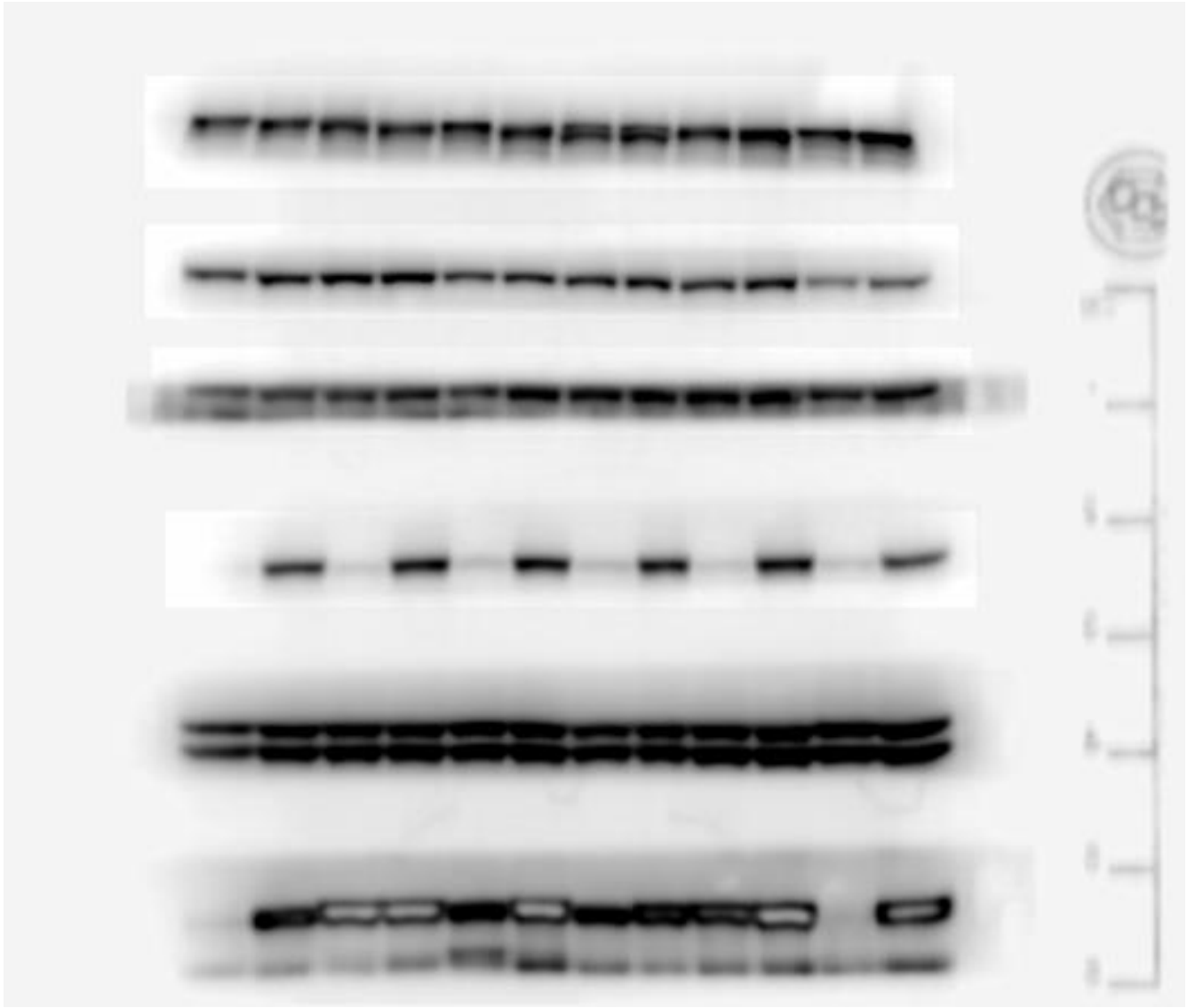
mTOR – FIG4A
ACLy
HSP90
p-AKTser
ERK
p-S6

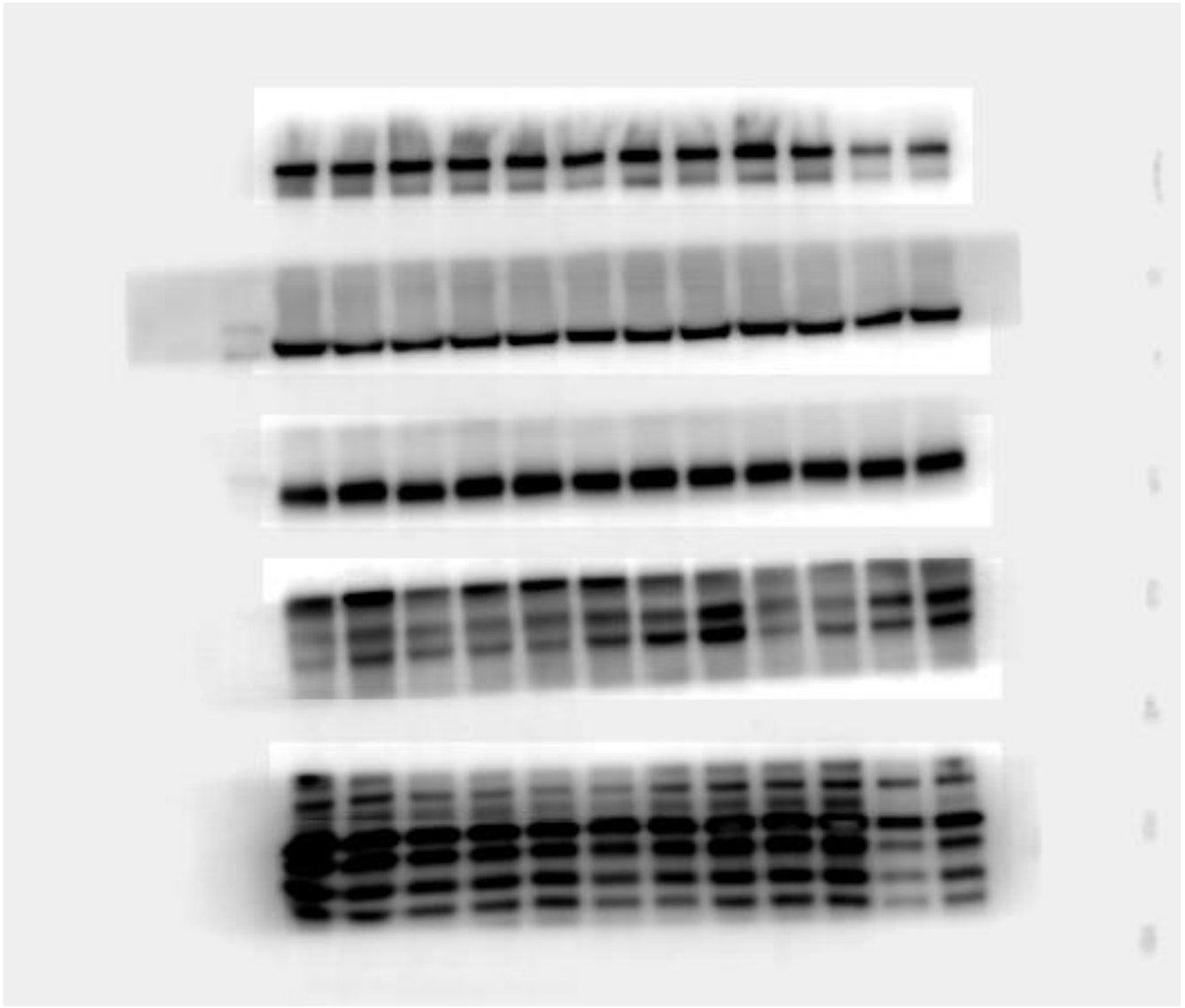
p-ACC
PGC1a
AKT
p-ERK
ARG1

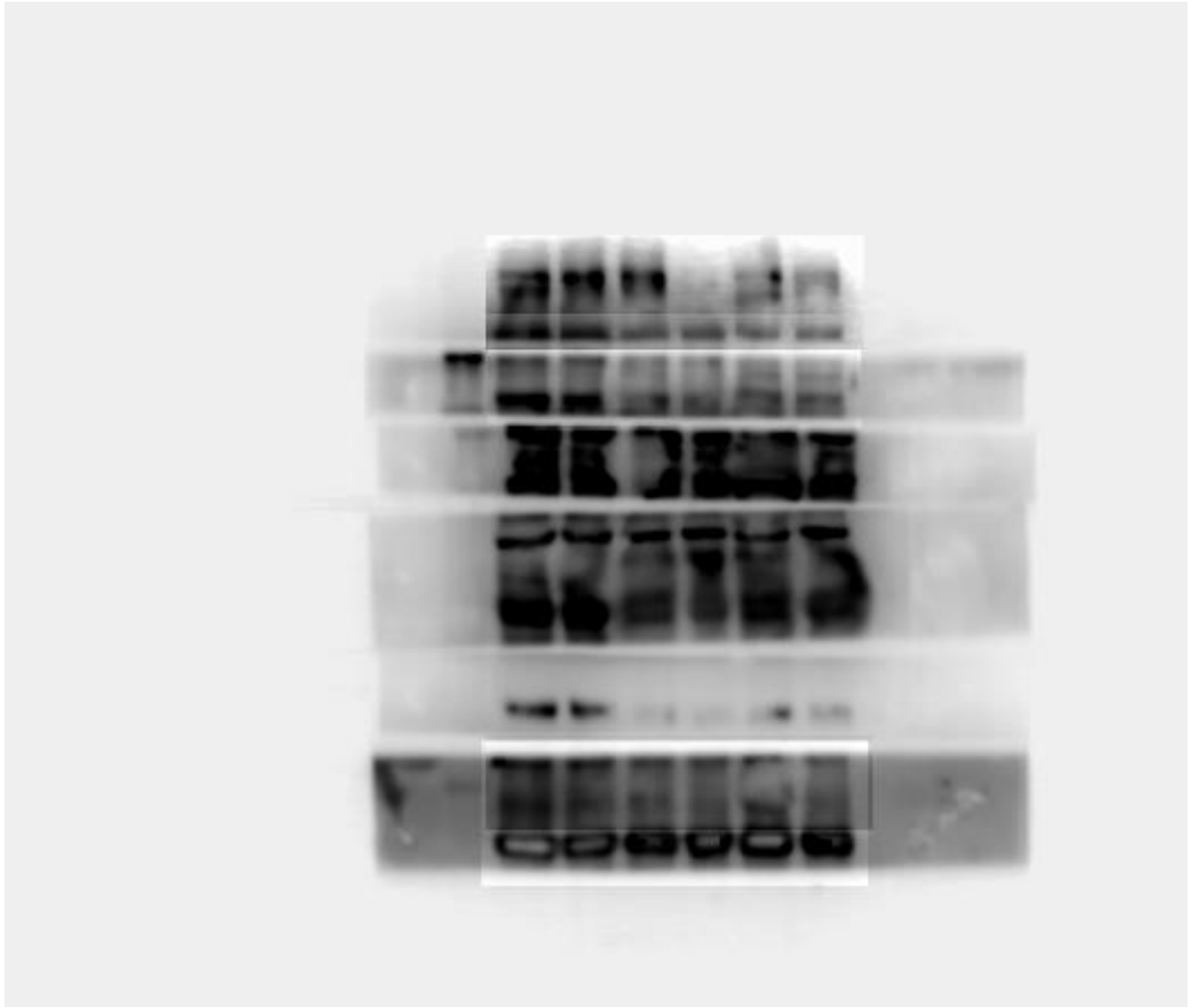
mTOR
SIRT
ATF6
p53
Actin
PCNA

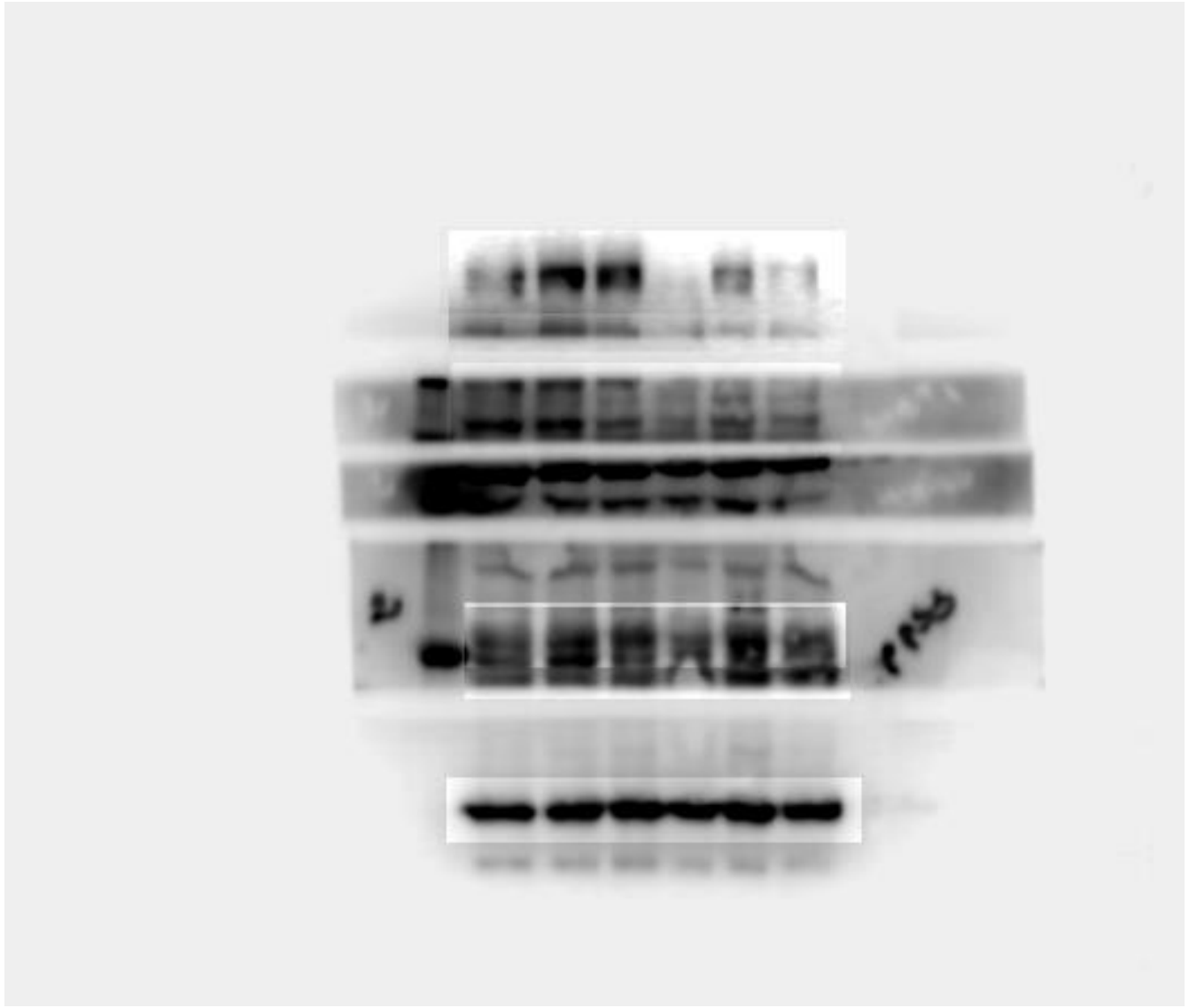

p-mTOR

SIRT – FIG3U

HSP90

p-p53 - FIG3U

GAPDH – FIG3U

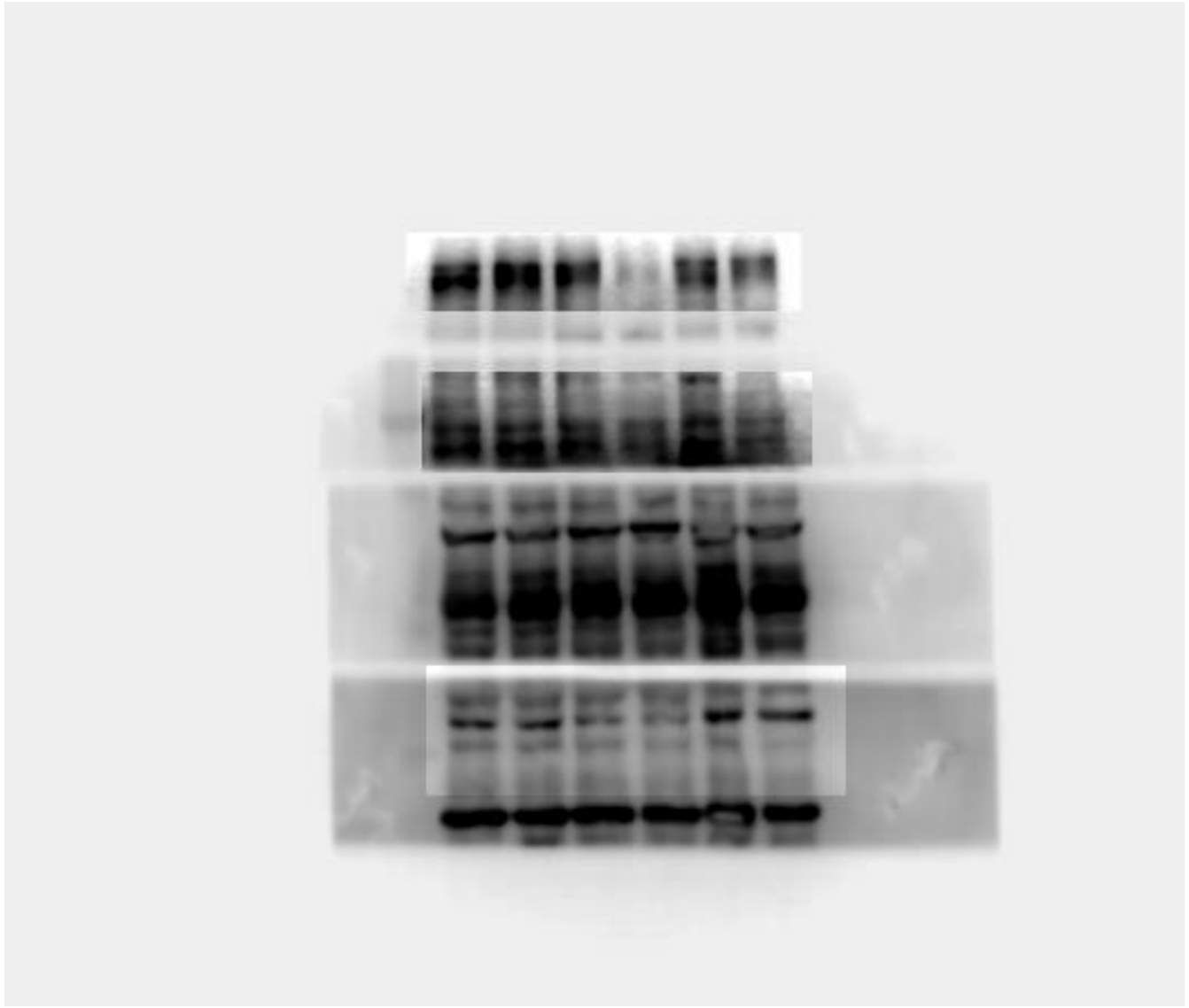

mTOR

p-RB

p53 - FIG3U

PCNA – FIG3U

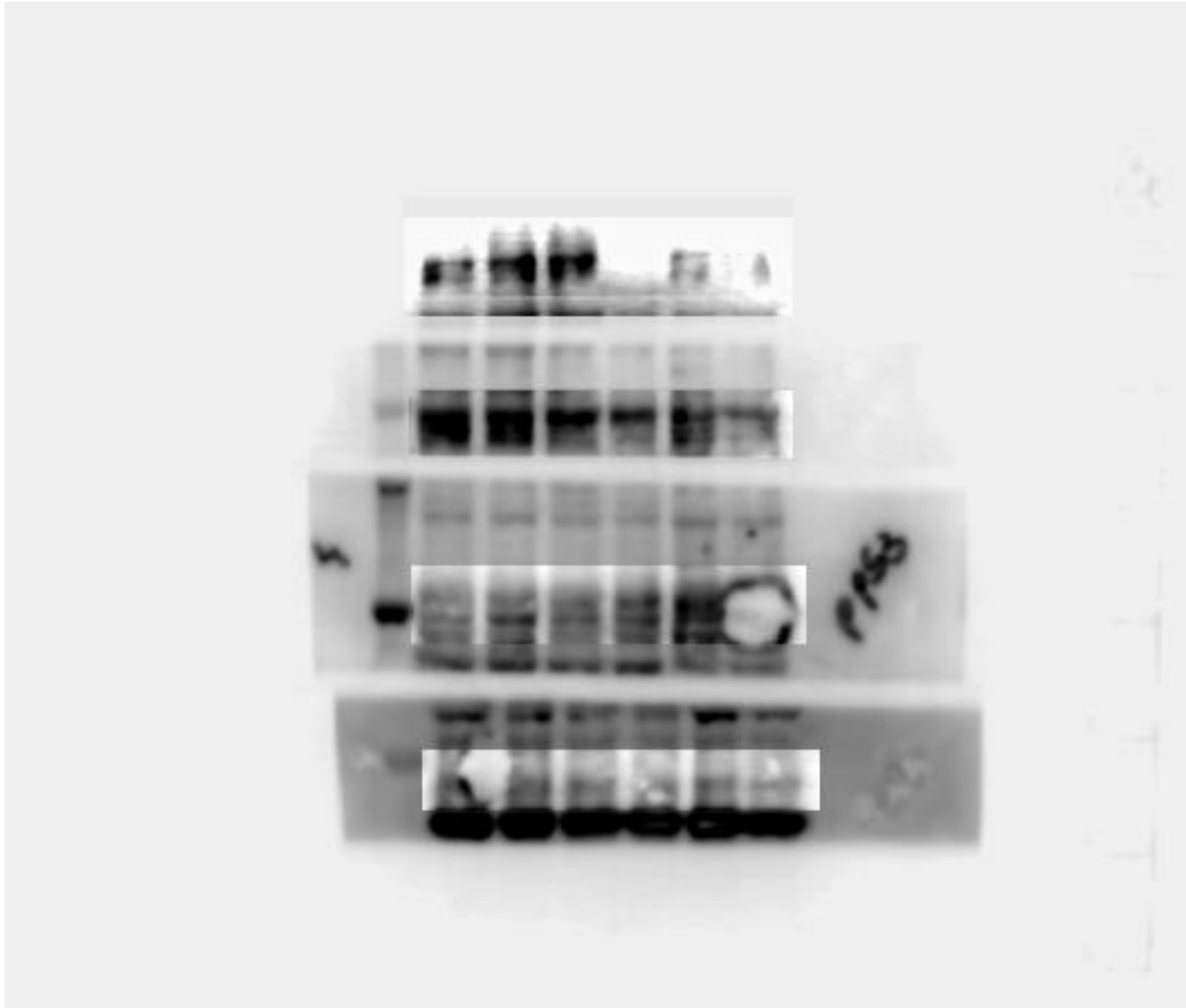
p-mTOR
p-RB – FIG3U
p-p53
PCNA

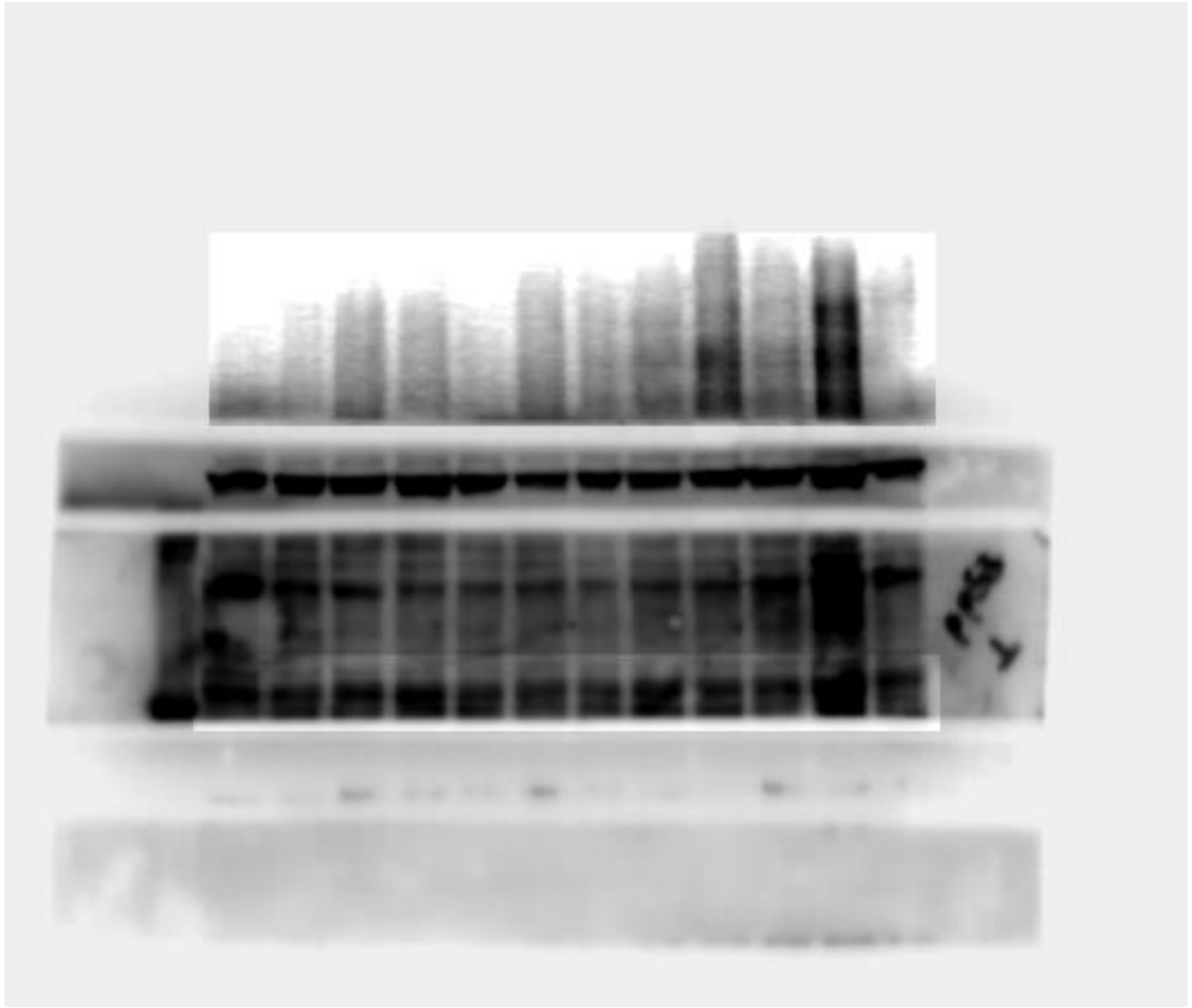
SIRT
HSP90
p-p53
PCNA

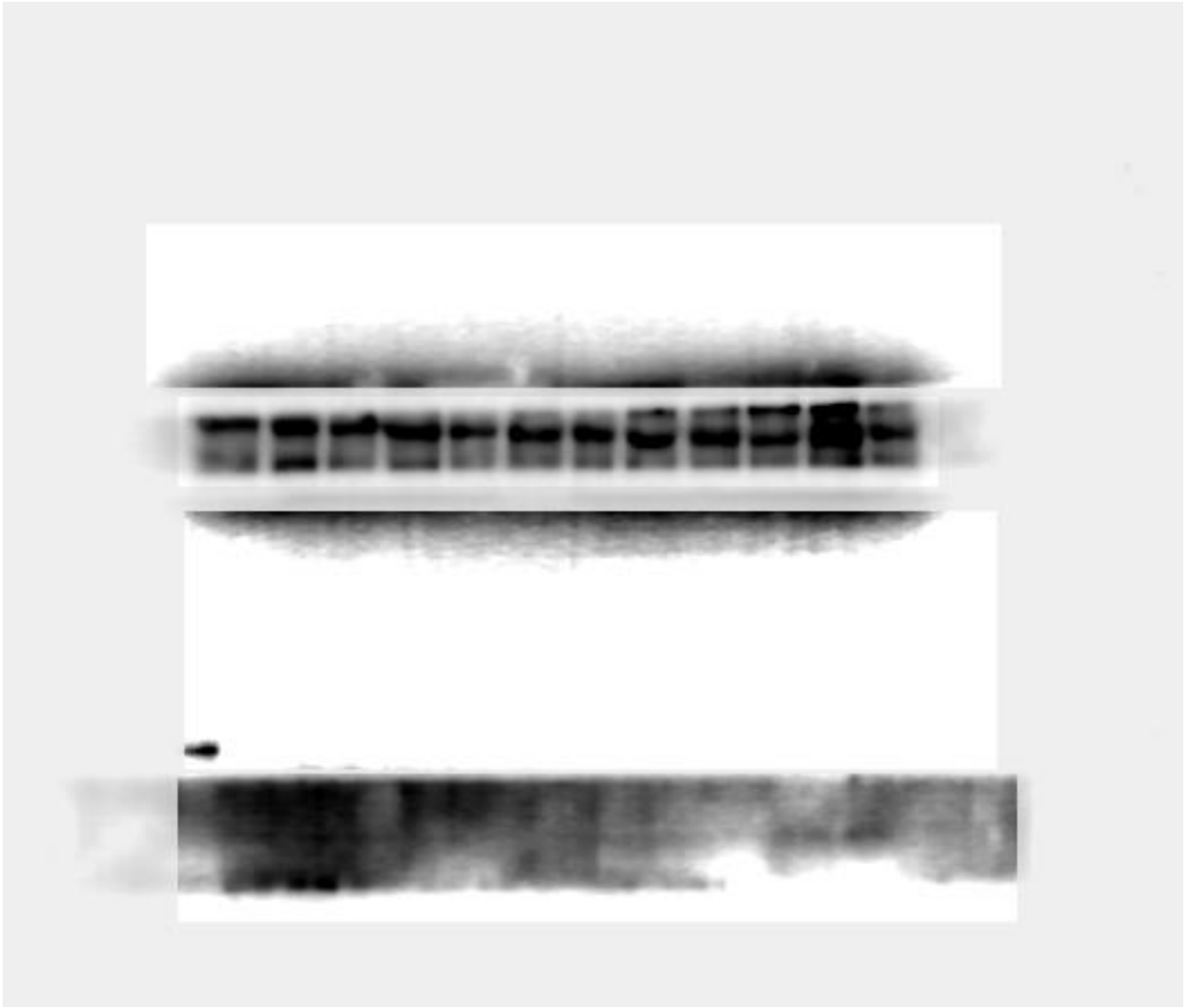
p-RB
ATF6
p-chk2
Actin
PCNA

SIRT

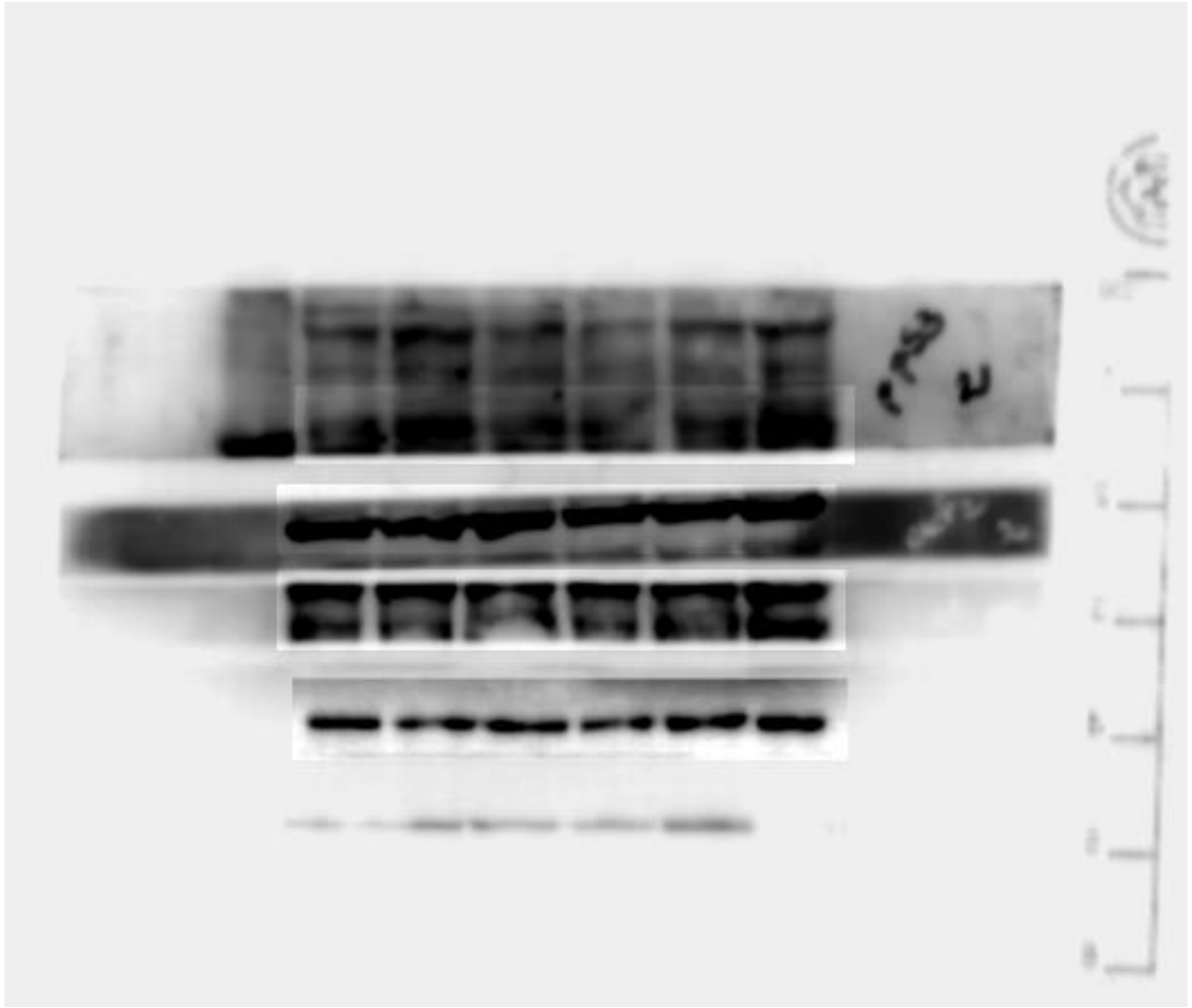
p-p53
HSP90
ATF6
Actin
Actin